Methods of Characterizing Gas-Metal Arc Welding Acoustics for Process Automation

by

Joseph Tam

A thesis
presented to the University of Waterloo
in fulfillment of the
thesis requirement for the degree of
Master of Applied Science
in
Mechanical Engineering

Waterloo, Ontario, Canada, 2005

I hereby declare that I am the sole author of this thesis. This is a true copy of the thesis, including any required final revisions, as accepted by my examiners.

I understand that my thesis may be made electronically available to the public.

Abstract

Recent developments in material joining, specifically arc-welding, have increased in scope and extended into the aerospace, nuclear, and underwater industries where complex geometry and hazardous environments necessitate fully automated systems. Even traditional applications of arc welding such as off-highway and automotive manufacturing have increased their demand in quality, accuracy, and volume to stay competitive. These requirements often exceed both skill and endurance capacities of human welders. As a result, improvements in process parameter feedback and sensing are necessary to successfully achieve a closed-loop control of such processes.

One such feedback parameter in gas-metal arc welding (GMAW) is acoustic emissions. Although there have been relatively few studies performed in this area, it is agreed amongst professional welders that the sound from an arc is critical to their ability to control the process. Investigations that have been performed however, have been met with mixed success due to extraneous background noises or inadequate evaluation of the signal spectral content. However, if it were possible to identify the salient or characterizing aspects of the signal, these drawbacks may be overcome.

The goal of this thesis is to develop methods which characterize the arc-acoustic signal such that a relationship can be drawn between welding parameters and acoustic spectral characteristics. Three methods were attempted including: Taguchi experiments to reveal trends between weld process parameters and the acoustic signal; psycho-acoustic experiments that investigate expert welder reliance on arc-sounds, and implementation of an artificial neural network (ANN) for mapping arc-acoustic spectral characteristics to process parameters.

Together, these investigations revealed strong correlation between welding voltage and arc-acoustics. The psycho-acoustic experiments confirm the suspicion of welder reliance on arc-acoustics as well as potential spectral candidates necessary to spray-transfer control during GMA welding. ANN performance shows promise in the approach and confirmation of the ANN's ability to learn. Further experimentation and data gathering to enrich the learning data-base will be necessary to apply artificial intelligence such as artificial neural networks to such a stochastic and non-linear relationship between arc-sound and GMA parameters.

Acknowledgements

I wish to thank my supervisor, Dr. Jan Huissoon for his continued support and faith in me throughout this research. I really appreciate his insight and guidance while allowing me the freedom to discover and to "try things my way". I would also like to acknowledge the expertise of Dr. William Melek in his willingness to assist in teaching me about intelligent systems. His enthusiastic support and interest in my research and efforts have had a profound effect on the completion of this thesis. My peers and colleagues have been of significant importance to me, particularly the technical wizardry of Edmon Chan whose abilities have made this a humbling yet gratifying experience. Also, the assistance of Neil Rettinhouse, Nick Bourdon, (Jackie) Jangbahadur Singh Mann, and Bhadresh Lad in the lab is greatly appreciated.

I would also like to acknowledge the financial support of the Ontario Research and Development Challenge Fund (ORDCF) and the Natural Sciences and Engineering Research Council of Canada (NSERC).

Above all, I wish to express my gratitude for the unwavering love, support, and faith of my partner in life, Samantha Tam, without whom I would have never come this far.

Table of Contents

List of Figures

List of Tables

Chapter 1
Introduction

1.1 Background

When basic automation was initially introduced to the welding industry, it was implemented as open-loop control; where process outputs have no bearing on process input parameters. As a result, the scope of arc-welding applications that could employ automation was limited to those that were simple and well characterized. The experienced human welder, being the best available closed-loop process controller, was still called upon for challenging applications involving complex geometries, poor fit-up, or unpredictable environments.

However, as applications of material joining branch into areas such as the aerospace, nuclear, and underwater industries, new challenges arise. Specifically, the levels of quality and accuracy required are exceeding human capacity, and more importantly, many of these weldments are located in environments that exceed human physiological tolerances. As a result, increasing emphasis is being placed on closed-loop automation of arc-welding processes. This in turn has necessitated improvements in the areas of modeling, sensing, and controlling arc-welding processes. Recent advances in the fields of high-speed sensing, data acquisition, processing hardware and software, and intelligent controls have inspired and facilitated numerous studies into varying methods of characterizing and refining the arc-welding process.

Of these available technologies, the most prominent and successfully employed in current industry are high-speed vision/laser ‘seam-tracking’ systems like the Liburdi Laser Seam Tracker [1] which,

combined with low-cost, software-based data acquisition cards for PCs create the platform upon which fully automated arc-welding can be realized. The major advantages of using PC based systems, indicated by Lucas et al [2], are low-cost, customizability and upgradeability. Although the challenge of complex joint geometry and poor fit-up can be addressed by such commercially available systems, the same type of equipment can be utilized to realize greater weld quality and consistency by controlling the welding process itself.

One such area of investigation is the use of airborne acoustic signals to provide insight and feedback about the gas metal arc welding (GMAW) process. Motivation for this advancement evolved from the general acknowledgment amongst professional welders that arc-sound provides as much useful feedback as vision [2] in controlling the process. In some cases, there is no choice but to employ fully automated welding systems utilizing vision and acoustic feedback. This is essential when the welding process is done where human activity is not admissible, such as deep-sea underwater welding, [3].

Along with the availability of economical computing power [4] comes the ability to practically apply the concepts of fuzzy logic and neural network control schemes to industrial processes including arc welding [5]. Furthermore, these modern techniques have also been used in attempts to identify and characterize arc acoustic signals [6].

1.1.1 GMAW Overview

Before surveying existing strategies for sensing and control, it is beneficial to briefly present an overview of the physics and input/output parameters that affect the arc-welding process. Readers familiar with GMAW may choose to advance to the next section.

The ultimate goal of arc welding is to join two or more materials, through fusion, such that the joint exhibits a sufficient strength and fracture toughness. In general, the heat required for melting and subsequent fusion of material is generated by an electric arc bridged between the workpiece and the welding electrode in an inert atmosphere that helps to the prevent oxidation. The current passing through this arc is generally in the range of 200 A to 600 A depending on the material thickness, electrode diameter and shielding gas mixture.

More specifically, GMA welding uses a 'consumable' wire electrode that melts and continuously deposits material into the joint during the process. The mode in which the metal is deposited changes from short-circuit to globular to spray and finally to rotational, Figure 1-1, with increasing current density. Typical manufacturing applications prefer globular and spray transfer modes of operation as they offer the best balance between material deposition speed, penetration, and bead aesthetics. However, short-circuit transfer mode is used in some heavy structural joining applications while rotational transfer mode is still being investigated by researchers as a viable method of ultra-high-speed material deposition.

In essence, it is the combination of arc stability and regulation of the rate and mode of 'metal transfer' that dictates the quality of the final weld. These properties are the integration of many interdependent aspects of the process, thus making GMA welding a fully coupled, highly non-linear multivariable process. Doumanidis et al [7] have identified three dominant qualities that need to be controlled, albeit indirectly: fusion zone geometry, heat affected zone properties, and thermally induced deflections and residual stress. Due to the challenges inherently presented by GMA welding control,

attempts at classical modelling and control techniques have met with little success [8, 9]. Nonetheless, they have helped to characterize and identify those input and feedback parameters pertinent and measurable for automation purposes. Input variables have been separated into two categories by the American Welding Society (AWS), [9] and are listed with the feedback parameters of interest in Table 1-1.

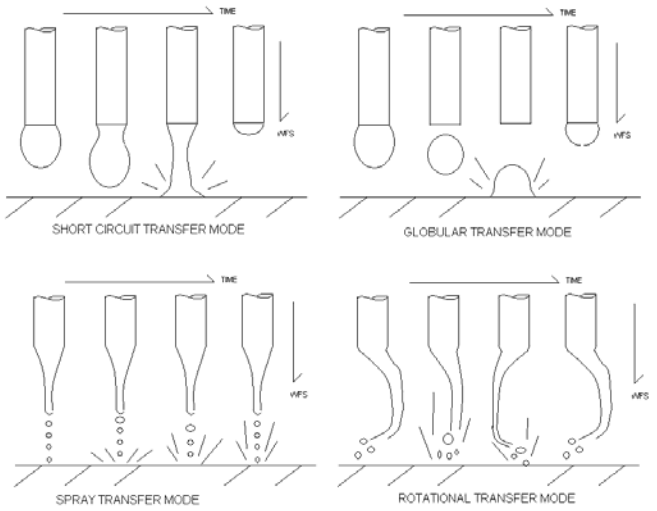

Figure 1-1: GMAW Metal Transfer Modes

Table 1-1: GMAW input and feedback parameters as identified by AWS [10]

Input Parameters	Feedback Parameters
Preset Parameters: - Joint Geometry - Material composition - Filler wire composition - Shielding gas mixture *Variable Parameters:* - Open Circuit Voltage/Waveform - Contact-tip to Work Distance (CTWD) - Orientation of torch to work piece - Torch Travel Speed - Wire Feed Speed (WFS) - Shielding Gas Flow Rate	- Arc voltage - Current - Weld penetration - Bead height - Bead width - Metal transfer mode - Metal transfer rate - Arc acoustics - Arc radiation emissions - Joint geometrical deviations - Base metal temperature gradients

Historically, real-time and non-destructive measurement of some of the listed parameters has been difficult or impossible due to restrictions in data volume, acquisition speed, and unavailability of technologies. For example, when developing a multivariable model for controlling GMA welding, Doumanidis et al.[7] points out that developing control systems for complicated, non-linear, multi-variable processes is complicated when sensing problems including inaccuracies and noise are present. Fortunately, there have been rapid advances in cost-effective and new sensing technologies in the past two decades. Armed with these tools and combined with heuristic knowledge accumulated by expert welders, new strategies for characterizing and detecting feedback parameters continue to evolve.

1.1.2 Review of Arc Acoustic Research

The airborne acoustics emitted by a welding arc are an indirect indicator of the arc stability and metal transfer characteristics. It is a well established fact that experienced human welders are able to maintain and direct the welding arc using a combination of their visual and auditory senses, [11]. In 1967, Jolly [12], published a study on GMA welding acoustics as an indicator of the occurrence of cracks in a welded joint. He concluded that sound pressure increases with arc length (voltage) and welding current. While investigating the pressure waves caused by arcing faults in an electrical substation, this relationship was formally defined in 1979 by Drouet and Nadeau [13], as:

$$S_a(t) = k\left[V(t)I(t)\right] \tag{1}$$

with

$$k = \alpha(\gamma - 1)/c^2$$

Where:

- S_a: time integral of acoustic signal
- V: arc voltage
- I: current
- α: geometrical factor

γ: adiabatic expansion coefficient of air
c: velocity of sound in arc

Later, Drouet and Nadeau [14] proceeded to refine this relationship while performing experiments using graphite electrodes. They discovered that the acoustic signal is specifically attributed to the instantaneous change in electrical power of the arc column, and not of the whole arc. In other words, there are no acoustic emissions due to the cathode and anode fall regions. This correspondence between the sound pressure level of the arc and electrical power has yielded significant practical use in applications where traditional direct measurements of the arc voltage are either not feasible or not reliable. Drouet and Nadeau, who originally established the relationship, capitalized upon its usefulness in applications to arc furnaces and currently hold a patent to the use of the technique of acoustic voltage measurement. In 1979 and 1980, Arata et al. [15, 16] made measurements confirming the strong relationship between sound pressure level (SPL) and electrical characteristics and also revealing the influence of sound on the molten weld pool. They also discovered that there is synchronization between sound impulses and short circuit transfer, confirming what expert human welders have claimed, but never proven.

This prompted experiments and investigations into the relationship between metal transfer mode and arc acoustics. Mansoor and Huissoon [17] performed experiments using sound level meter (SLM) measurements and subsequent FFT analysis to identify acoustic emission characteristics of different metal transfer conditions. Utilizing a professional welder's heuristics, weld parameters for spray, globular, and short circuit transfer modes were arrived upon. Using these parameters, welds were performed while acoustic data were simultaneously gathered. Of particular interest were the resulting frequency spectra for each transfer mode. In spray transfer mode, a distinct 3.6kHz peak was observed, while globular transfer resulted in a triangular frequency band ranging from 2.5kHz to

7kHz dominant about 5kHz. This result is significant in that it defines the guidelines for future development and research of acoustic based quality control.

In an attempt to perform on-line monitoring based on the arc noise signal, Prezelj and Cudina, [18] identified two mechanisms of interest pertaining to short circuit transfer acoustics. The first is the impulse associated with peak current during the short, as reported earlier by Arata et al [15]. The second is the duration between peaks where "turbulent" noise resides and is attributed to arc oscillation and cracking of material due to inner tension relaxation. This turbulent noise was observed, through time based spectral analysis of the signal, to prevail above 5 kHz. Considering this, they proceeded to develop a non-linear relationship between the amplitude of sound pressure, *p(t)*, and current, *I*.

$$p(t) = C_1\left[V\dot{I} - 2RI\dot{I} - L\left(\dot{I}^2 + I\ddot{I}\right)\right] \tag{2}$$

Using numerical analysis and least squares estimation (LSE), the factor of proportionality, C_1, resistance, R, and inductance, L were determined. Despite the time variance of these parameters, comparison of calculated results with experimental data proved to be in excellent agreement. Furthermore, the relationship is able to reject the "turbulent" noise, thus increasing the accuracy of measurements. The authors concluded that, in conjunction with an adaptive algorithm, this method is promising for on-line monitoring of stability and quality without background and reverberation noise contamination.

So far, the discussion has been limited to research and investigations into understanding or characterizing arc acoustics with little mention to practical manifestations of these results. In fact, several preliminary but promising papers have been published within the past decade demonstrating the ability to utilize arc acoustics in real-time monitoring and adaptive control applications.

Chawla and Norrish [19] successfully demonstrated online identification of 'good' and 'poor' flux-cored arc welding (FCAW) wire using sound data. Mathematical models were derived from a correlation study of the integrated sound data with measured values of droplet size and arc length. Application of the models with on-line sound data enabled the characteristics of different wires to be determined. With 11 out of 14 successful trials using this method, they concluded that application of arc-acoustics as a quality measurement technique is possible, but limited. Excessive background noise during welding was reported to have contributed to the erroneous cases.

Kaskinen and Mueller [20] pursued acoustic arc length control by converting the measured sound pressure to an equivalent arc voltage for feedback into the original controller. The resulting system was reported to be competitive at any reasonable arc length and superior to the original signal at very short lengths.

Arc-sound signals have also been utilized by Murugesan et al [21] in monitoring and controlling the deposition thickness in an electric arc-spraying process. They succeeded in dynamic characterization of sound signals in the time domain using an auto-regressive moving average (ARMA) model with numerator and denominator of order 4 and 3, respectively. The peak value of the resulting Green's function was found to have a polynomial relationship with the deposit height for a given spray air

pressure. This value, obtained on-line, is used as a controller feedback signal indicating current deposit height.

1.1.3 Intelligent Methods in Arc Acoustics

It is interesting to note that the preceding cases have either used the arc acoustics as an indirect measurement of power characteristics or a qualifier of 'good' or 'poor' qualities. Furthermore, these experiments have only been based on statistical analysis or classical modeling tools. Unfortunately, the restrictions imposed by these techniques are that it is difficult or impossible to deal with noise polluted, erroneous, erratic, or even incomplete data. Additionally, on-line qualification of weld quality is performed based on 'crisp' information i.e. where a value is either above or below a specified threshold. GMAW being a highly coupled, non-linear multiple-input multiple-output (MIMO) process, designing a fully integrated control system around these short-comings is especially difficult. As mentioned previously, the introduction of intelligent control and analysis tools made viable by cost-effective computing power has alleviated some of these difficulties and provided further insight into parameter interactions.

Available literature shows that the use of artificial neural networks (ANN) is the preferred choice for identifying and classifying salient information from erratic data. As presented by Smith and Lucas [5], "[ANNs] attempt to simulate…biological neural networks…The main advantage… is that they learn from examples…" The most appealing aspect of ANNs is that it allows for the construction of systems from existing data without a priori knowledge concerning the interactions between input and output pair data.

More specifically, much research has been performed using ANNs to analyze airborne acoustic signals. Taylor-Burge et al. [6] developed a hybrid system combining a 'self-organising' network paradigm with high-speed FFT computation for real time corrective control of submerged arc welding (SAW). A 64 data point FFT operating at a sampling frequency of 20 kHz was applied to the acoustic data. These data were then used as training inputs to the self organising feature map (SOM). The SOM model utilizes a competitive learning technique as opposed to taught responses. The SOM was reported to have successfully separated and classified low, high and optimum voltage settings based on acoustic emissions.

Matteson et al, [22] developed a weld acoustic monitor (WAM) for process control. The WAM makes use of an ANN capable of generating its own classification rules based on a back propagation learning procedure. The procedure is based on a database of known GMAW acoustic signals of acceptable and unacceptable quality along with a corresponding confidence level. It was reported that the resulting ANN is robust and able to judge weld quality in a noisy production environment.

1.2 Objectives

As part of the larger effort to develop a fully automated GMAW system, this thesis investigates methods of extracting and characterizing data encoded in the arc-acoustic signal. Attempts at using arc acoustic signals for controlling and detecting weld processes have been implemented before, as discussed in the background. The premise of many of these previous studies was to characterize the acoustic signal based on overall sound pressure level (SPL) [3, 12, 13, 14, 18, 19, 20] or general spectral shape of the signal [17, 22]. The majority of these studies utilizing SPL as feedback were not repeatable under industrial or uncontrolled conditions due to environmental noise.

Unlike these previous experiments and implementations, this thesis seeks to identify and map salient acoustic spectral characteristics to specific changes in welding parameters. The result of this approach is a potentially more robust and noise insensitive form of acoustic feedback. Moreover, the exploration of expert human welder dependency on acoustic characteristics including time delays and spectral harmonics is pursued. Furthermore, acoustic spectral characteristics are applied to an artificial neural network (ANN) to establish a relationship from acoustics to welding parameters. Once trained, the network has the potential to act as non-linear feedback transfer function for closed-loop process control. The development, execution, and results of these experiments are described in the chapters to follow.

Chapter 2 discusses initial experiments to identify temporal changes in spectral characteristics due to continuously changing weld parameters using short-time Fourier transforms. It also presents the development of Taguchi experiments and a spectral clustering algorithm used in correlating process parameters to spectral bands. In order to better corroborate these relationships, Chapter 3 presents the development of psycho-acoustic methods and experiments in which expert human welders were asked to perform welding tasks while listening to modified acoustic feedback. In Chapter 4, the development, training, and verification of an artificial network capable of predicting weld parameters from acoustic spectra is presented. Finally, Chapter 5 presents conclusions and puts forth recommendations for future study and development.

Chapter 2
Parametric Arc-Acoustic Characterization

2.1 Introduction

Much of the content in this chapter is directly taken from [23], a paper written by the author and submitted to *Science and Technology of Welding and Joining*, an international peer reviewed journal on applied technology in the field of welding and joining science.

Previous studies have shown that arc acoustic emissions can be used to identify the metal transfer mode and to detect process problems such as lack of shielding gas [2], as well as for establishing relationships with arc electrical characteristics [3], and control of arc length [20]. In many of these studies, the investigators have only been able to relate the general sound pressure level (SPL) to weld characteristics. To our knowledge, only cursory investigations have been conducted to identify how and which frequency components change with changing parameters.

By studying changes in the GMAW acoustic signal spectra and identifying salient frequency bands pertaining to changes in welding parameters, we were better able to define important feedback content. Of significance is the relationship between arc-voltage and acoustic emissions. As part of our investigation, we conducted preliminary experiments to identify the level of correlation between these two front-end sources of feedback during spray-transfer. A discussion of the spectral analysis techniques and results of these experiments are presented.

Specifically, this thesis of arc-acoustic characterization focuses on associating spectral changes to weld process parameters. To do this, we employed several spectral analysis techniques including:

fast Fourier transform (FFT), short-time Fourier transforms (STFT), and recursive spectral cluster identification. The following three sections provide the background to these approaches as well as Taguchi methods, and are followed by implementation, results, and implications. The results of these experiments and analysis will be summarized with descriptions pertaining to their potential significance as control feedback.

2.2 Short-Time Fourier Transform (STFT) Analysis

A useful technique for visualizing changes in the frequency content of a signal over time is to assemble a sequence of frequency spectra as a 3 dimensional surface. A frequency spectrum plots the signal power as a function of frequency, and is obtained from a time domain signal as the Fourier transform of the signal. The continuous Fourier transform relates a time function *g(t)* to a complex frequency response *G(f)* according to Eq (3).

$$G(f) = \int_{-\infty}^{\infty} g(t) e^{-j2\pi ft} dt \tag{3}$$

The use of a continuous Fourier transform allows for an infinite frequency resolution since integration occurs over an infinite length of time. In practice, this is implementated by discrete integration over *N* data points and *k* finite frequency bands to form the discrete Fourier transform (DFT) as:

$$G(k) = \frac{1}{N} \sum_{n=0}^{n=N-1} g(n) e^{-j2\pi kn/N} \tag{4}$$

By using a finite number of samples, the spectral band lengths or frequency resolution, R_f, of the DFT is also limited. For a signal sampling frequency of F_S, the frequency resolution of a DFT of length N can be computed by Eq. (5).

$$R_f = \frac{F_S}{N} \tag{5}$$

The FFT algorithm improves the speed and memory usage of DFT computations by efficient reorganization of the effective computation matrix formed by Eq. (4). Utilizing the efficiency offered by FFT analysis, STFT analysis is implemented.

Short-time Fourier transform (STFT) analysis uses a series of FFT spectral plots arranged in temporal sequence to generate a visual representation of spectral changes in the signal as a function of time. An example to illustrate this is shown in Figure 2-1, where multiple frequency spectra (FFT1 through FFT9) recorded t_D seconds apart exhibit differences in signal power due to a parameter changes during the interval between recordings. Over a larger number of intermediate spectra recorded, the development of this change in spectral content can be observed as a function of time (or as a function of the varying parameter). For improved view-ability, these 3 dimensional STFT plots are often shown in plan view as contour plots or with the signal power color coded (e.g. Figure 2-8).

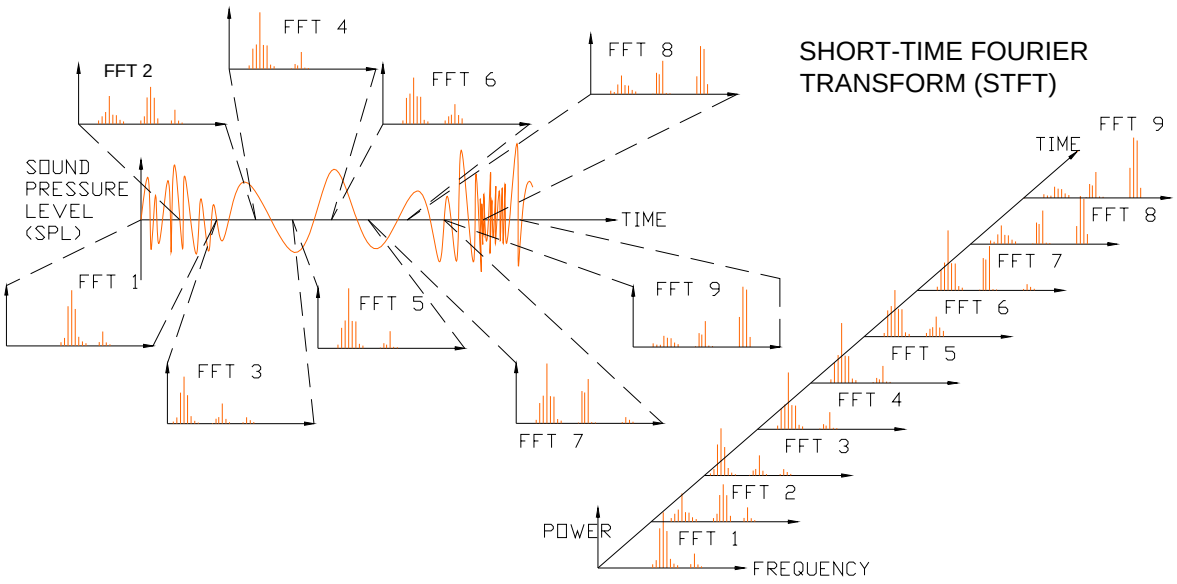

Figure 2-1: Illustration of how a STFT plot is generated from a time-dependant acoustic signal.

The STFT technique is useful for analyzing signals that are quasi-static with respect to FFT lengths. In fact, the expected rate of change of significant spectral components should be at least an order of magnitude less than the frequency resolution, R_f, of each FFT. This constraint is necessary to properly capture variations in spectral component magnitudes due to process parameter changes. To prevent sudden spectral changes from one FFT window to the next, the windows used for the analysis of a given signal are arranged to overlap each other.

2.3 Recursive Spectral Cluster Identification

While STFT plots are useful visual analysis tools, it is also useful to be able to identify 'significant' features within a spectrum and to be able to associate numerical values (e.g. frequency or power) with these features. A cursory inspection of a typical frequency spectrum for a GMA weld (Figure 2-2), shows key frequency components (peaks) are present and that such a spectrum could be divided into frequency bands so that each band contains a significant peak. The recursive spectral cluster

identification technique was used to systematically subdivide the measured 20Hz – 16kHz frequency range of the spectrum into a predefined number of bands. Prior to clustering, the measured acoustic data were first transformed to the human octave-based perception of sound, since one of the objectives of this research is to determine what a human welder listens for when controlling the weld process.

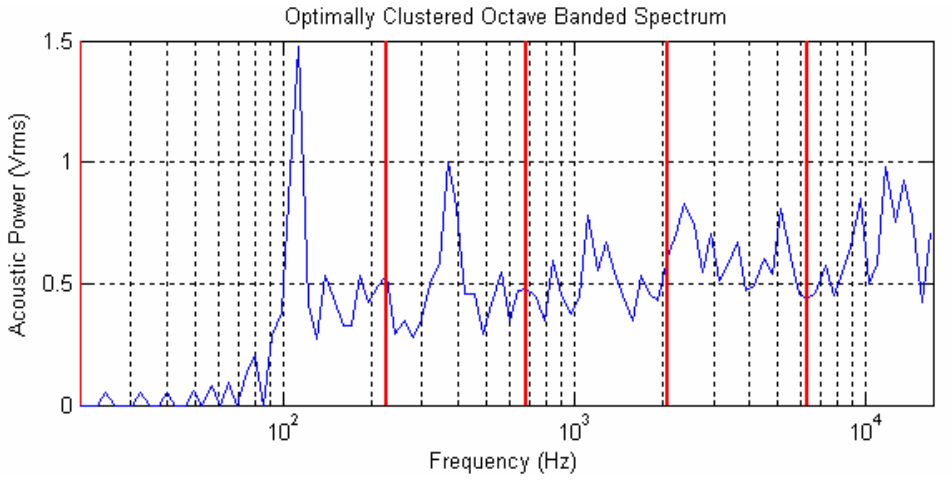

Figure 2-2: Optimally clustered octave-banded spectrum using recursion cluster identification algorithm

The overall procedure was thus as follows: for a selected (constant) set of welding parameters, the acoustic signal was recorded for 10 seconds; 4 equally spaced data sets (4096 samples per set) were extracted from the steady state recording (Figure 2-3), and the sub-audio content removed using a digital high-pass filter with a 20 Hz cut-off frequency. An FFT was applied to each data set, and the resulting spectrum then underwent octave band transformation to better represent human sound perception. Once transformed, each of the resulting logarithmic spectra undergo recursive cluster identification to identify common and dominant frequency components between clusters and between experiments.

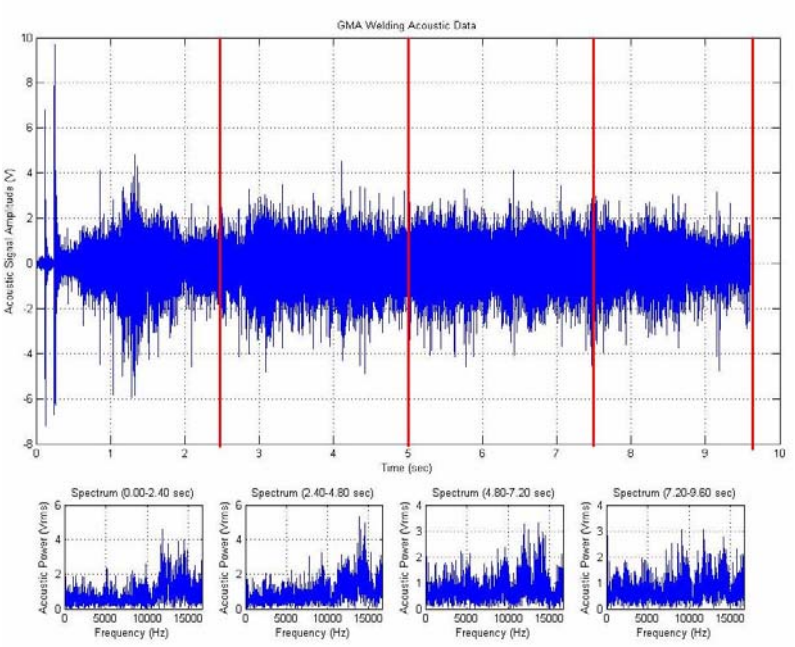

Figure 2-3: Time domain acoustic signal and associated spectra for four equally spaced data segments

The objective of the acoustic spectral anaylsis was to investigate whether changes to weld process parameters can be associated with changes in the acoustic spectrum. Rather than monitor individual frequences for changes in amplitude, frequency bands were monitored within the spectrum for changes in band center frequency and scatter. The recursive spectral cluster identification technique provides a method of systematically subdividing the measured 20Hz – 16kHz frequency range of the spectrum into a predefined number of bands. The upper range, 16kHz, is selected based on the Nyquist sampling criterion which states that the sampling frequency of a data-acquisition device must be at least twice as fast as the highest frequency of interest. At 33kHz per channel, our DAQ can at best record information below 16kHz.

However, since the objective is to classify the audible spectrum, it is first necessary to transform the measured acoustic data to accommodate human octave based perception of sound.

2.3.1 Octave Band Transformation

Human hearing is not a linear function of frequency, and as such, the frequency spectra were transformed using 1/10th octave bands. The octave band boundaries were computed according to Eq.(6).

$$\begin{aligned} f_{C_{n+1}} &= 2^{1/m} f_{C_n} \\ f_{L_n} &= \frac{f_{C_n}}{2^{1/(2m)}} \\ f_{U_n} &= 2^{1/(2m)} f_{C_n} \end{aligned} \tag{6}$$

Where:

m: octave band fraction (m=10 in this case)

f_{Cn+1}: center frequency of n'th band

f_{Ln}: lower frequency boundary of n'th band

f_{Un}: upper frequency boundary of n'th band

Based on the frequency boundaries computed above, the original spectral data, *G(f(k))* was transformed to the logarithmic scale, *G(n)*, according to Eq.(7).

$$G(n) = \sum_{f(k)=f_{L_n}}^{f_{U_n}} G(f(k)) \tag{7}$$

An example of this fractional octave band transformation is illustrated in Figure 2-4.

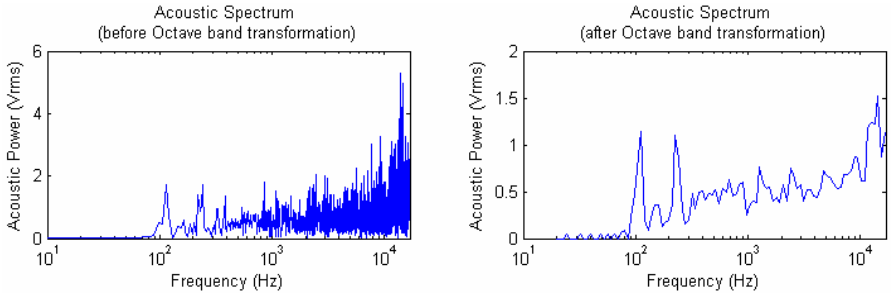

Figure 2-4: 1/10th octave band transformation of acoustic spectrum

Not only does the octave band transformation yield representative spectra for human hearing, it also reduces the effective number of frequency bins from 2048 to 98. Having fewer frequency bins is very effective in facilitating a quicker clustering algorithm, as discussed next.

2.3.2 Recursive Cluster Boundary Identification

The most noticeable aspects of a given acoustic spectrum are the major peaks and the 'distribution' of acoustic power – these will describe the sound heard while the signal was recorded. In order to be able to make a comparison between two spectra taken under different welding conditions, it is necessary to be able to characterise the 'peakiness' and overall distribution. The approach chosen was to specify the number of clusters into which the spectrum should be subdivided, and then determine the location of the subdivision boundaries. To perform this spectrum subdivision in a consistent manner, a recursive algorithm was developed in Matlab to compare the level of scatter in the data within the specified number of clusters.

The scatter S within cluster n consisting of frequency bins N_L to N_U is computed as:

$$S_n = \sum_{j=N_L}^{N_U} p(j).(j - m_n - N_L)^2$$

Where:

p(j): acoustic power of frequency bin *j*

m_n: geometric mean of the cluster, calculated as:

$$m_n = \frac{\sum_{j=N_L}^{N_U} p(j).(j - N_L)}{\sum_{j=N_L}^{N_U} p(j)}$$

As mentioned above, following the octave band transformation the discrete spectrum consists of 98 frequency bins, and these were grouped into k frequency bands (or clusters) based on the scatter of the acoustic power within each band. The number of combinations in which the 98 bins can be grouped into k clusters is ${}_{97}C^{k-1}$. Using a brute force approach (evaluating every possible cluster combination) means that for our practical compuation purposes, k was limited to 5, resulting in approximately 3.6 million groupings to be evaluated for each spectrum. For each possible cluster set combination, the scatter of the acoustic power within each of the 5 clusters was computed, and these were averaged to provide a global cost function for that particular cluster set combination. Once all 3.6 million cost functions were computed, the lowest value was selected as the opitmal cluster combination. With 4 spectra per weld, a total of 80 minutes was required per weld using a 2.4GHz Pentium IV. Figure 2-2 illustrates an optimally clustered octave-banded spectrum where the optimum boundaries for the five layers have been illustrated as solid vertical lines super-imposed on the octave-banded PSD.

Having identified cluster boundaries for each spectrum, the dominant frequency from each cluster is identified. This simply involves searching for and recording the frequency at which maximum power occurs within each cluster. This method is simple and yields relatively consistent results when used on steady-state data.

2.4 Taguchi Method

Having established a method of repeatably characterizing the acoustic signal, we seeked a method of generalizing how these characteristics change with different welding parameter levels. The Taguchi method is a simple and efficient parametric method of identifying the effects of changing weld parameters to changes of specific acoustic characteristics. The design of Taguchi experiments involved several steps: 1) choosing independent variables and levels; 2) calculating total degrees of freedom; 3) selecting an appropriate orthogonal array to ensure an equal number of experiment levels are used; 4) drawing the required linear graph and adjust to match a standard linear graph to dictate which effects and cross-effects will be assessible upon anaylsis.

2.4.1 Choosing Independent Variables and Levels

The choice of independent variables is determined by the number of adjustable weld parameters for the given equipment. The parameters of interest were chosen as voltage, wire-feed-speed (WFS), contact-tip-to-workpiece-distance (CTWD), torch-speed, torch-angle, wire diameter, and gas flow rate.

As part of Taguchi experiments, it is necessary to select the number of levels for each parameter under investigation. Since GMAW is inherently non-linear, it is reasonable to expect acoustic trends between operating levels to change in a non-linear fashion. As such, it was decided to carry out

experiments with three operating levels for each independent variable, with the exception of wire diameter (Table 2-1).

With the experiment parameters and associated levels selected, proper parameter combinations were decided upon. These combinations will ensure that the experiments yield representative results and associations between acoustic data and welding parameters.

Table 2-1: Independent variable operating levels for Taguchi experiments. Note the differences between numerical values of the operating levels between wire diameters. This is necessary to accommodate for proper spray-transfer operating envelopes for each respective wire size.

Wire Diameter [in]	**0.035**			**0.0625**		
	Low	**Med**	**High**	**Low**	**Med**	**High**
CTWD [in]	0.551	0.650	0.787	0.551	0.650	0.787
Torch Speed [in/sec]	0.354	0.472	0.591	0.472	0.591	0.709
WFS [in/sec]	8.333	10.833	12.500	6.300	7.874	9.449
Voltage [V]	26	29.5	33	24	29	34
Gas [ft^3/min]	30	40	50	30	40	50
Torch Angle [deg]	30	0	-30	30	0	-30

2.4.2 Calculating Degrees of Freedom

The degrees of freedom (DOF) are the number of factor and interaction comparisons necessary to derive a complete conclusion concerning the effect of parameter levels for a given experiment. Eq.(8) shows how this is computed:

$$
\begin{aligned}
DOF_{\text{main\_effects}} &= \sum_{i}^{N} (n_i - 1) \\
DOF_{\text{interactions}} &= \sum_{j}^{M} DOF(A_j) \times DOF(B_j) \\
DOF_{\text{total}} &= DOF_{\text{main\_effects}} + DOF_{\text{interactions}}
\end{aligned}
\tag{8}
$$

Where:

A,B: experiment parameters

N: number of factors (main effects)

n_i: number of levels for factor 'i'

M: number of interactions

To compute the DOF of these experiments, interactions of interest were identified. Since it is known that there is a strong correlation between the electrical and acoustic behaviour in GMAW [13, 14, 24], it was reasonable to investigate the interaction of those factors which have strongest influence on electrical characteristics. Thus, the interactions of interest were; Voltage / WFS, Voltage / CTWD, and CTWD / WFS.

Having seven main effects and three interactions, each with 3 levels of operation, the number of degrees of freedom for this experiment was 26.

2.4.3 Orthogonal Array Selection

An orthogonal array is one that is designed so that each level for each factor occurs an equal number of times. The appropriate orthogonal array was selected from a set of standard arrays based on the

required degrees of freedom, as determined previously. In this case, for a three level experiment, a L27(313) orthogonal array [25] was selected to match the required 26 DOF.

2.4.4 Linear Graphs

This graphical method allows for systematic assignment of factors within the orthogonal array without confounding the effects of factors and interactions [25]. The graphs were constructed of vertices and edges, representing main effects and interactions, respectively. Numbers were associated with each vertex and edge corresponding to the columns in which each factor or interaction is to be placed within the orthogonal array. With seven main effects and three interactions, Figure 2-5 represents the required linear graph chosen from a standard list provided in [25].

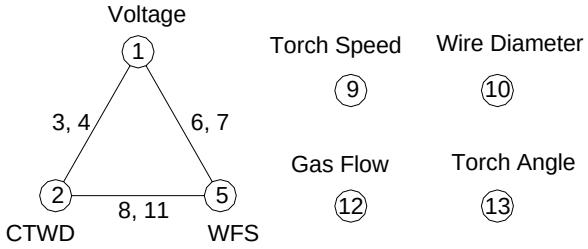

Figure 2-5: Linear graph used for assigning factors and interactions to the appropriate columns of a L27(313) orthogonal array.

The resulting factor level listing was then generated based on the linear graph and orthogonal array. Although the wire diameter factor has three levels, only two diameters were available for testing. To accommodate this, we decided to perform two experiment sets where the medium level for wire diameter was assigned to either small or large diameters in each (Table 2-2). By approaching the problem this way, we were able to maintain orthogonality in the experimental design by maintaining an equal number of occurences for each level of each factor. Moreover, additional data points generated by the extra experiments will allow for a more accurate analysis.

Table 2-2: Use of two experiment sets to assign wire diameter levels for maintaining orthogonality in experiment design scheme.

Orthogonal Array Level	Actual Wire Diameter Levels (Experiment Set 1)	Actual Wire Diameter Levels (Experiment Set 2)
High	High (0.0625")	Low (0.035")
Med	High (0.0625")	Low (0.035")
Low	Low (0.035")	High (0.0625")

2.5 Analysis of Taguchi Data

In order to identify dominant acoustic characteristics with respect to changing weld parameters, the analysis of data collected from the experiments included: level average analysis; signal-to-noise (S/N) analysis; and frequency-of-occurrence analysis.

2.5.1 Level Average Analysis

Level average analysis investigates the mapping of welding parameters to salient acoustic characteristics by considering how much the output parameter mean is affected by changes in control parameter levels.

The primary effects and interaction effects of input parameters on a given output parameter was computed by Eq. (9):

$$P = \frac{\sum_{i=1}^{N} \bar{m}_i}{N} - \frac{\sum_{j=1}^{M} \bar{m}_j}{M} \tag{9}$$

Where:

P: Primary or interaction effect

m_i: Means of output parameters pertaining to level of highest effect.

m_j: Means of output parameters pertaining to level of lowest effect.

N: Number of experiments at each level

For this investigation, each of the five possible spectral bands was considered as an output parameter and was subjected to level average analysis.

2.5.2 Signal-to-Noise Analysis

It became apparent that because level average analysis utilizes the mean of dominant frequency components from each spectrum, some effects may be underestimated due to anomalous or non-clustered data points that can skew the computed means. Fortunately, signal-to-noise analysis should be sufficient to identify those effects which were scattered (noisy), or well clustered, thus giving a better indication as to which effects were truly dominant.

The signal-to-noise (S/N) ratio (Eq. (10)) was developed as an indicator of how well a given process will perform in the presence of noise. In this context, it was used as an indicator of how consistent changes in spectral components are with respect to changes in welding parameters. When used in conjunction with results generated by level-average analysis, it will help pinpoint the exact frequency bands that deserve attention for a given set of welding parameters.

The S/N equation, in dB, was defined as:

$$S/N = -10 \cdot \log \left| \frac{y_1^2 + y_2^2 + \ldots + y_n^2}{n} \right| \qquad (10)$$

Where:

$y_1, y_2, \ldots, y_n$: Data point values

n: Number of data points under consideration

In general, the larger the S/N ratio, the more salient or confident one would be of a specific spectral component.

2.5.3 Frequency of Occurrence Analysis

Although the statistical mean and S/N of spectral clusters yielded indications of the ranges within which critical characteristics lie, it failed at identifying specific spectral components. To accomplish this, the data for dominant spectral bands were subjected to frequency-of-occurrence analysis.

Frequency-of-occurrence analysis was a better representation of the mode of each data set. It simply calculates how often data values occur within a range of values and plots a histogram (Figure 2-6). Due to the acoustic nature of the anaylsis, the data ranges were arranged logarithmically in $1/10^{th}$ octave bands.

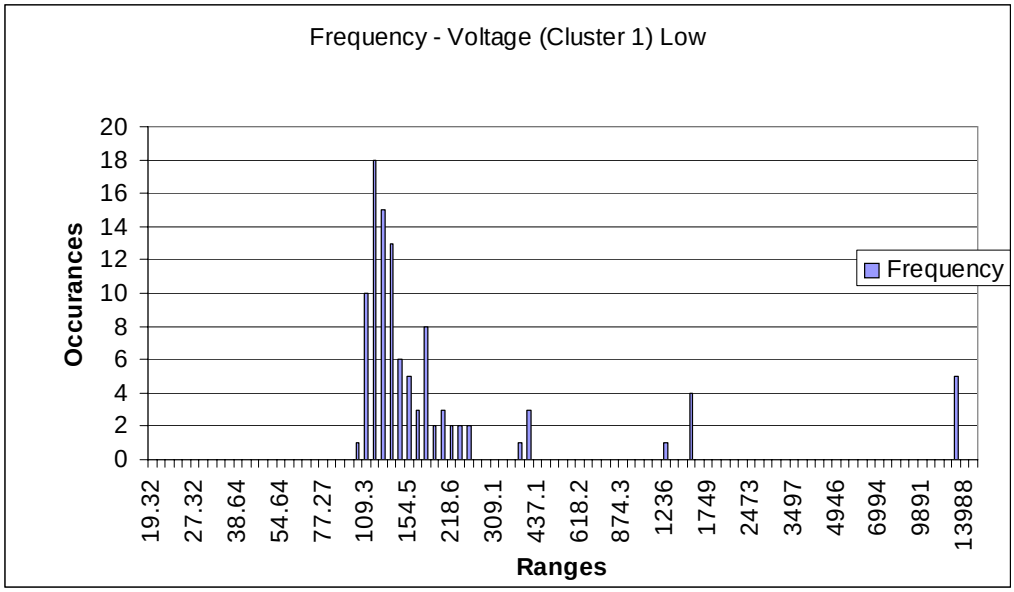

Figure 2-6: Sample histogram generated using frequency of occurrence analysis to identify characteristic frequency bands of significance.

2.6 Experimental Apparatus and Execution

The experimental apparatus is illustrated in Figure 2-7. Acoustic data was collected through a custom built microphone pre-amplification circuit that includes a built-in analogue anti-alias filter with a 12.5 kHz corner frequency. This signal was then digitally stored on a PC using a PCI 9114 data acquisition card with a sampling frequency of 33.3 kHz per channel. Also collected were voltage and current data measured using a LEM LV-100 voltage transducer and a LEM LT-1000 Hall effect current transducer, respectively.

Welding equipment included a FANUC 210i Arc Mate robot in conjunction with a Lincoln Powerwave 455 configured for constant voltage operation. All welds were performed on plain carbon steel plates using copper-free steel wire. All were bead-on-plate welds using 0.125" plate for 0.035" wire and 0.250" plate for 0.0625" wire.

Initial investigations of the relationship between arc voltage/current and arc acoustics were carried out with the same apparatus using 0.0625" wire. Voltage and current were manually varied, independently, while the torch manipulator traversed the work-piece. Table 2-3 lists the parameters under which these experiments were carried out.

For the Taguchi experiments, each weld was performed, non-consecutively, three times. The parameters used are described in the Taguchi method discussion. This facilitates the signal-to-noise analysis and also establishes a level of confidence when identifying dominant frequency clusters.

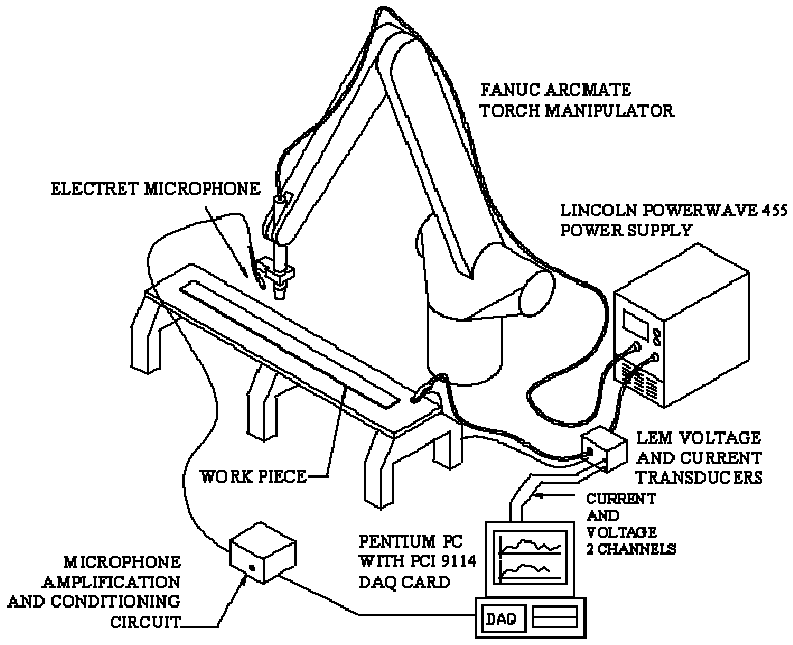

Figure 2-7: Illustration of experimental apparatus used in parametric arc-acoustic study

Table 2-3: Parameters used in initial study of arc-acoustic correlation with welding parameters.

Experiment No.	Voltage [V]	WFS [in/sec]	CTWD [in]	Torch Speed [in/sec]
1	28-34	5	0.787	0.590
2	32	3.5-4.0	0.787	0.590
3	32	2.67-3.83	0.787	0.590
4	24-34	3.33	0.787	0.590
5	24-29-22	3.33	0.590	0.590

2.7 STFT Results

Figure 2-8 to Figure 2-12 illustrate the changes in the arc-acoustic spectra as voltage and WFS values were changed while welding. Each STFT has been plotted with the same scaling to better represent relative magnitudes in frequency components between tests. The frequency scale on the STFTs are on a log-scale to better represent changes in lower spectral components. Furthermore, low-pass

filtered traces of arc-voltage and current are included above the STFT plot to indicate where and why changes occurred.

In general, the plots show that change in voltage is the most prominent influence on acoustic spectra. Inspecting Figure 2-8, we see that below 31V (before 8 seconds), the STFT show prominent frequencies in the 7kHz to 9kHz bands as indicated by the bright purple peaks. Once the voltage crosses the threshold of 31V however, these high frequency content disappear giving way to dominant low frequency components in the 150Hz to 300Hz range. Similar inspection of the subsequent figures reveal significant spectral bands and general trends. The spectral bands of significance in this cursory study has been identified as the 50Hz to 500Hz band and 4500Hz to 9800Hz band. More specifically, for the welding parameters used in these tests, increases in voltage up to approximately 31V results in a distinct shift in spectral bands from the 50Hz to 300Hz into the 4500Hz to 9800Hz range but drops back down to the lower frequency bands once the threshold of 31V is exceeded.

Although the STFT results yield a visual representation of how spectral attributes change with welding parameters, they do not give a clear indication as to which combinations characterize specific welding parameter sets. With respect to our objective to better map these acoustic characteristics to process parameters in a repeatable fashion, we can conclude that the STFT can serve well as indicators of spectral portions that deserve attention. However, repeatable methods are required to be able to better extract well defined parameters from the sound signal.

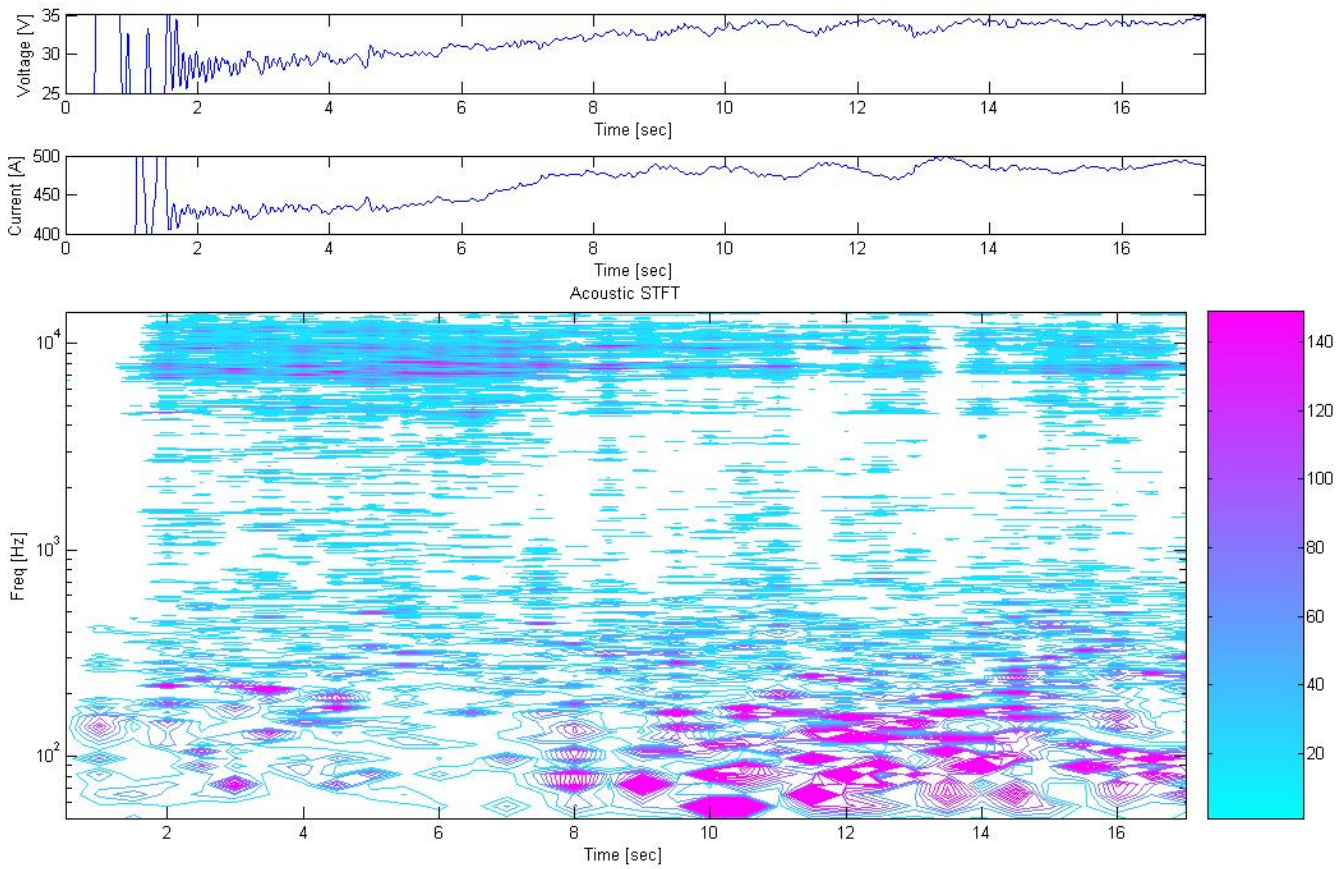

Figure 2-8: Experiment 1 STFT results. Increase in voltage from 28V to 34V at 5.0 in/sec WFS shows a shift in frequency from 7kHz - 9.8kHz band to 50Hz - 300Hz band.

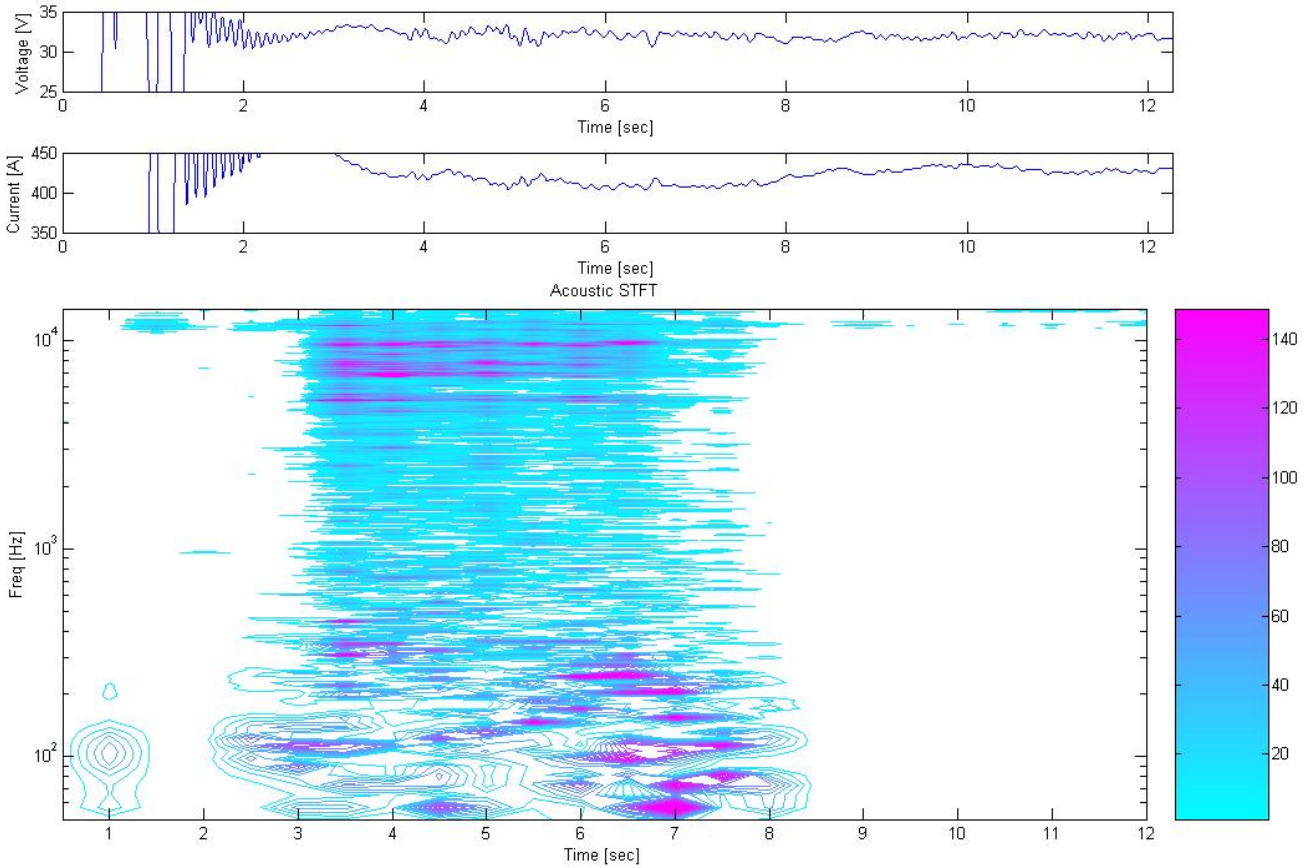

Figure 2-9: Experiment 2 STFT results. Increase in WFS from 3.5 in/sec to 4.0 in/sec results in the disappearance of high-amplitude frequency components in the 4.5kHz - 9.8kHz and 50Hz - 400Hz bands

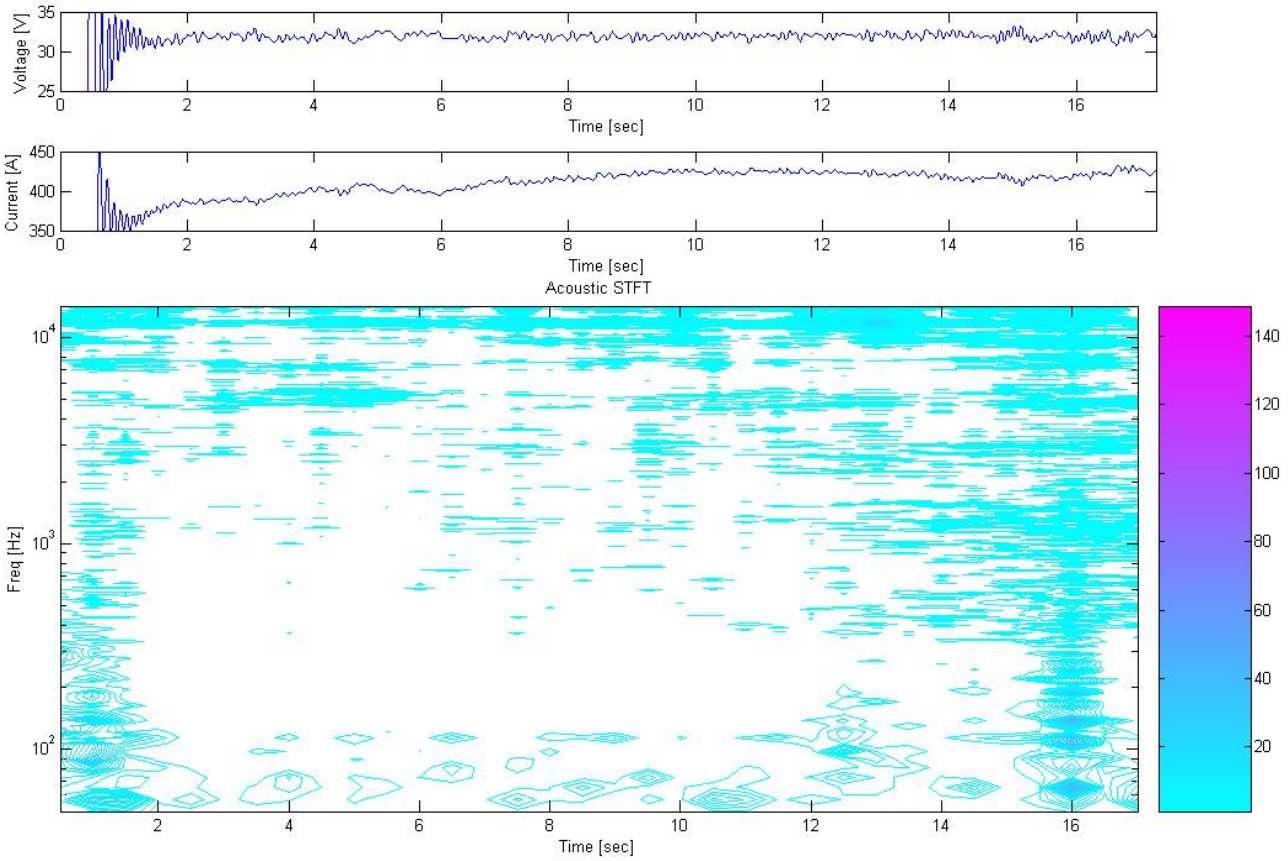

Figure 2-10: Experiment 3 STFT results. Increase in WFS from 2.67in/sec to 3.83in/sec results in no significant spectral changes.

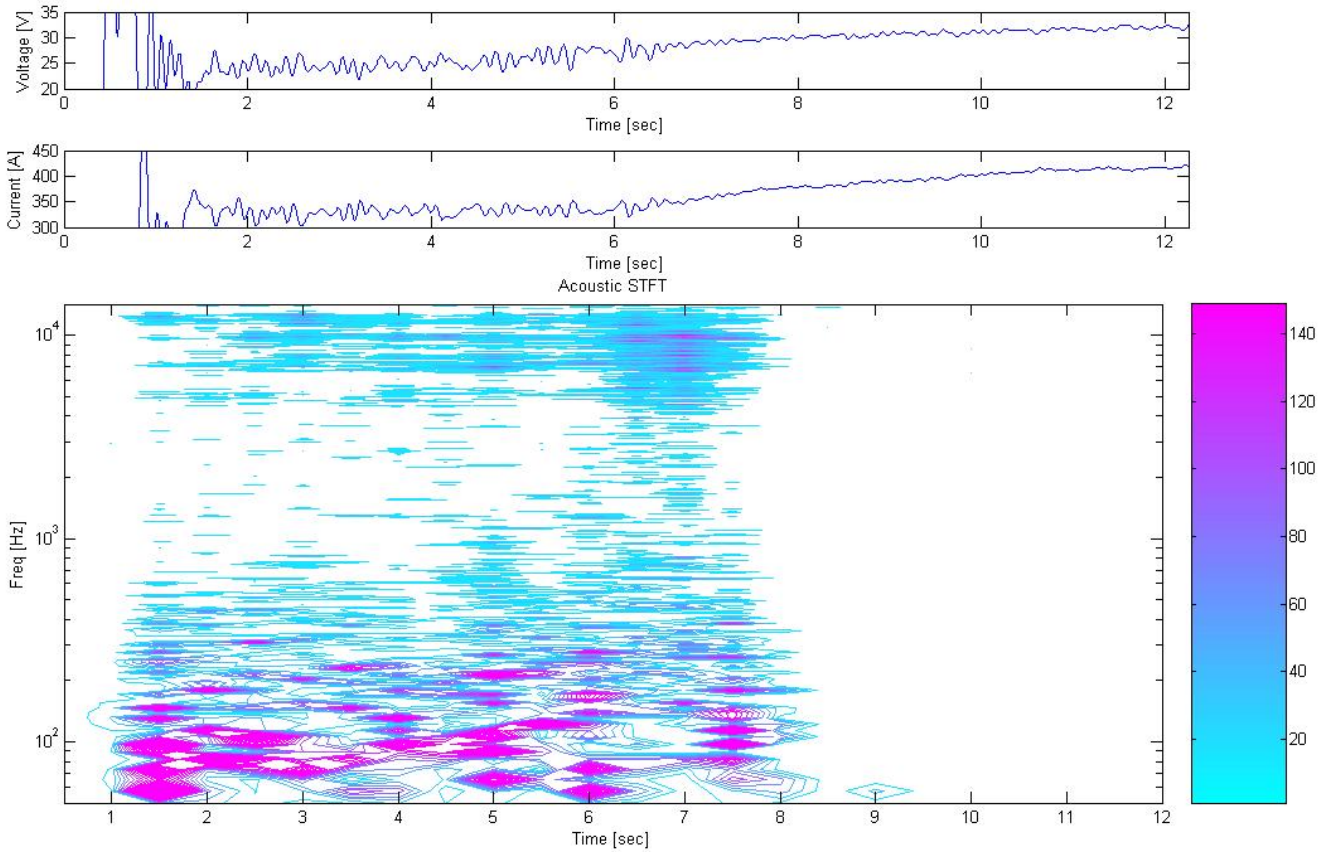

Figure 2-11: Experiment 4 STFT results. Increase in voltage from 24V to 34V at 3.33in/sec WFS results in disappearance of all significant spectral attributes indicating a very soft arc. Between 27V to 30V, spectral components in 4.5kHz and 9.8kHz range become prominent as well as a shift of lower frequency components from 200Hz to 400Hz.

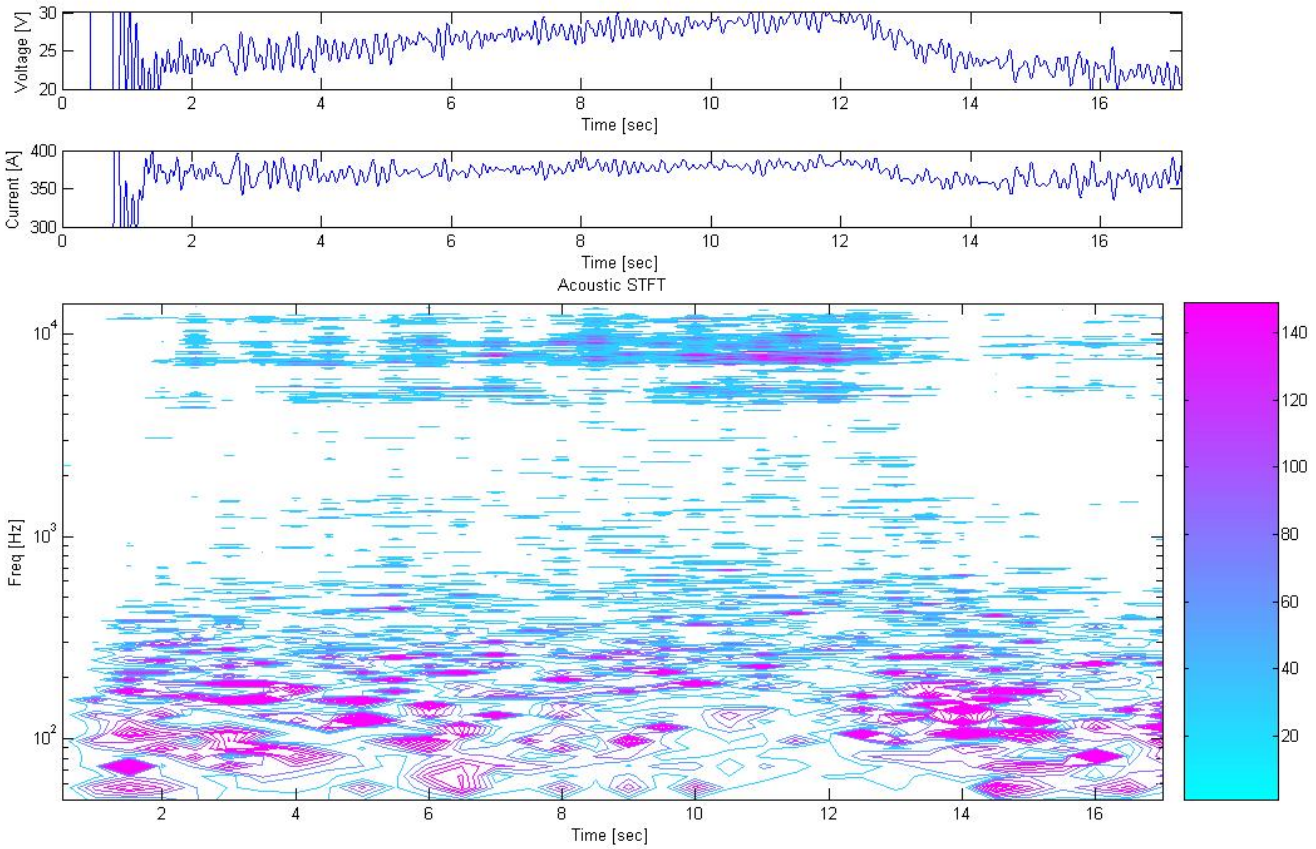

Figure 2-12: Experiment 5 STFT results. Increase in voltage from 24V to 29V at 3.33in/sec WFS results in appearance of spectral components in 6.0kHz -10.0kHz band around 27V to 29V, as shown before. Also, consistency of lower frequency components in 200Hz-400Hz bands at voltages below 27V is present.

2.8 Level Average and S/N Results

Tandem assessment of the level average and S/N results can be used to identify significant input parameters for each spectral band. Figure 2-13 shows an example of how input parameters and interactions which have significant level average effect as well as high S/N ratio are considered.

For level-average analysis, maximum and minimum response ranges are used to determine the factor selection threshold. In Figure 2-13, the shaded columns indicate those factors and interactions which have response ranges exceeding the selection threshold. In other words, the change in mean frequency levels due to these factors and interactions are most prominent.

A similar selection process is performed for the S/N results using the maximum S/N ratio for each factor or interaction. Furthermore, the response range in the S/N analysis gives an indication of how the salience and consistency of the given frequency band changes due to changes in each factor or interaction. For example, as voltage increases from low to high, the S/N ratio decreases. This indicates that spectral components centered about 338Hz will be more consistent at low voltage settings while those components centered about 3645Hz will be less consistent at high voltage settings.

	Frequency Band 1 - Level Average Responses													
		Input Factors and Interactions												
	Input Parameter Level	**Voltage**	**CTWD**	**A x B**	**A x B**	**WFS**	**A x C**	**A x C**	**B x C**	**Torch Speed**	**Wire Dia.**	**B x C**	**Gas**	**Torch Angle**
Dominant Frequencies (Hz)	**Low**	338	1025	2542	1628	2139	1667	1718	1747	851	2608	1704	2980	509
	Med	807	1805	1562	1535	837	1877	2179	1625	1930	1248	2708	1446	1070
	High	3645	2275	1002	1942	2128	1561	1208	1733	2324	1248	693	679	3525
	Response Range:	**3307**	**1250**	**1540**	**408**	**1302**	**317**	**971**	**121**	**1473**	**1360**	**2014**	**2301**	**3016**
Level Average Selection Threshold:		**1205**												
	Freqency Band 1 - S/N Responses													
		Input Factors and Interactions												
	Input Parameter level	**Voltage**	**CTWD**	**A x B**	**A x B**	**WFS**	**A x C**	**A x C**	**B x C**	**Torch Speed**	**Wire Dia.**	**B x C**	**Gas**	**Torch Angle**
S/N Ratios (dB)	**Low**	-48.58	-59.36	-65.17	-56.81	-67.94	-60.67	-62.40	-60.22	-57.89	-64.00	-62.80	-64.59	-53.79
	Med	-56.79	-57.57	-53.85	-61.20	-52.97	-61.30	-58.00	-59.75	-60.10	-57.27	-59.66	-60.15	-62.10
	High	-71.54	-61.62	-59.53	-60.53	-57.63	-56.58	-58.14	-58.58	-60.56	-57.27	-56.09	-53.81	-62.65
	Response Range:	**22.97**	**4.05**	**11.32**	**4.40**	**14.97**	**4.72**	**4.40**	**1.64**	**2.67**	**6.73**	**6.71**	**10.78**	**8.86**
	Max S/N:	**-48.58**	**-57.57**	**-53.85**	**-56.81**	**-52.97**	**-56.58**	**-58.00**	**-58.58**	**-57.89**	**-57.27**	**-56.09**	**-53.81**	**-53.79**
S/N Ratio Selection Threshold:		**-53.85**												

Figure 2-13: Level average response and S/N response analysis spread-sheet. Grey columns indicate input parameters having the greatest response effect for the specific frequency band.

Figure 2-14 through Figure 2-18 provides a graphical summary of how the S/N ratios and respective mean frequency clusters change with significant parameter levels.

From level-average and S/N analysis, voltage changes appear to have the most significant impact (Figure 2-14). Specifically, at low voltage levels, distinguishing spectral components were more salient particularly for lower frequency components below 500 Hz. As voltage increases, signal salience generally decreases with a shift towards higher frequency components above 2 kHz. This trend is in agreement with the physical phenomenon of increased droplet transfer rate. However, it is puzzling to see lower frequency clusters identified as being above 2 kHz. This does not seem to conform to the idea that droplet transfers occur at rates no higher than 1 kHz. Upon closer examination, it seems that the acoustic signal behavior obeys this rule at lower voltages. However, once transition into spray transfer is made, higher frequency components are observed. Thus,

according to these results, it can be hypothesized that in globular transfer mode (lower voltages) the acoustic signal is actually dominated by and is related to the frequency of droplet transfer. When we make the transition into spray-transfer this hypothesis no longer holds and higher frequencies are observed. However, this observation is not corroborated by the STFT analysis performed earlier (Figure 2-8) where the opposite is true. This leads us to believe that level-average analysis may not be providing as much insight into acoustic characteristics as we like.

The second parameter that seemed to have the best salience and direct impact on acoustic parameter changes was the contact-tip-to-workpiece-distance (CTWD) (Figure 2-15). From the analysis, it appears that an increasing CTWD will increase lower cluster frequencies from approximately 1.9 kHz to 3.5 kHz. Again, this seems to make sense since effective arc voltage increases with increasing CTWD, and as such, we expect an increase in transfer frequency. Also, at shorter CTWDs, the process is possibly in a transition phase between globular and spray-transfer, thus lowering droplet frequency. Another observation from Figure 2-15 is that, in general, the dominant frequency bands converge around the 3.6 kHz range at larger CTWDs.

Proceeding to the analysis on effects of wire-feed-speed (WFS), Figure 2-16 shows some uncertain trends. At medium WFS rates, there is a general shift in the lower cluster bands toward 900 Hz. In a more general sense, our analysis suggests a distinct shift in transfer modes as WFS goes from low to high.

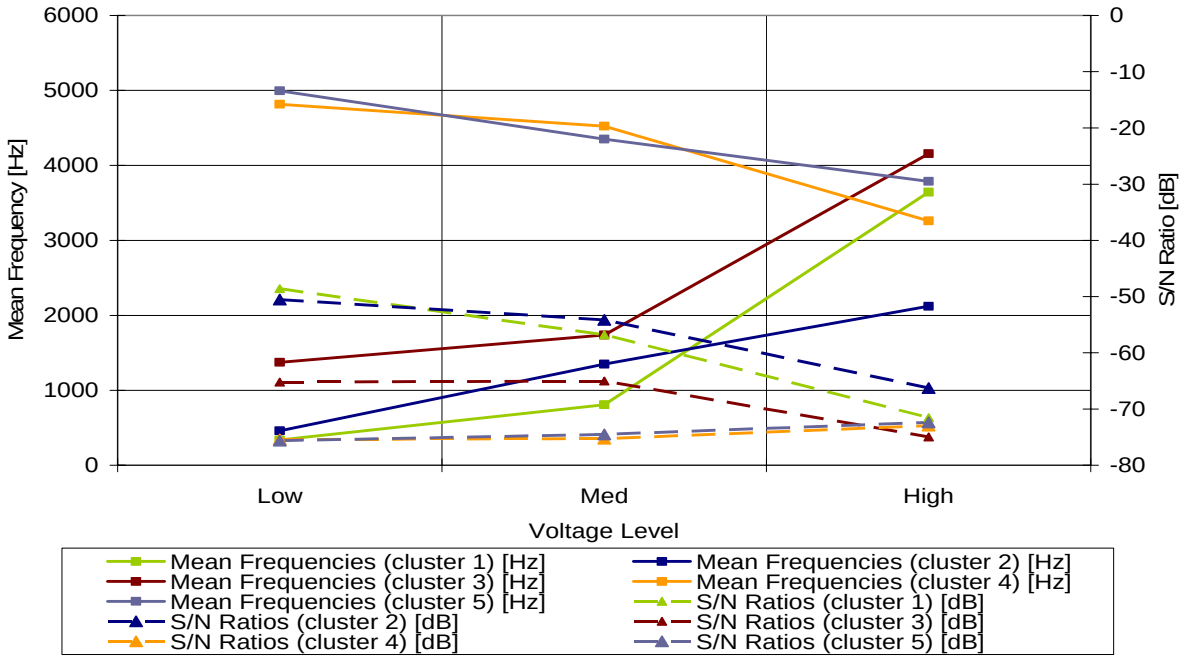

Figure 2-14: Dominant level average and S/N response due to voltage level change

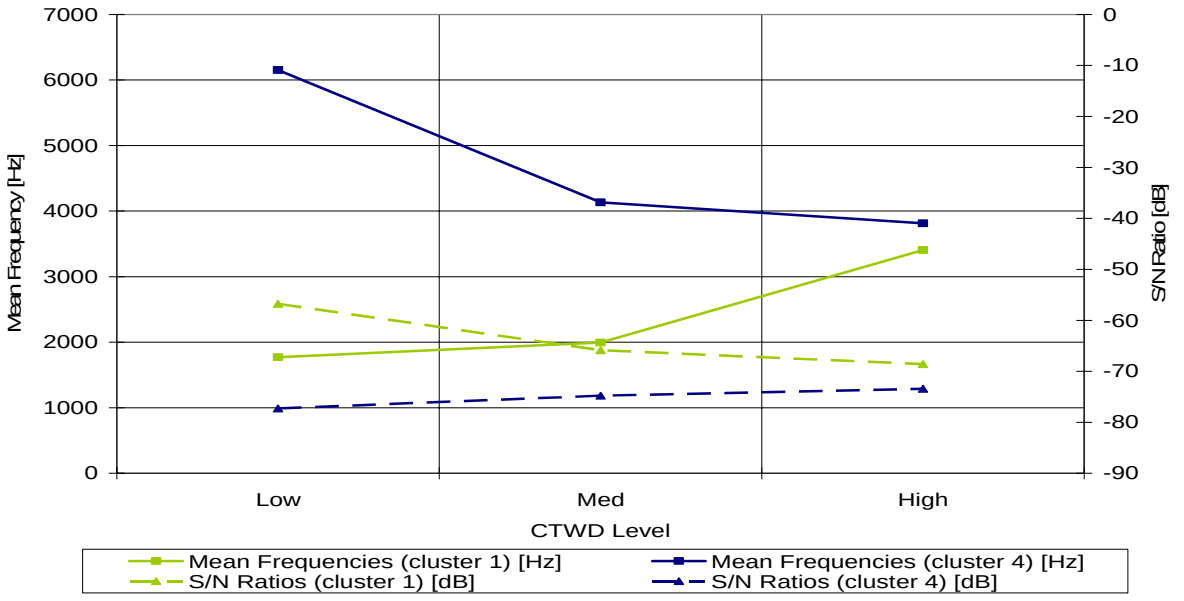

Figure 2-15: Dominant level average and S/N responses due to CTWD changes.

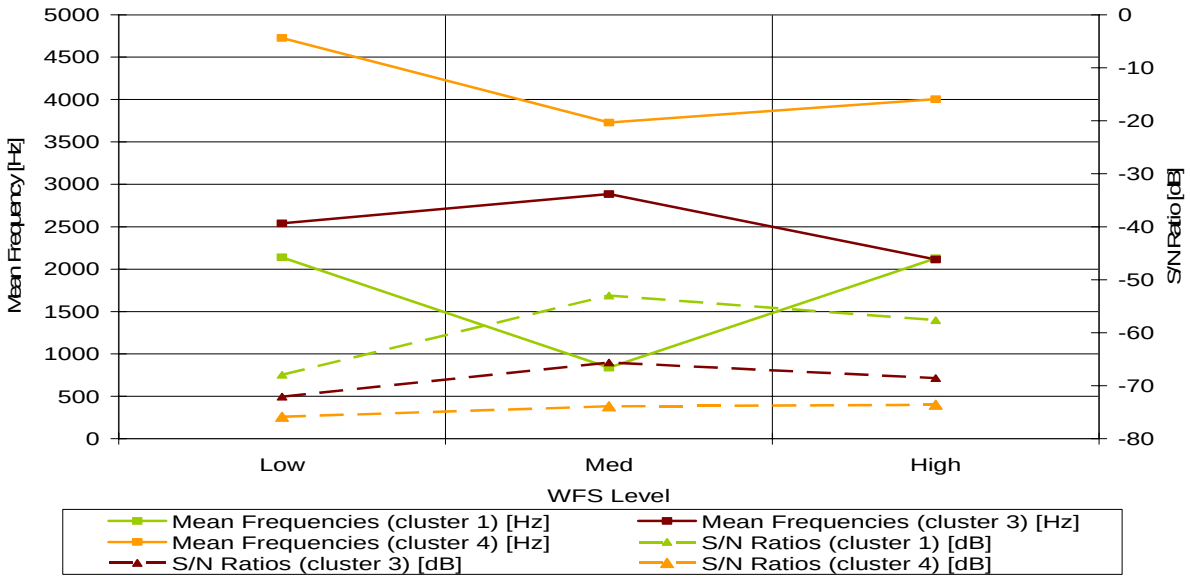

Figure 2-16: Dominant level average and S/N responses due to WFS changes.

By moving the torch angle from positive (pushing) to negative (dragging), Figure 2-17 reveals an increase in lower cluster frequency content from 500 Hz and a lowering of upper frequency cluster content from 5.4 kHz to a converging cluster of approximately 3.6 kHz. Salience in these components generally decreases with a negative torch angle.

Finally, the effects of gas flow rate are shown in Figure 2-18. As gas flow increases, the general trend is shown to be a decrease in lower frequency components. However, upper harmonic frequencies increase noticeably. Salience for all clusters is relatively constant with respect to changes in gas flow-rate.

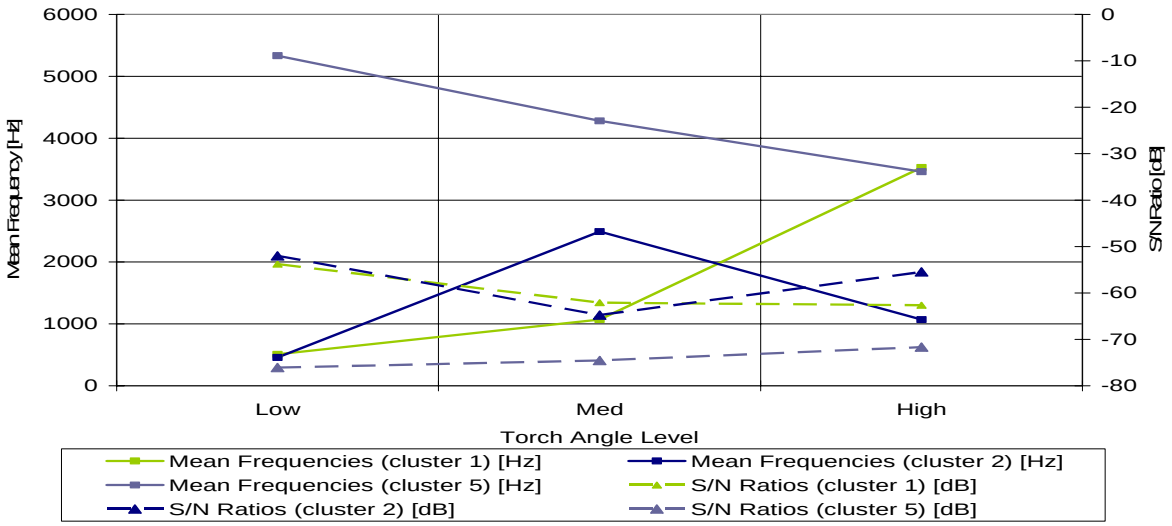

Figure 2-17: Dominant level average and S/N response due to torch-angle changes

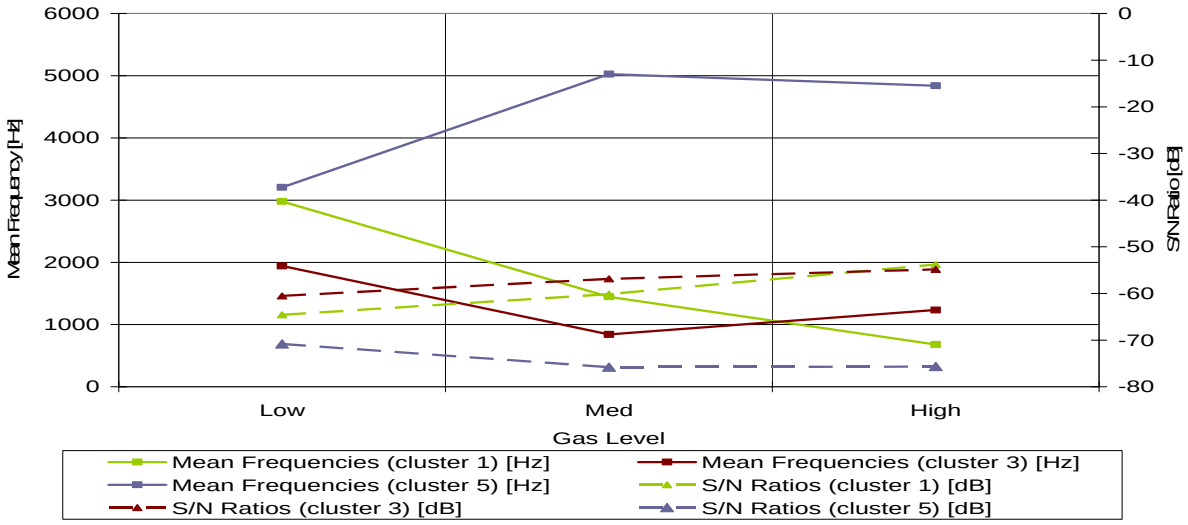

Figure 2-18: Dominant level average and S/N responses due to gas-flow-rate changes.

2.9 Frequency of Occurrence Results

Each significant spectral band identified by level-average and S/N ratio analysis was subjected to this analysis. The most commonly occuring frequency for each case was then identified and the collective results plotted against their respective parameter levels (Figure 2-19 through Figure 2-21). Only those cases which exhibited significant changes in dominant frequencies are presented. The frequency-of-occurance analysis has greatly reduced the number of significant parameters and associated levels when compared to the level average analysis, illustrating how it reduces the confounding effects of non-clustered data points.

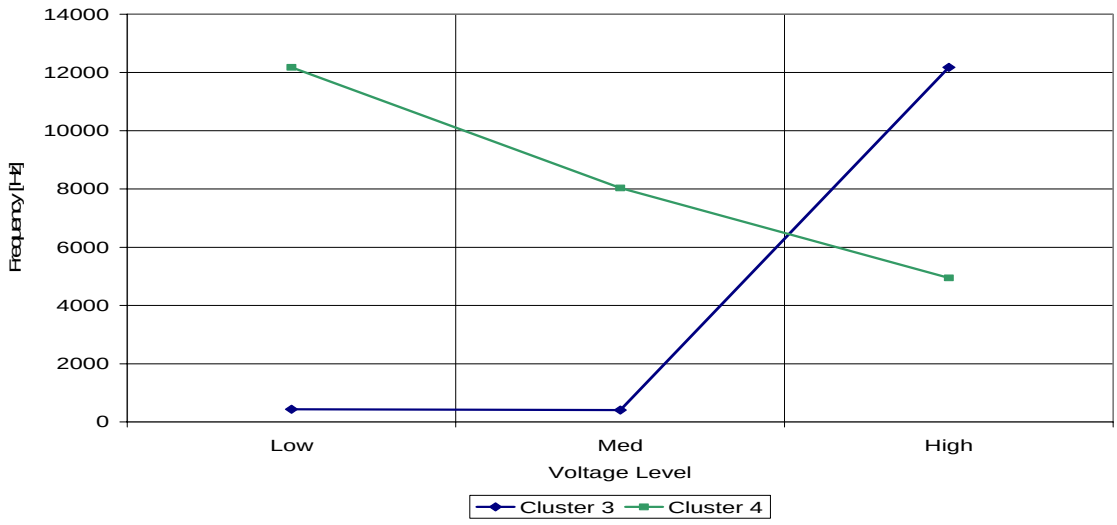

Figure 2-19: Dominant spectral bands identifiying changes in key sound characteristics with changing voltage as identified using frequency of occurrence analysis.

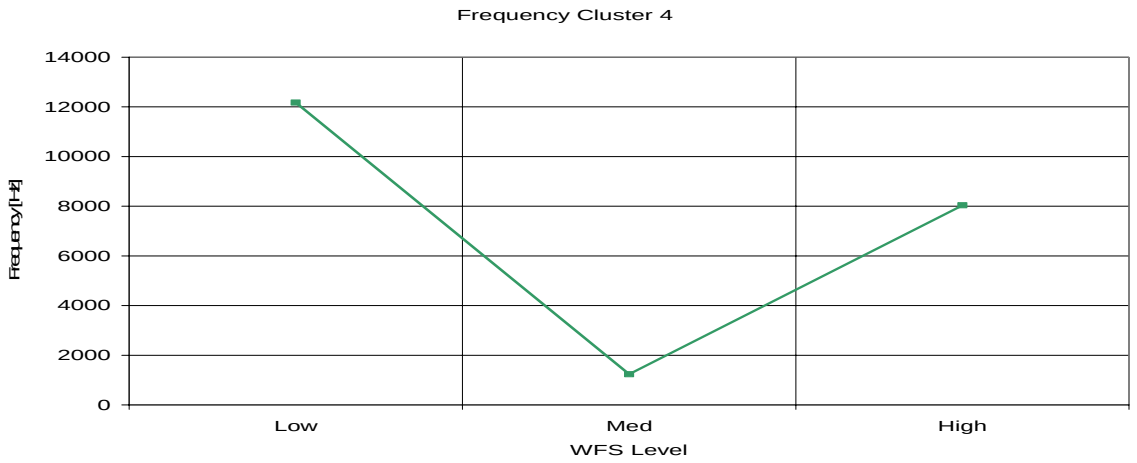

Figure 2-20: Dominant spectral bands identifying changes in key sound characteristics with changing WFS as identified using frequency of occurrence analysis.

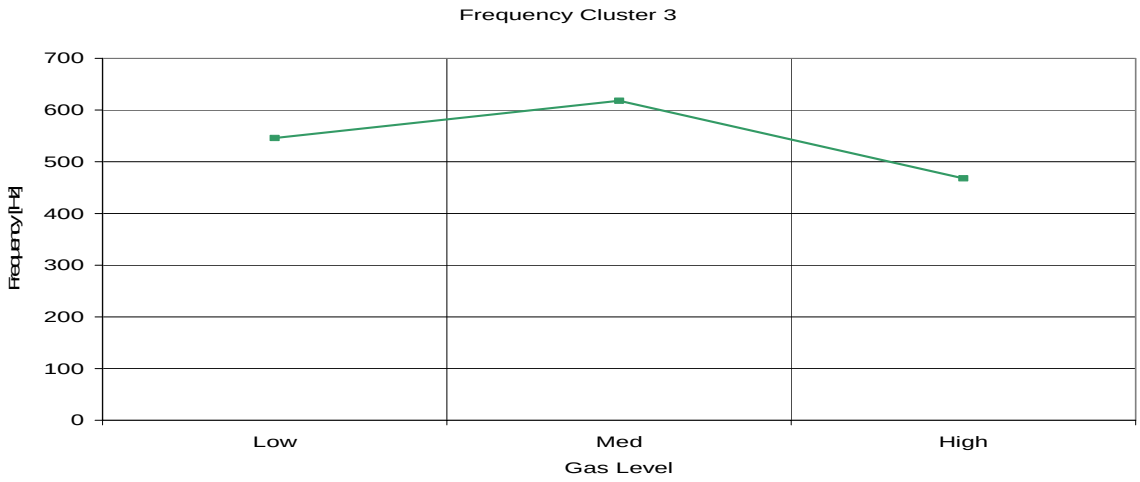

Figure 2-21: Dominant spectral bands identifying changes in key sound characteristics with changing gas flow rate as identified using frequency of occurrence analysis.

2.10 Recursive Boundary Identification Algorithm

Briefly described before, the algorithm developed for identifying optimal spectral cluster boundary placement is effectively a brute-force approach in which every possible boundary combination is evaluated. This section provides elaboration as to how the algorithm works and implementation challenges.

Each octave transformed spectrum contains 98 possible boundary positions. Every boundary combination is considered and its respective global scatter computed. Each combination was explored using a recursive algorithm. The algorithm initially sets two permanent boundary positions at the beginning and end of each spectrum. It then proceeds to evaluate boundary combinations starting with all boundaries clustered in the left, after which it moves the right most boundary one space to the right. It then calls itself to perform the same routine for the remaining boundary positions within the current configuration and continues to propagate. This occurs exponentially until the termination condition was met for the most recent function call, at which point, back-propagation through the recursion history occurs. The termination condition was defined, in this case, as when the sub-set of boundary combinations has been exhausted, or when the right most boundary combination has been considered. This procedure was demonstrated in Figure 2-22 with a simple six-bin four-boundaries example. Given four possible boundary positions for two non-static boundaries, the total number of possible combinations is six, computed by ${}^{4}C^{2}$.

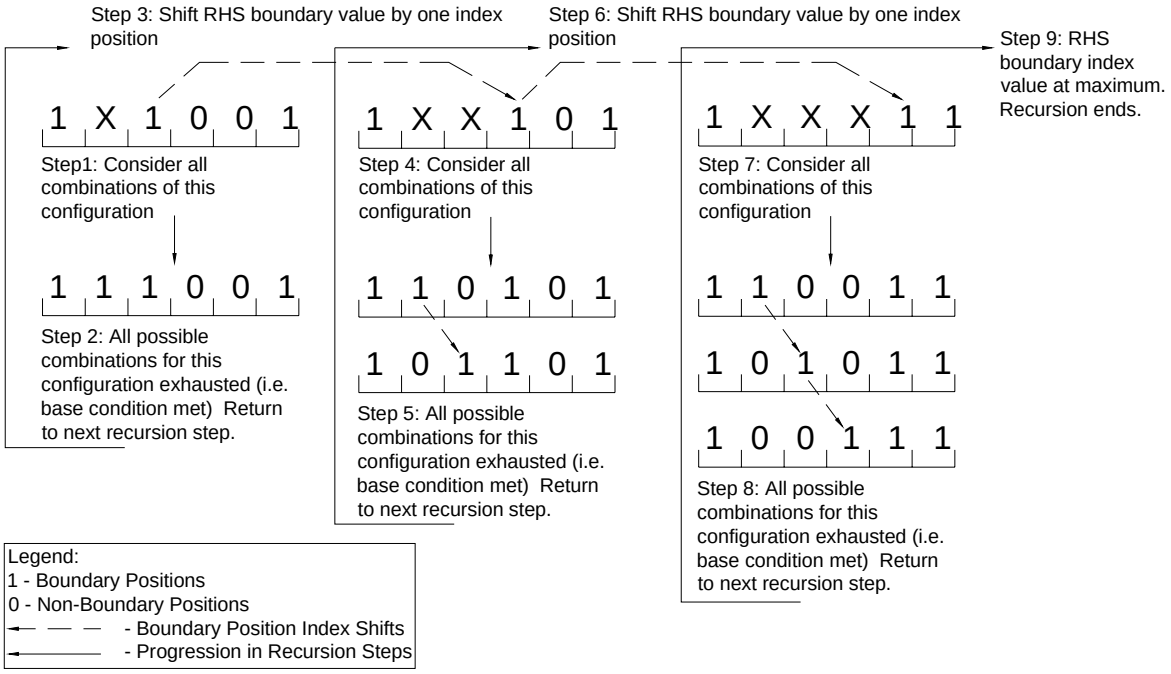

Figure 2-22: Illustration of how all boundary positions are considered using recursion algorithm. The boundary positions at the head and tail are inherently static since they represent the beginning and end of the data set.

After each boundary combination is considered, the individual scatters of each spectral cluster are computed and averaged to form a global cost function. This value is effectively a measure of how well each boundary combination represents spectral grouping. The lower the value, the better the clustering achieved for a given boundary set. When all combinations have been considered, the boundary combination with the lowest cost function is selected. Detailed code-listing of this algorithm can be found on the accompanying CD (refer to Appendix A for files listing).

Ideally, a complete spectral analysis would incorporate another layer in the algorithm which would continue to increase the number of clusters considered (while applying the recursive algorithm for

each) until an optimal cost function value has been found. The result would be both an ideal cluster grouping and ideal boundary placement for a given spectrum.

Unfortunately, our analysis was restricted to using only five clusters (six boundary positions) for each spectrum. The reason for imposing this restriction was immediately apparent when the number of boundary combinations was computed for 98 positions and five clusters ${}^{98}C^{(4)}$; approximately 3.6 million global cost computations. Executing the code in Matlab on a Pentium IV running at 2.4GHz and 512 Kbytes of RAM required approximately 20 minutes per spectrum. Increasing to six clusters would require ${}^{98}C^{5}$ or 67.9 million global cost computations. The resulting 19 fold increase in computation time is impractical. Even if it were feasible to decrease computation time, it would not guarantee reaching an ideal cluster grouping without evaluating even more possible cluster groupings.

Chapter 3
Arc-Acoustic Characterization through Psycho-Acoustic Experiments

3.1 Introduction

Much of the content in this chapter is directly taken from [26], a paper written by the author and submitted to *Science and Technology of Welding and Joining*, an international peer reviewed journal on applied technology in the field of welding and joining science.

Acoustic feedback plays an important role for expert welders when performing gas metal arc welding (GMAW). In fact, most professional welders agree that arc-sound provides as much useful information concerning the process as vision does [2,19]. When performing gas-metal arc welding (GMAW), the welder's attention is usually completely consumed by the task. Professional welders are typically able to detect minute variations, through vision and sound, in process parameters and adjust for them.

However, the salient characteristics of acoustic signals used by welders have never been experimentally identified, nor has the welder's reliance on these signals been experimentally confirmed or quantified. Better understanding of this untapped source of feedback can take us one step closer to fully automating GMAW using expert human judgment.

In this work, we explore the temporal and spectral acoustic reliance of professional welders through psycho-acoustic experiments. Specifically, these tests involve real-time alterations of acoustic signals

while changing welding parameters to observe any changes in welder performance. Presented are the experimental apparatus and signal processing techniques used in executing the experiments. Of particular focus will be the process of developing and testing the apparatus to achieve acceptable experimental results.

To support the motivation for this study, our experimental apparatus is first used to confirm the welders' reliance on acoustics. Our experiments then focus on attenuating, or removing, specific spectral components of that sound to determine their significance on welder performance. Furthermore, we also experiment with applying time delays to determine whether or not tracking instabilities can be induced in the human welder.

Discussions concerning experiment development will include: human factors considered when designing experiments, why specific spectral bands were selected, results of experiments, and implications in intelligent applications.

3.2 Experimental Apparatus

The general experimental apparatus is schematically illustrated in Figure 3-1. The microphone is attached to the welder's helmet and powered by a custom built microphone amplification circuit (Appendix B) that includes an anti-aliasing filter with a 12.5 kHz corner frequency and 60dB/decade roll-off.

This signal is then processed by an Analog Devices ADSP-21065L digital signal processor (DSP) for playback to the welder. The DSP board samples at 48 kHz and provides 1 Kbytes of RAM. The headphone (KOSS UR15C) worn by the welder has a dynamic range of 25 Hz to 15 kHz and is powered by a custom built, portable audio amplification circuit (Appendix C).

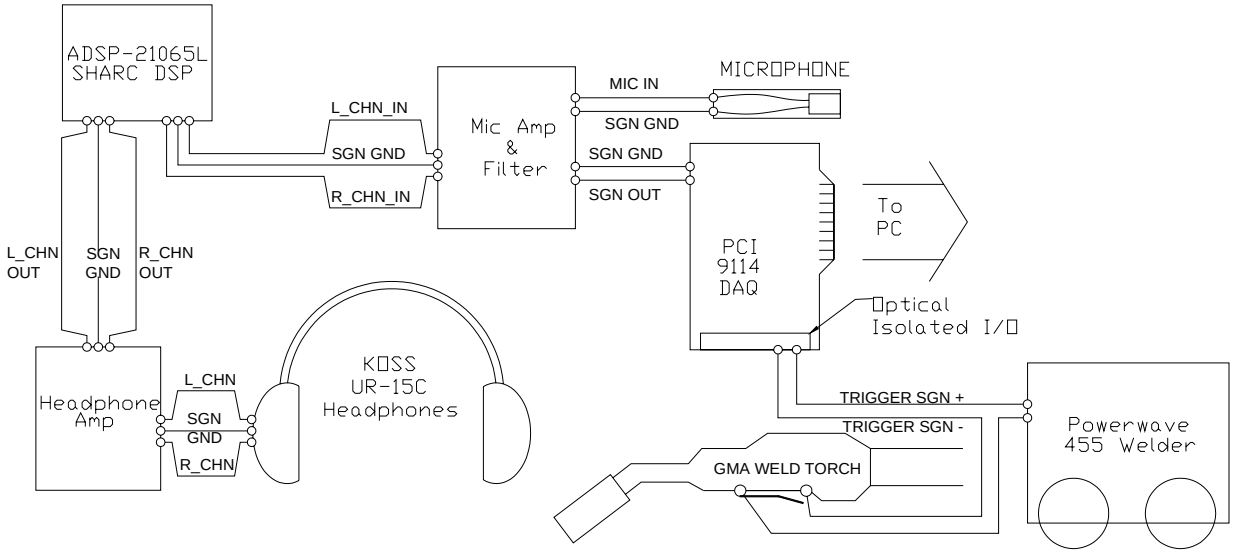

Figure 3-1: Schematic of experimental apparatus used in psycho-acoustic experiments.

The microphone signal was collected, along with welding power-supply voltage and current, using a PCI 9114 data acquisition card with a sampling frequency of 33.3 kHz per channel. These data allowed post review of the welders' performance based on correlation between power and acoustic variations. In other words, the data collected confirms whether or not control was maintained by the welder under different acoustic conditions.

Furthermore, indication of welder control is confirmed by video recording of torch movement during experiments. A Pulnix A70 CCD camera is located at one end of the welding fixture and mounted

behind a #10 optical welding filter to reduce over-saturation (Figure 3-2). In an attempt to overcome change in scale due to perspective, two steel wires are fastened one inch apart beside the welding fixture. This allows reflected arc light to provide scale to the image when reviewing the video.

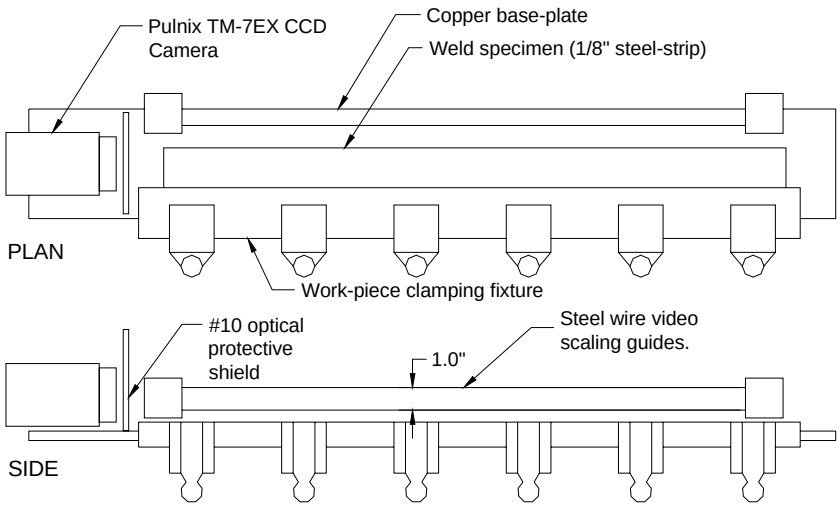

Figure 3-2: Camera mounting configuration for observing welder torch movement during experiments.

The welding power supply, a Lincoln Powerwave 455, was configured for constant voltage operation. All welds performed were bead-on-plate using 0.125" mild-steel specimens, 0.035" wire, and pure argon shielding gas.

3.3 Signal Processing Techniques

The experiments in this work test for welder response due to changes in acoustic feedback. More specifically, real-time modifications of this feedback, including time-delay and spectral band attenuation, is made possible by signal processing algorithms implemented on the DSP. This section describes the development of these algorithms and associated implications.

Several considerations were made with respect to sound quality being delivered to the welder. Initially, the primary concern was attenuation of external and actual arc-sounds during the experiments. Initial tests proved that the combination of head-phone padding and adequate sound amplification provided ample attenuation and outside noise rejection. Secondly, algorithms and implications in signal processing and filter design were considered with respect to limitations of the DSP.

After several test trials, complaints concerning the sound reproduction were brought to our attention by the welder. This prompted an investigation into the frequency response of the entire apparatus and the subsequent design of an arbitrary frequency response filter to improve sound fidelity. In implementing this filter, limitations imposed by the DSP and methods of circumvention are presented.

3.3.1 Time Delay Algorithm

A time delay can be implemented with the ADSP-21065L board and its built in CODEC. The algorithm takes advantage of the processor's circular buffer capability and onboard RAM. The circular buffer is effectively a reserved length of memory that is written to and read from in consecutive locations. When the pointer reaches the end of the memory segment, the next pointer is automatically directed to the beginning of the memory block and over-writes the oldest existing data. The necessary time delay, t_D, is based on the sampling frequency, F_S, and defined by assigning the length of the circular buffer, L_D, which is computed by $L_D = t_D \cdot F_s$. In our experiments, time delays of 10msec, 100msec, 200msec, and 400msec were applied. The DSP code listing can be found in the accompanying CD (file listings can be found in Appendix A).

3.3.2 Windowed-Sinc Band Reject Filters

By rejecting specific frequency bands from the feedback signal, we attempt to ascertain those bands that were critical to the welder's decision making process. To do so, three aspects of filter performance were considered; 1) adequate attenuation, 2) steep attenuation roll-off, and 3) time-domain response fidelity.

The necessary level of attenuation is dictated by the human threshold of hearing, 0 dB or 2 x 10-5 Pa of sound pressure level (SPL). Since the headphones are rated for a maximum output of 92 dB SPL, the attenuation of the filter should be ideally 92 dB SPL, assuming that full power is actually applied to the headphones. Attenuation roll-off needs to be as steep as possible so that components outside the stop band are not unnecessarily attenuated. Finally, the fidelity of the filter's temporal response should be affected as little as possible so that the feedback is not distorted in an unpredictable manner.

Unfortunately, it is impossible to satisfy all of the above criteria given known filtering techniques. Since we were more interested in identifying spectral components of the signal used by welders, finite impulse response (FIR) windowed-sinc filters were chosen due to their performance in the frequency domain. However, their uses come at the expense of excessive ripple and overshoot in the time domain response.

An ideal, discrete, low-pass sinc filter with a cut-off frequency of f_c and signal sampling frequency, F_S, is defined by the FIR kernel, $h[i]$, and computed as:

$$h[i] = \frac{\sin(2\pi(f_C \cdot F_S)i)}{i\pi} \tag{11}$$

This infinitely long filter is made practical by symmetrically truncating the kernel, shifting it so that all values are positive, and applying a Blackman smoothing window to it. The shifting is done to accommodate the DSP's positive indexing system (i.e. i >= 0). Windowing is necessary to reduce "ringing" in the frequency domain caused by the abrupt end to the kernel due to truncation. The resulting equation for a low-pass Blackman windowed-sinc kernel of length $M+1$is [27]:

$$h[i] = \frac{\sin(2\pi(f_C \cdot F_S)(i - M/2))}{i - M/2}\left[0.42 - 0.5\cos\left(\frac{2\pi i}{M}\right) + 0.08\cos\left(\frac{4\pi i}{M}\right)\right] \tag{12}$$

By using the Blackman window, a stop-band attenuation of 74dB can be achieved. Although this does not satisfy the desired attenuation of 92dB, it reduces sound level to 18dB; quieter than a recording studio [28]. The roll-off bandwidth is defined from 0dB to 100dB attenuation and can be reduced by increasing windowed-sinc filter length, *M*. However, experimentation revealed that optimal DSP operation is limited to filters of about 200 points or less. With this consideration and additional processing overhead in mind, a filter length of 128 points was chosen, resulting in an impressive roll-off of approximately 120dB/decade.

Band-reject filters are constructed by the sum of normalized kernel values of a low-pass and high-pass windowed-sinc filter. The high-pass filter portions were formed by spectral inversion of a low-pass filter, as illustrated in Figure 3-3. After summation, the filter kernel is normalized by:

$$h_N[i] = \frac{h[i]}{\sum_{i=0}^{M} h[i]} \tag{13}$$

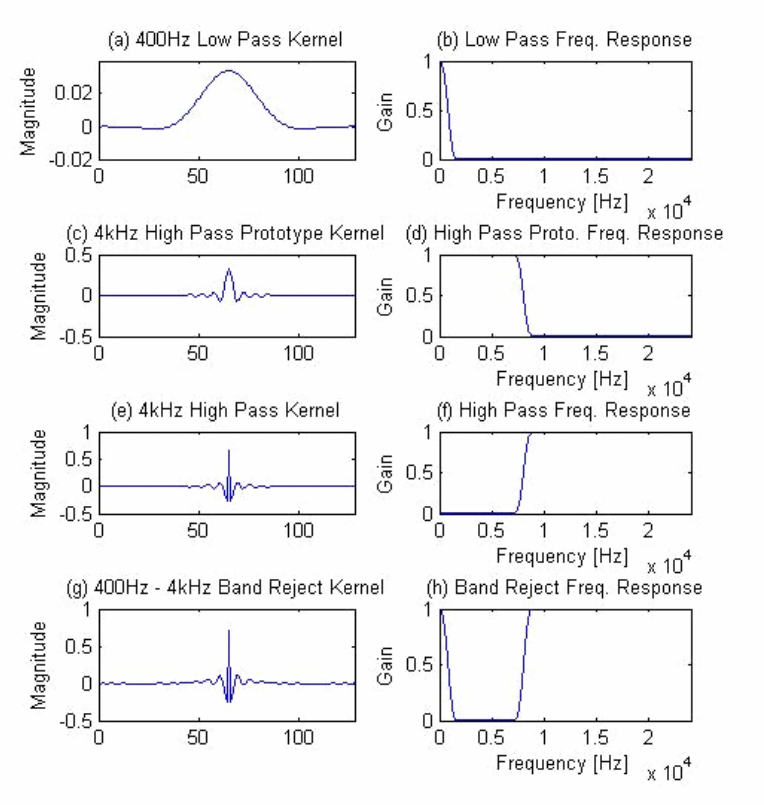

Figure 3-3: (a) 128pt. 400 Hz low-pass kernel, (b) FFT of 400 Hz low-pass kernel, (c) 128pt. 4 kHz low-pass kernel as prototype for high-pass kernel, (d) FFT of 4 kHz low-pass kernel, (e) Spectrally inverted 4 kHz low-pass kernel to form 4 kHz high-pass kernel, (f) Corresponding FFT of spectrally inverted high-pass kernel, (g) 128pt. band-reject kernel formed by summation of (a) and (e), (h) FFT of band-reject kernel.

3.4 Initial Apparatus Assessment

Initial tests of the acoustic apparatus were conducted with a professional welder. The DSP was configured for direct throughput, allowing the welder to hear the arc acoustics with no modification. He was allowed to perform welds with and without headphones, and was afterwards asked about the quality of sound reproduction.

The welder complained of a "windy" sound that was preventing his proper judgment of the process. Without the headphone, he was immediately able to identify that he was welding too slowly for the given WFS and promptly adjusted his welding speed to suit.

The significance of this initial test was that it confirms the necessity of acoustic feedback and that there is information encoded in the sound that cannot be ascertained from visual feedback alone. In fact, post review of the welds showed consistent undercutting on those made when headphones were used. This indicates that, without proper acoustic feedback, the welder was not aware that the torch speed was too slow and allowed unnecessary filler deposition into the bead.

However, in order to conduct the psycho-acoustic experiments described above, it was apparent that improvements needed to be made to the apparatus to ensure proper sound reproduction.

3.4.1 Measuring Circuit Frequency Response

Prompted by the welder's description of a "windy" noise, it was hypothesized that the cause was due to an uneven frequency response of the acoustic circuit. Firstly, we needed to assess the circuit's frequency response with the microphone as input, and headphones as output. The circuit is shown in block-diagram form (Figure 3-4a). We realized that it would not be practical to assess this circuit

response using the microphone as input since this would require a flat response tone generator. However, since the system is linear, it is possible to rearrange the sequence of components without affecting the resulting system transfer function. Thus, we used the headphones as input while probing the headphone amplification circuit output signal (Figure 3-4b). To minimize extraneous noise from affecting readings, the microphone is embedded in foam padding with the headphones mounted around the assembly (Figure 3-4c). It is then placed into a foam insolated box to attenuate external sound and vibration.

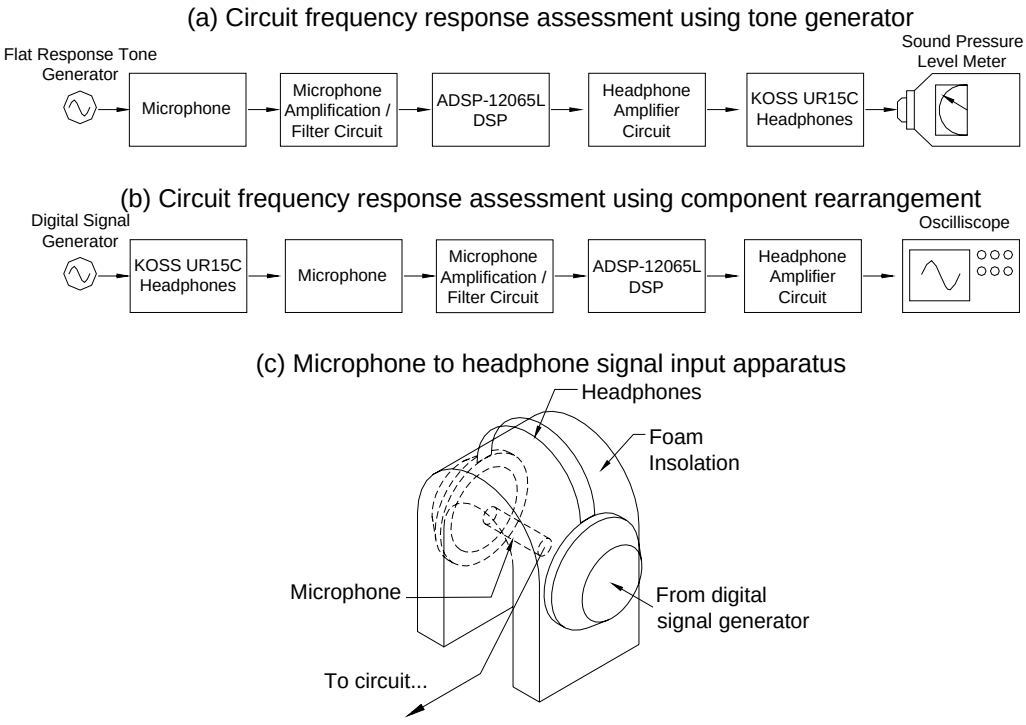

Figure 3-4: Assessment of circuit frequency response if a tone generator and sound pressure level meter are used, (b) Assessment of circuit frequency response by rearranging components and using signal generator and oscilloscope, (c) Microphone and headphone apparatus used for frequency response assessment.

3.4.2 Sound Fidelity Enhancement

Sinusoidal signals of constant amplitude with frequencies ranging from 10 Hz to 15 kHz were applied to the headphones using a digital signal generator. The resulting circuit output gain is plotted (Figure 3-5) indicating attenuation at low frequencies and some high-frequency ripple. By flattening the frequency response, we can achieve better fidelity in signal reproduction. This was achieved in several steps including; 1) determine a system model using Bode plot analysis, 2) invert system in the discrete domain using z-transform, 3) implement an inverted system as compensating FIR filter in DSP.

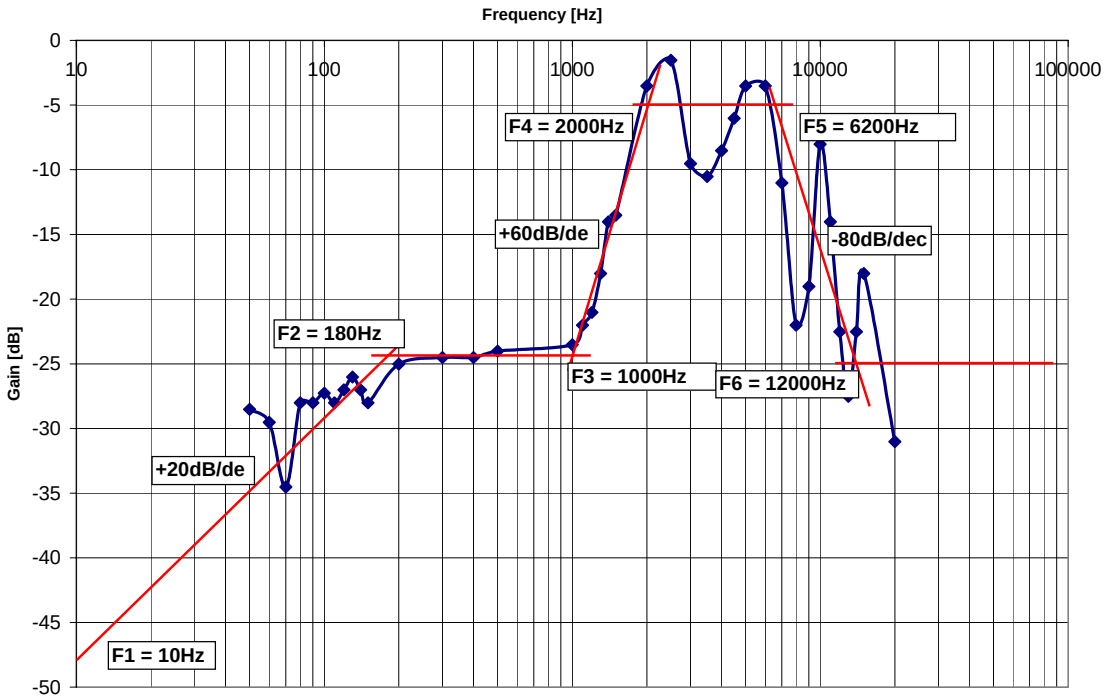

Figure 3-5: Acoustic circuit frequency response. Bode plot analysis using asymptotic approximations and corner frequencies used for identifying the circuit transfer function.

In Bode analysis, significant corner frequencies and their associated logarithmic slopes are used to approximate the equivalent system transfer function. Figure 3-5 illustrates the asymptotic approximations, slope values, and corner frequencies used to derive the audio circuit transfer function:

$$G(s) = \frac{10.261 \cdot (s + 62.83)(s + 6283)^3 (s + 7.54 \times 10^4)^4}{(s + 1131)(s + 1.257 \times 10^4)^3 (s + 3.89 \times 10^4)^4} \tag{14}$$

The system is then converted to the z-domain using the bilinear transformation and then inverted by swapping poles and zeros, resulting in the following discrete transfer function:

$$G(z) = \frac{22.080 \cdot (z - 0.999)(z - 0.877)^3 (z - 0.120)^4}{(z - 0.977)(z - 0.769)^3 (z - 0.423)^4} \tag{15}$$

The frequency response of the above transfer function is generated in Matlab using the "bode" command, and subjected to an inverse fast Fourier transform (IFFT), the results of which are coefficients representative of the system time-domain impulse response (Figure 3-3a). When performing the IFFT, the system phase response was purposely set to zero for a zero-lag response from the filter. To generate the proper compensating FIR filter coefficients, the IFFT values were rearranged to the familiar shifted impulse response form (Figure 3-6b), truncated, Blackman windowed, and normalized. The reasons for truncation and windowing are the same as those for the sinc-filters.

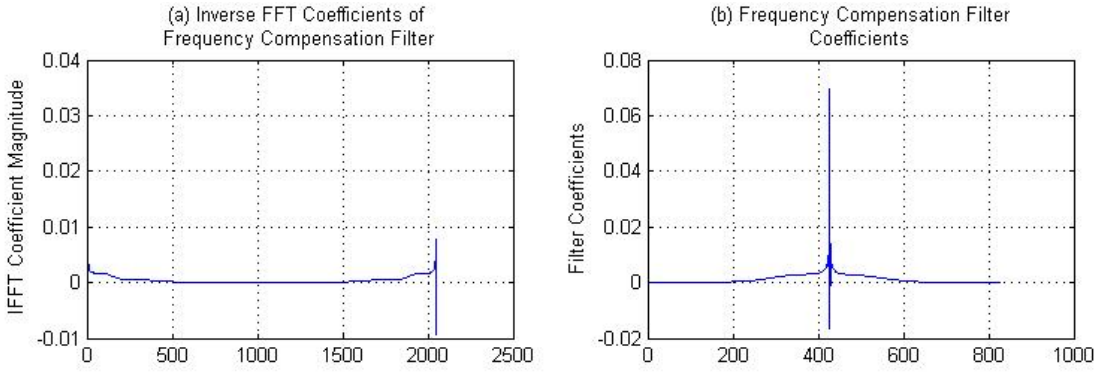

Figure 3-6: (a) Coefficients resulting from IFFT performed on frequency response of filter, (b) Rearrangement of IFFT coefficients, truncation, and Blackman windowing to produce required frequency compensation filter kernel.

However, it was discovered that because the filter's frequency response is effectively arbitrary in nature (when compared to low-pass kernels) its performance is highly sensitive to the amount of truncation and length of the IFFT. In conjunction with hardware limitation on kernel lengths, it was necessary to experiment with all these factors to achieve a reasonable frequency response without compromising the DSP's ability to properly process the signal without aliasing. Prior to application, the response of the filter kernel is confirmed in Matlab using the "FFT" function. Figure 3-7 and Figure 3-8 show how dramatically the filter's response is affected by the amount of truncation and IFFT length. After several iterations, it was decided to implement the filter using an IFFT length of 1024 points and a truncation that results in a 256 point filter kernel.

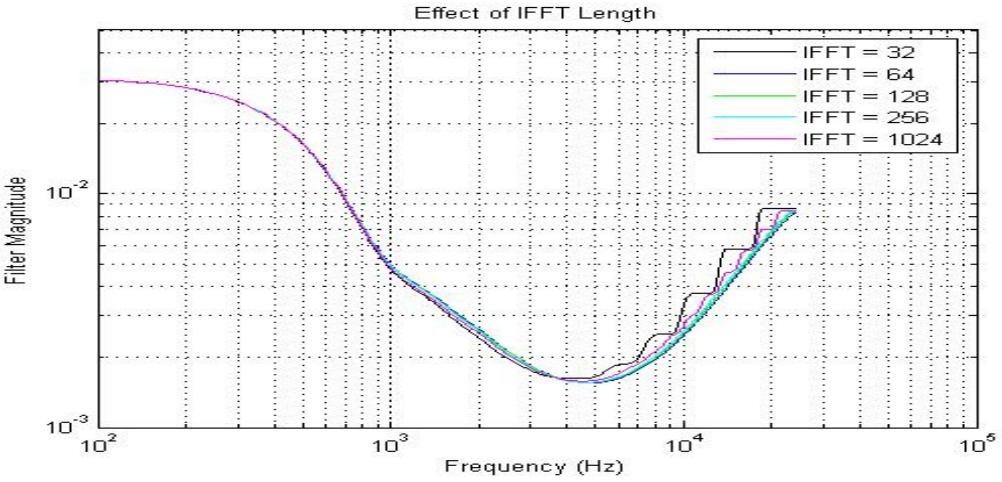

Figure 3-7: Resulting filter frequency response with changing length of IFFT analysis. Note the degradation at higher frequencies due to short IFFT length.

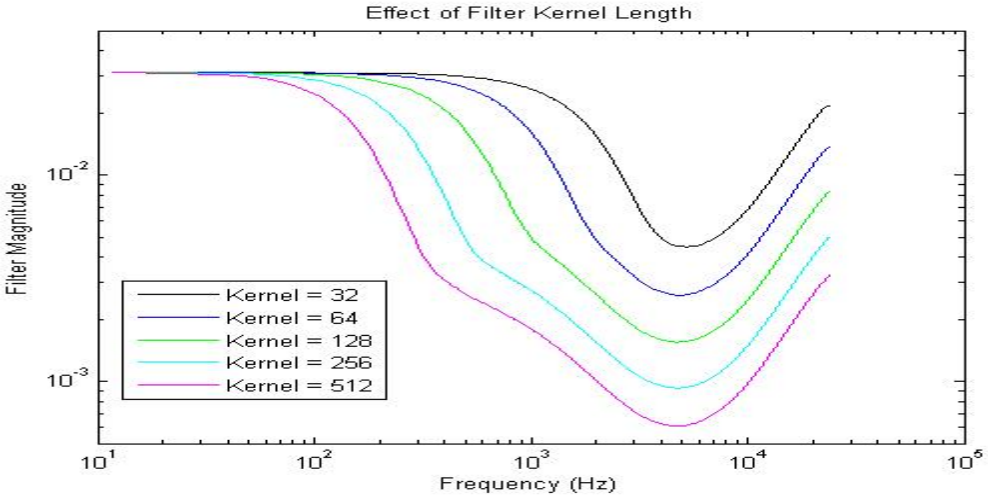

Figure 3-8: Resulting filter frequency response with changing kernel length.

The filter was then tested using the same method as that for assessing the circuit's original frequency response. Figure 3-9 shows the marked improvement in flattening the circuit's response. Finally, a professional welder was invited to try several trial welds using the improved system. The welder was

then asked about the quality of the reproduced sound, and more importantly, their ability to detect process changes. They responded that the filter implementation dramatically improved sound fidelity.

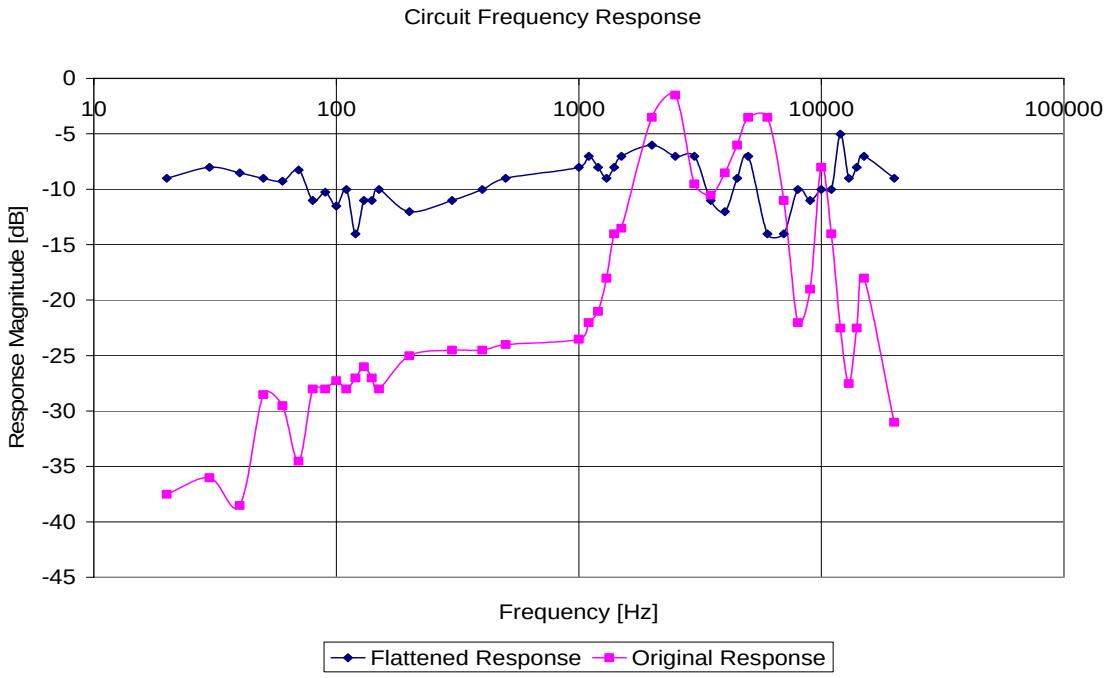

Figure 3-9: Comparison of circuit frequency response before and after implementation of fidelity improvement filter.

3.5 The Human Welder Model

To better understand how they work and fit into the GMAW process, we first modelled a human welder as a black-box controller as part of a closed-loop control system. Secondly, an information processing model was used to illustrate processes contributing to a welder's situation awareness. From these models, we were able to exploit attributes of the closed-loop system to help determine and give indication of the level of reliance professional welders have on acoustic feedback.

3.5.1 Closed-Loop Control Model

Modelling the manual GMAW process as a closed-loop system (Figure 3-10) allows us to clearly identify parameters which the human welder has immediate control over, as well as how information fed back to the welder may have an effect on performance.

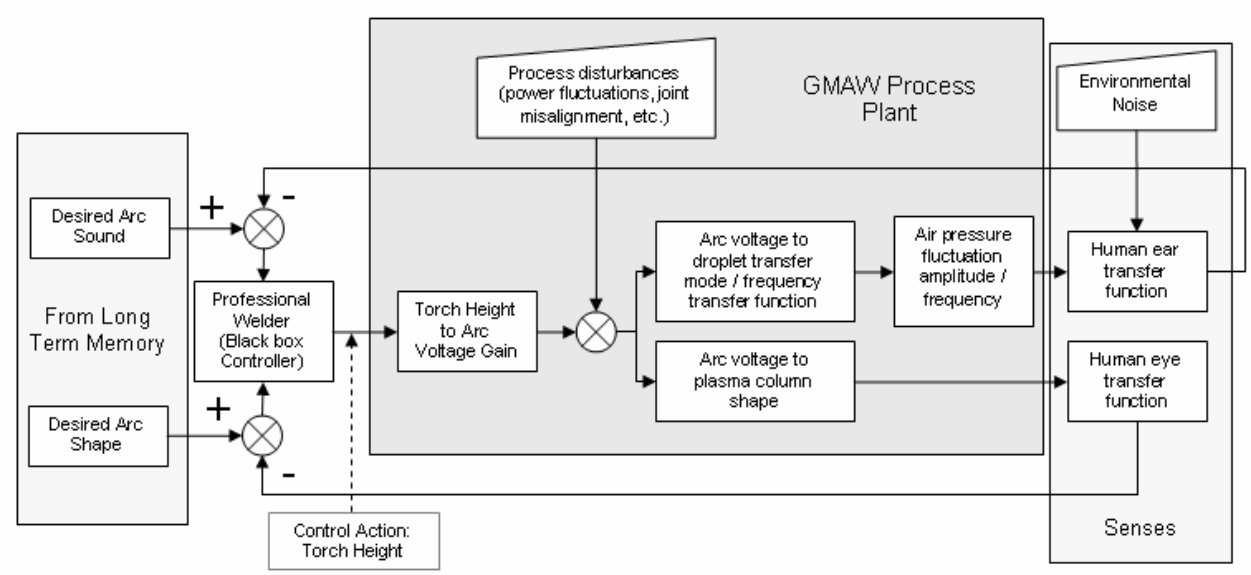

Figure 3-10: Closed-loop model of manual GMAW with embedded human welder controller.

As mentioned before, the primary sources of feedback are sound and vision. More specifically, visual feedback aids the welder in judging arc shape, adjusting torch orientation, and seam tracking. Acoustic feedback, on the other hand, gives an indication of the droplet transfer mode; short, globular, or spray.

Moreover, as a controller, the professional welder has the task of comparing the feedback to some input signal. In our case, the input signal comes in form of the welder's knowledge and memory of

what the process should look and sound like. In our closed-loop model, this is simply depicted as the difference between feedback and input. However, in reality, the situation awareness and decision making process is far more complex and is influenced by several aspects of cognitive ergonomics, as will be discussed later.

A welder's immediate control action in GMAW includes torch height, orientation, and speed. The first two effectively dictate arc length and ultimately arc voltage during welding. Incidentally, for a given wire-feed speed (WFS), metal transfer mode changes from short-circuit to globular to spray with increasing voltage. As such, welders typically "tune" their arc by moving the torch closer or further away from the work-piece to achieve the desired transfer mode. Torch speed, on the other hand, dictates the energy density being delivered to the work-piece, and subsequently, joint penetration.

In GMAW, process disturbances in the form of misaligned joints and power supply fluctuations can make a welder's job very challenging. From the standpoint of a closed-loop controller, the welder is made aware of these disturbances through acoustic and visual feedback. Unlike a computerized closed-loop controller, environmental noise and distractions are not easy to filter or attenuate and play a significant role in the quality of the feedback. It is the welder's job to distinguish salient components of the signal from noise.

3.5.2 Information Processing Model

To better understand how professional welders accomplish their control task, we adopted [29] a situation-awareness and information processing model (Figure 3-11). This model explains how specific cognitive and memory processes are used in filtering feedback and decision making.

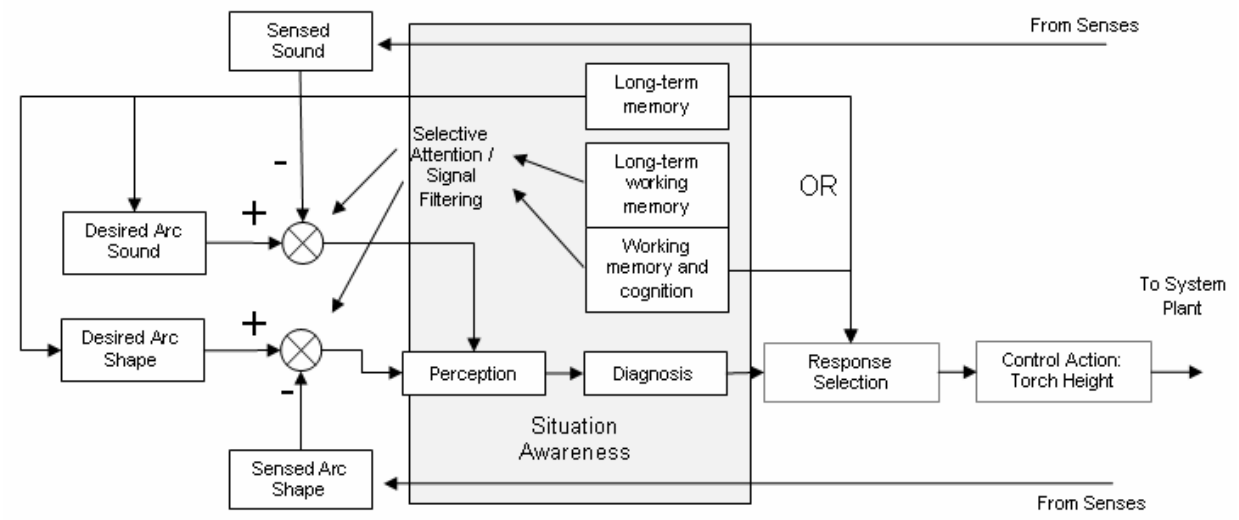

Figure 3-11: Situation awareness model of human welder controller. Working memory as well as long-term working memory is used in signal filtering. Long-term memory is used for decision making as well as dictating desired process output.

Signal filtering in humans occurs purely as a cognitive exercise. Selective attention is directly related to the theory of signal detection and situation awareness. According to this theory, there are two discrete states to feedback: signals and noise. In our case, the signal would be changes to characteristic sound components while noise would include reverberations, wire-feeder servo sounds, and power-supply hum.

Signal detection theory also assigns four possible response states based on the welder's decision and the presence of an actual signal. These states are: hits – signal is present and is properly detected; misses – signal is present and not properly detected; false-alarms – signal is not present but perceptively detected; and correct rejection – signal is not present and not detected. According to the model, a welder judges the presence of a signal based on two memory components: long-term and working memory. These two aspects work in conjunction to provide a gauge of how the present

signal compares to that of a moment ago and also of what it should be from recent experience. This is almost analogous to a self-adapting fuzzy controller where the output gains are continuously adjusted based on optimal desired arc-sound and shape as well as adapting the immediate optimal feedback profile to recent sound and shape. By doing so, even new extraneous noise specific to present circumstances can effectively be filtered. This ability is best illustrated when volunteer welders described their ability to diagnose a problem with an arc just by listening to it when walking by a welding arc. So despite environmental noises and not being right beside the weld, it is still possible for professional welders to detect the characteristic aspects of arc sound.

The control output of the situation awareness model is torch height, which also serves as an indicator of whether or not the welder detected changes as well as an indicator of whether or not the acoustic changes are important to arc control.

3.5.3 Response Instabilities

From the situation awareness model, it takes a finite amount of time for the welder to filter and decide upon a control action. In theory, if a phase lag is present in the feedback that happens to be out of phase with the welder's situation awareness cycle, there should be a direct impact on their ability to track changes when a disturbance is introduced.

Psychological research into the effect of acoustic feedback delay [29] has shown that approximately 400 to 500 milliseconds of delay are sufficient to induce unstable or poor performance by participants. By performing experiments where time delay is introduced in acoustic feedback, we can confirm this hypothesis in welders. Furthermore, it will give an indication as to the level of reliance that welders have on sound.

This is important because if a welder can still perform well with this delay, it means that visual feedback is adequate compensation which would indicate a duality between the two senses in GMA welding.

3.5.4 Acoustic Spectral Dependency

Acoustic signals can be effectively divided into three components, magnitude, frequency, and phase. In the context of human hearing, only the magnitude and frequency are of consequence. Phase differences between frequencies can be considered random due to environmental reverberation, and as such is usually not detectable by humans.

Again drawing upon the situation awareness model, we wanted to determine if the welder is still capable of proper control when specific spectral components are missing from acoustic feedback. More specifically, we wished to determine the specific spectral bands that are critical to proper control.

We hypothesized that frequency bands under 1 kHz would play the largest role in characterizing the transfer mode. To illustrate why this might be so, consider how the dynamics of droplet transfer affect the surrounding air. Before detachment, the plasma arc between electrode and work piece is of a shorter length (Figure 3-12) causing a build up in local heat and thus expansion in the surrounding inert-gas and air. Upon detachment, the arc immediately lengthens (Figure 3-12) causing a sudden change in pressure due to reduced heat. This cyclic pulsation produces what the welder perceives as arc sound. The hypothesized critical frequency bands are suspected because GMAW metal droplet transfer occurs at rates no higher than 1 kHz.

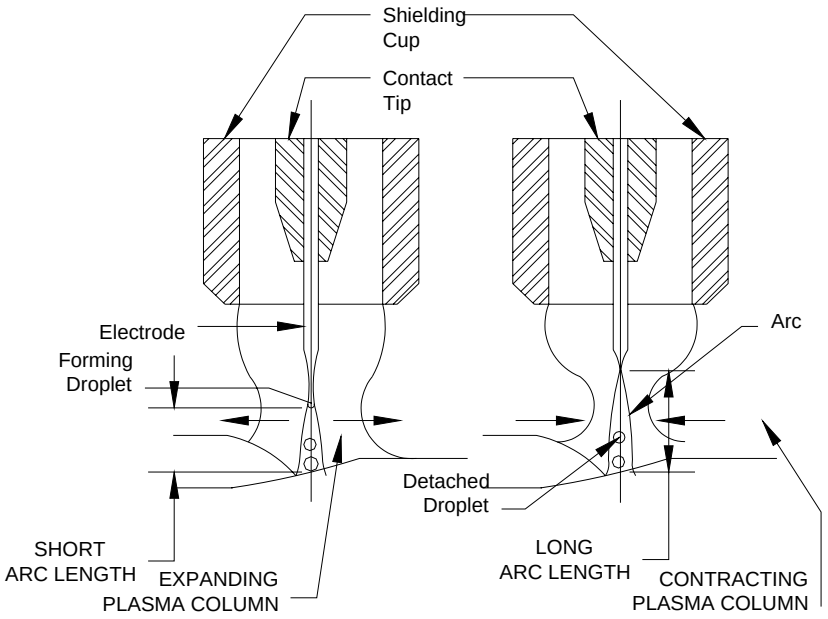

Figure 3-12: Expansion and contraction of plasma column causes pulsations in surrounding air creating arc-sound. The length of, and hence heat produce by, the arc changes the rate of droplet detachment from the electrode. In spray transfer mode, this rate typically remains well below 1 kHz.

However, we realize that in addition to the base frequency bands, humans are able to detect differences in timbre of a tone. In other words, we are capable of detecting the difference between a violin and flute when they emit the same note. As such, our experiments will also examine how associated harmonic frequency bands play a role in welder control.

3.6 Psycho-Acoustic Experiments

There were three primary objectives to the experiments; 1) confirm welder reliance on acoustic feedback for control, 2) confirm hypothesis concerning the onset of instabilities as a result of acoustic feedback delay, and 3) identify acoustic frequencies that serve as cues to human welders when tuning the arc.

To do this, we asked welders to perform three sets of welds. The first gauges the welder's ability to perform the task without acoustic feedback. The second investigates the effects of time-delayed feedback. Finally, the third experiment identifies characteristic spectral components and their harmonics used by welders during operation. All welders were told to maintain spray-transfer to the best of their ability.

In addition to the recorded data, each welder was asked to complete a task-loading index questionnaire. The results collected from the questionnaire are meant to act as a secondary indicator of how much mental and/or physical load was required of each weld.

3.6.1 Welding Without Sound

These experiments involved having the welder weld while listening to loud music through the headphones. The volume of the music was adjusted such that the arc sound was barely audible. The maximum volume of music being played had to be limited since we realized that it is impossible to completely eliminate the arc sound without damaging the welder's hearing. Nonetheless, by comparing weld data made with proper feedback and those without, these experiments yield an indication of the level of dependence on sound as well as the level of integral-separable distinction between the visual and audio cues. After arc-ignition, the welder was allowed to reach steady state before the process disturbance is introduced. Two types of disturbances were tested for in form of a sudden change in voltage and a sudden change in WFS. Table 3-1 summarizes the welding parameters used during experiments.

Table 3-1: Welding parameters used during psycho-acoustic experiments including: no-sound, band-reject, band-harmonic reject, and time-delay instability experiments.

	Voltage [V]	Wire-Feed-Speed [inches/sec]	Feedback on/off	Attenuated Bands [Hz]	Feedback Delay [millisecond]
1	29.5 >> 33.0	10.83	Off	n/a	n/a
2	29.5 >> 26.0	10.83	Off	n/a	n/a
3	29.5	10.83 >> 12.50	Off	n/a	n/a
4	29.5	10.83 >> 8.33	Off	n/a	n/a
5	29.5 >> 33.0	10.83	On	4750	n/a
6	29.5	10.83 >> 12.50	On	550	n/a
7	29.5 >> 33.0	10.83	On	220	n/a
8	29.5 >> 33.0	10.83	On	150	n/a
9	29.5 >> 33.0	10.83	On	4750 + harmonics	n/a
10	29.5	10.83 >> 12.50	On	550 + harmonics	n/a
11	29.5 >> 33.0	10.83	On	220 + harmonics	n/a
12	29.5 >> 33.0	10.83	On	150 + harmonics	n/a
13	29.5 >> 33.0	10.83	On	n/a	10
14	29.5 >> 33.0	10.83	On	n/a	100
15	29.5 >> 33.0	10.83	On	n/a	200
16	29.5 >> 33.0	10.83	On	n/a	400
17	29.5	10.83 >> 12.50	On	n/a	10
18	29.5	10.83 >> 12.50	On	n/a	100
19	29.5	10.83 >> 12.50	On	n/a	200
20	29.5	10.83 >> 12.50	On	n/a	400

3.6.2 Time Delay Induced Instabilities

This set of experiments utilizes the DSP to introduce delay into the feedback signal. Like the previous experiment, the experiment progression introduces a disturbance to the process by a change in voltage and WFS to observe welder reaction. Unlike the previous experiment however, this change is meant to induce instability in welder control. Table 3-2 summarizes the welding parameters used during experiments.

Table 3-2: Single octave band-reject frequency rages used in experiments.

Experiments	Lower Frequency, f_L [Hz]	Center Frequency, f_C [Hz]	Upper Frequency, f_U [Hz]
4750 Hz	3358	4750	6717
550 Hz	389	550	778
220 Hz	155	220	311
150 Hz	106	150	212
4750 Hz + Harmonics	3358	4750	6717
	10076	14250	20153
	16794	23750	33588
550 Hz + Harmonics	389	550	778
	1167	1650	2333
	1944	2750	3889
	2722	3850	5445
220 Hz + Harmonics	155	220	311
	467	660	934
	778	1100	1556
	1089	1540	2178
	1400	1980	2800
150 Hz + Harmonics	106	150	212
	318	450	636
	530	750	1061
	742	1050	1485
	955	1350	1909
	1167	1650	2333

3.6.3 Acoustic Spectral Band Dependency

The spectral bands under investigation are determined a priori from level average, signal-to-noise ratio, and frequency-of-occurrence analysis performed on acoustic data collected during Taguchi experiments. This data determined that specific frequency bands are of particular prominence during

different voltage, WFS, and gas-flow rate levels. By attenuating these spectral bands, we hope to determine which are used by welders when arc-tuning.

Preliminary tests, as presented later, using narrow $1/3^{rd}$ frequency bands of attenuation yielded inconclusive results about welder reliance. As a result, we decided that employing octave-wide rejection bands may yield more conclusive results. The bands of interest, listed in Table 3-2, are one standard octave in width and centered about the frequency of interest. We realize that by enlarging the spectral rejection bands, the certainty of importance associated with these spectral components is reduced. Nonetheless, the approach is the only one capable of realizing our objectives.

In addition to the base frequencies of interest, we also suspect that process information is possibly also encoded in the harmonics of these frequencies. As a result, several "arbitrary-frequency-response" filters (Table 3-2) were created to test the effect of attenuating the harmonic frequencies as well. The experiments are carried out similar to the previous two experiments with disturbances introduced in form of voltage and WFS changes. Table 3-1 summarizes the welding parameters used during experiments.

3.6.4 Task Loading Index (TLX)

The TLX is a standardized method of subjectively measuring an operator's physical and mental workload based on six sub-scales. In general, the index evaluates the degree to which these six sub-scales contribute to the workload of a specific task. By its nature the TLX makes it possible to associate the type of workload demanded of the welder for each acoustic characteristic being tested. Although it has no value to automation of the process, it still serves as insight into how professional welders think or operate when faced with new situations and scenarios.

Data collection occurs in two stages; the first stage (Figure 3-13) asks the welder to rate each sub-scale, on a scale from 1 to 20, which best reflect their experience of the task, the second (Figure 3-14) establishes sub-scale weightings by asking the welder to select between a series of two factors the one which contributes more to the task.

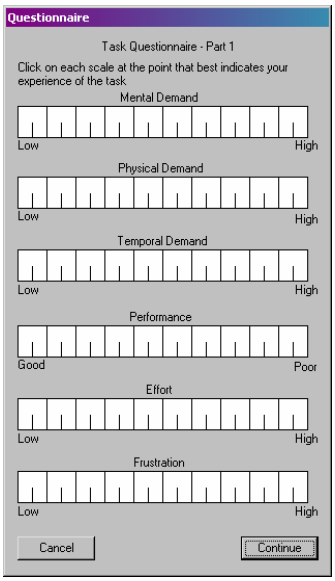

Figure 3-13: TLX Task Experience Questionnaire.

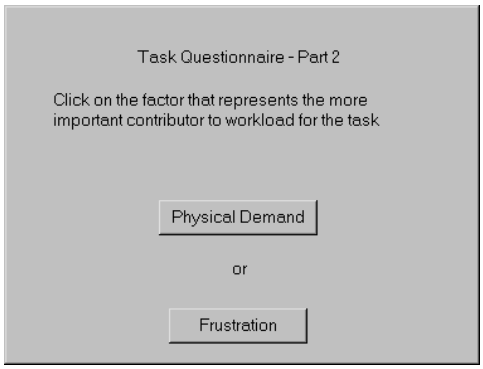

Figure 3-14: TLX Task Weighting Questionnaire.

The sub-scales in the TLX are; Mental Demand, Physical Demand, Temporal Demand, Performance, Effort, and Frustration. Table 3-3 lists a more comprehensive definition of these sub-scales. Moreover, the second section of the TLX facilitates the reduction of the between-rater variations in their interpretation and weighting of the six sub-scales by providing a metric of each welder's subjective assessment of each sub-scale's importance.

Table 3-3: TLX sub-scale level definitions.

Title	Description
Mental Demand	How much mental and perceptual activity was required (e.g., thinking deciding, remembering, etc.)?
Physical Demand	How much physical activity was required (e.g. controlling, activating, precision movement, etc.)?
Temporal Demand	How much time pressure does the participant feel to the rate or pace of task elements?
Effort	How hard did the participant have to work to accomplish necessary level of accomplishment?
Performance	How successful does the participant think they were in accomplishing the goals of the task? How satisfied were they of their performance in accomplishing said goals.
Frustration Level	How insecure, discouraged, irritated, and annoyed did the participant feel during the task?

3.7 Experimental Results

Three welders were tested using the above experiments. From this set of data, we were able to draw some conclusions concerning welder reliance on acoustic feedback. The data collected includes voltage, current, and audio traces of each weld performed. In addition to the indication of torch height variation provided by voltage and current data, the video recordings are also used as corroborating evidence.

3.7.1 Data Conditioning

In order to reveal any trends in the recorded data, it was necessary to subject the data to signal conditioning. All voltage and current signals are subjected to a 20Hz low-pass filtering to reveal alterations in arc voltage and current due to any changes in torch height. Similarly, the recorded

acoustic signal is subjected to a 20 Hz to 12.5 kHz band-pass filter to isolate audible signal components.

3.7.2 Apparatus Readiness Test – Results

As mentioned previously, preliminary tests were conducted to evaluate equipment readiness. The findings from these tests are presented here.

Confirming the findings during initial apparatus tests, Fig. 15 shows that a professional welder is unable to maintain a proper weld without acoustic feedback. The change in WFS is reflected as a DC change in current. The welder, without realizing the change through acoustic feedback, continues to weld without compensating, resulting in a change in voltage characteristics. However, because of the duality between vision and acoustics, the welder eventually attempts to compensate (6 second and 10 second mark) and is indicated by dips in the voltage trace.

Data from welds performed with time delays (Fig. 16) show distinct degradation in the welder's ability to compensate as delay was increased from 10 milliseconds to 400 milliseconds. This confirms that instabilities occur as a consequence of delayed feedback and 400 milliseconds is enough to cause completely unstable control conditions in human welders.

Results from initial band-reject experiments were inconclusive as indications of instabilities or degradation in welder performance were too minor or inconsistent. As mentioned previously, several factors were found contributing to this and were rectified by using wider spectral rejection bands and exploring welder dependency on timbre.

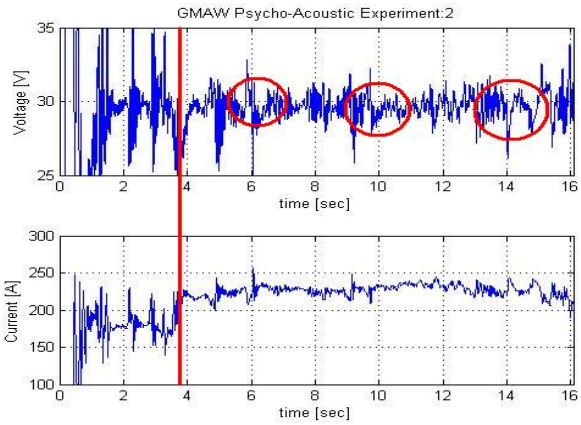

Figure 3-15: Voltage and current data recorded during a "no-sound" experiment. The red line indicates where a disturbance was introduced by changing the WFS. The red circles highlight where the welder attempts to compensate for changes in process parameters based on his visual feedback alone.

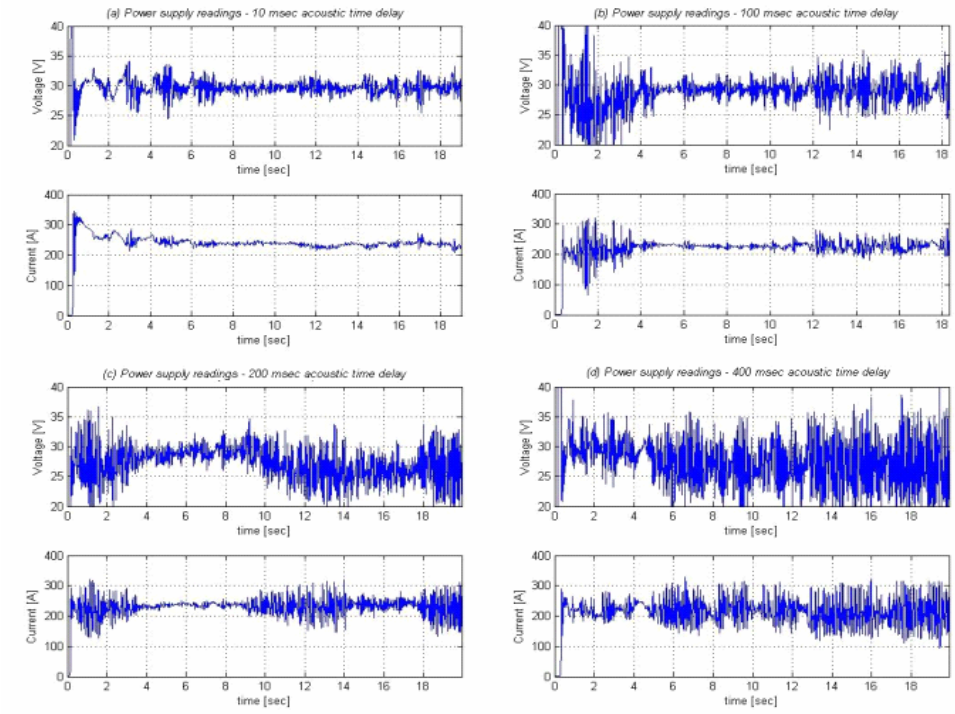

Figure 3-16: voltage and current data recorded during acoustic feedback delay experiments of (a) 10 msec, (b) 100 msec, (c) 200 msec, (d) 400 msec. These results illustrate how welder response significantly degrades as longer delays are introduced.

3.7.3 Welding Without Sound – Results

As indicated during preliminary tests, review of data collected during welds performed without sound shows that, in general, welders are incapable of tuning their arc to maintain spray-transfer when acoustic feedback is absent. Moreover, these results confirm that there is information encoded within the acoustic signal unavailable to the welder from visual feedback alone.

Evidence of incapacity to tune the arc is shown as low frequency fluctuations in voltage and current levels indicating changes in torch height (Figure 3-17). More extreme examples of a welder's inability to detect changes in the weld process due to the absence of sound is amply demonstrated in several instances when the process transitioned from spray to globular transfer mode without correction by the welder (Figure 3-18).

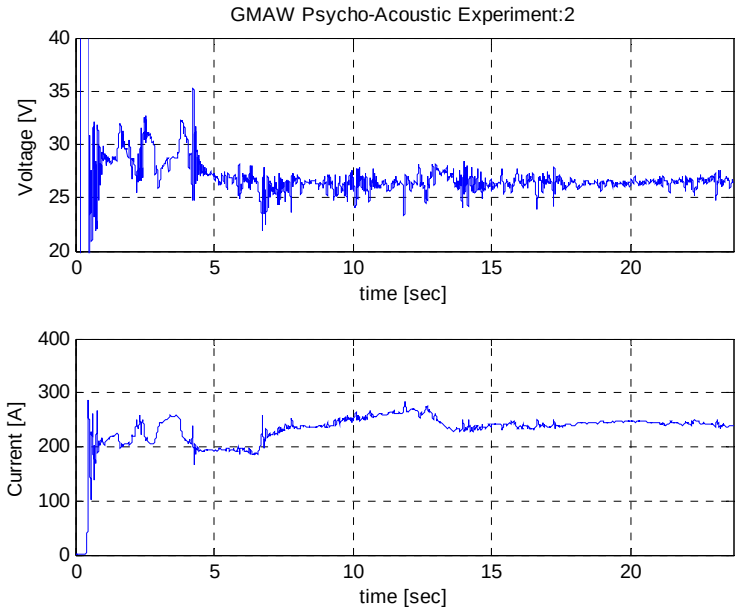

Figure 3-17: Wavering welder performance due to absence of acoustic feedback as shown in fluctuations in current and voltage due to unsteady changes in torch height.

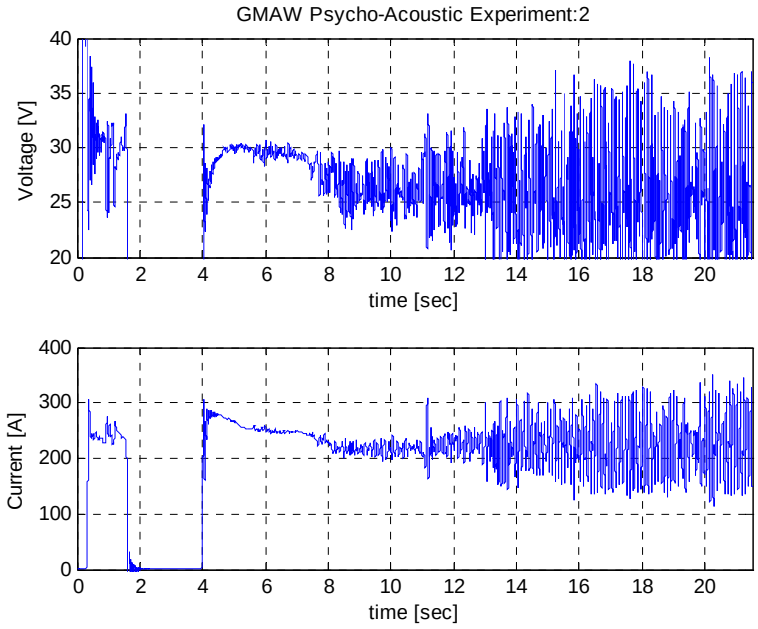

Figure 3-18: Deteriorating welder performance due to absence of acoustic feedback. Voltage and current traces show undesired transition to globular transfer mode.

TLX data from these experiments indicate that welders had a fairly frustrating time when welding without sound. In general, the overall task loading index, when welding without sound, was approximately 15% to 20% higher than that of welding with sound.

3.7.4 Feedback Delay Induced Instabilities – Results

Confirming the results of the preliminary tests, all three welders exhibited deterioration in control as the feedback delay was increased from 10 milliseconds to 400 milliseconds. The results also confirm our original hypothesis; that at feedback delays of 400 milliseconds, most welders are incapable of properly tuning their arc for spray transfer. An interesting distinction that emerged from

this study is that the effect of acoustic feedback delays is more significant for voltage changes compared to changes in WFS.

The corresponding TLX results (Figure 3-19) of welds done with time delays show a general decline in performance and increase in frustration as time delay increases. Furthermore, the TLX data supports the significance in voltage changes (Figure 3-19) versus WFS changes (Figure 3-20). This is generally shown as lower overall task loading for WFS changes as well as smaller changes in performance, mental demand and frustration. From the results of these time-delay studies, we can again confirm the existence of information encoded within the acoustic signal that has no duality component in visual feedback.

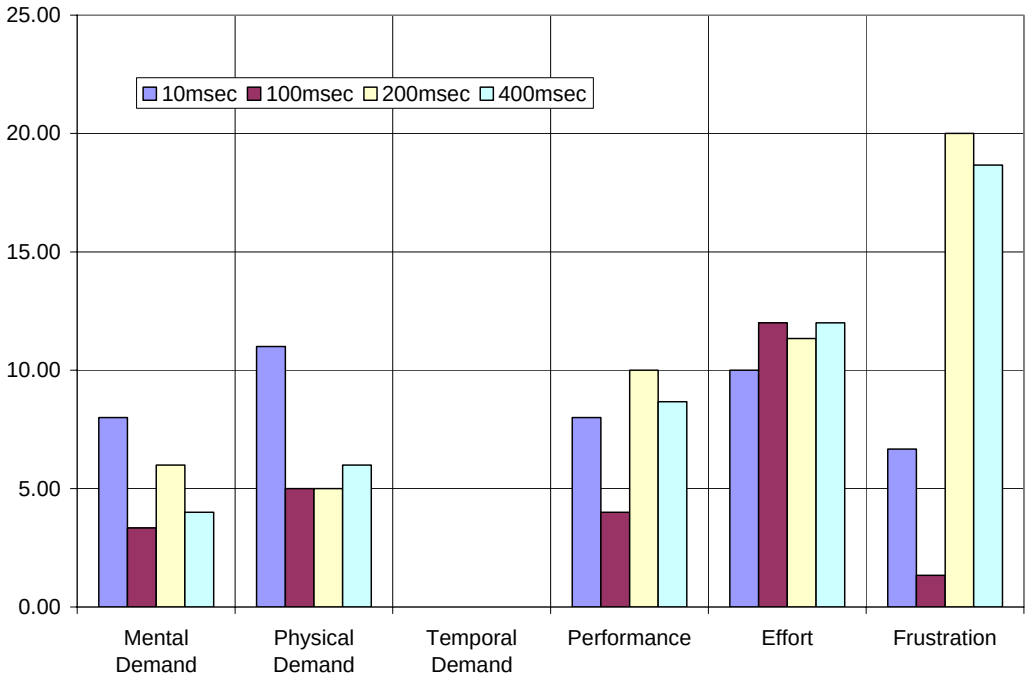

Figure 3-19: Time-delayed feedback TLX results - Welder task loading responses due to voltage change.

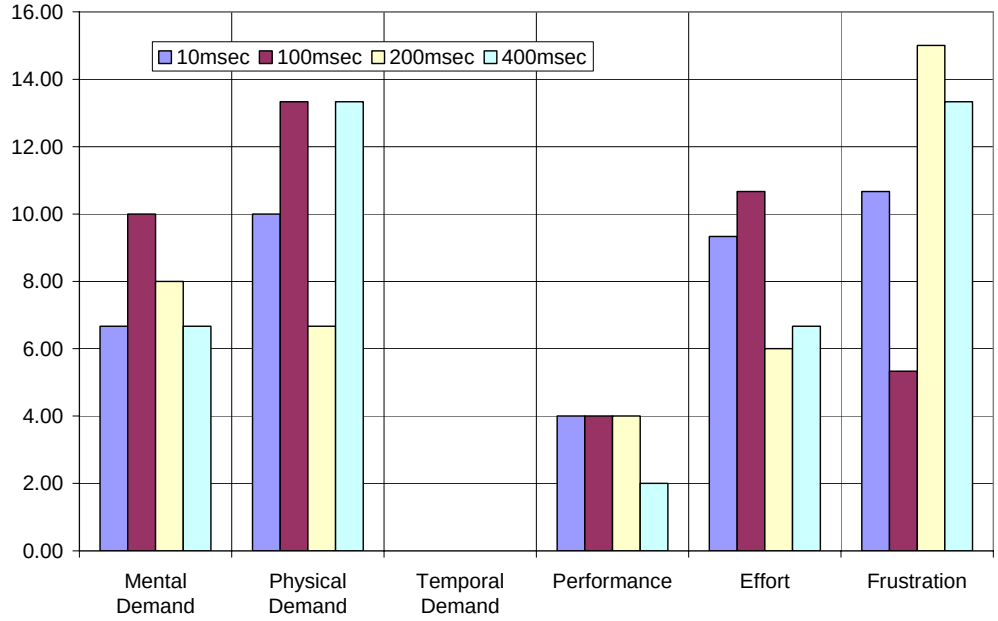

Figure 3-20: Time-delayed feedback TLX results - Welder task loading responses due to WFS change.

3.7.5 Spectral Dependency - Results

Unlike the no-sound and feedback delay experiments, data from the spectral dependency studies yield vague results. Disappointingly, increasing the rejection bands to single octave width made no significant difference to the welder's ability to respond to changes in voltage or WFS. Moreover, considering only three participants have been tested during the writing of this work, it is difficult to establish a statistical conclusion of which frequency bands are of importance.

On the other hand, review of the results from the harmonic band-reject experiments suggests some information may be encoded in the timbre of the above frequency components. Specifically, attenuation of 150 Hz and 220 Hz harmonics has noticeable effects on arc-tuning performance

(Figure 3-21 to Figure 3-26). A surprising result from one welder showed that the absence of harmonics of the 4750 Hz band resulted in an *increase* in ability to maintain spray transfer.

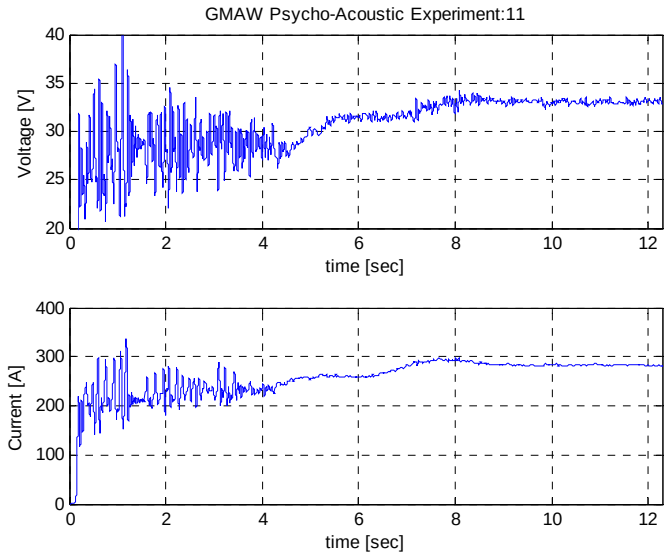

Figure 3-21: Welder 1 - Voltage and current traces of 220Hz + Harmonics attenuation experiment

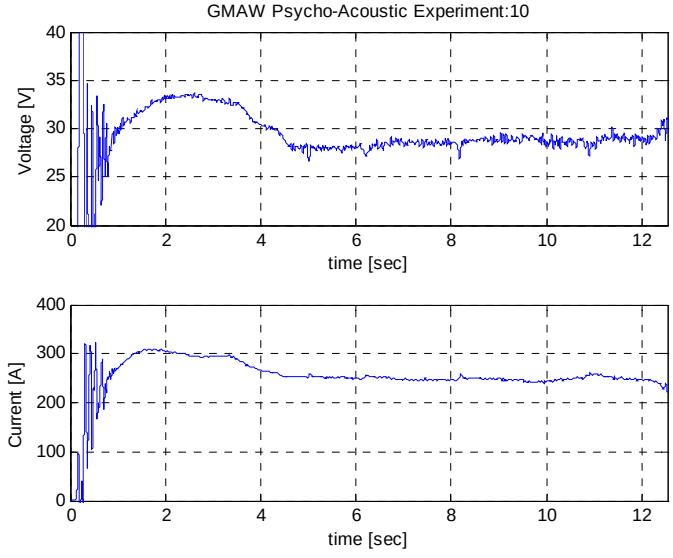

Figure 3-22: Welder 1 - Voltage and current traces of 150Hz + Harmonics attenuation experiment.

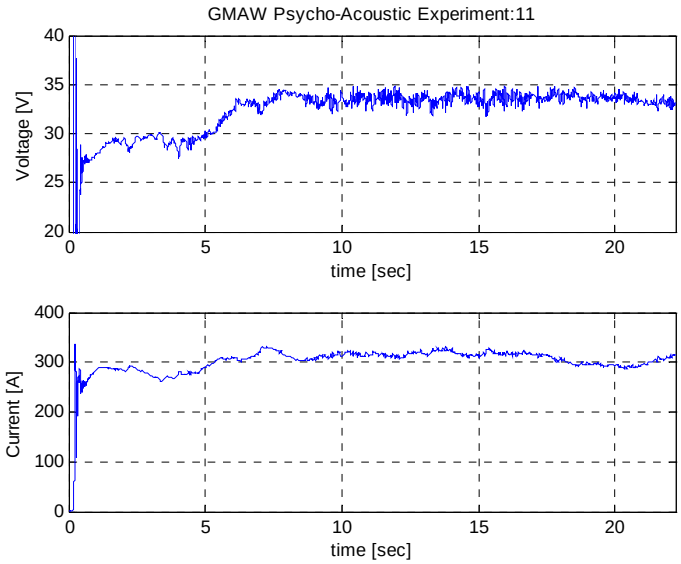

Figure 3-23: Welder 2 - Voltage and current traces of 220Hz + Harmonics attenuation experiment

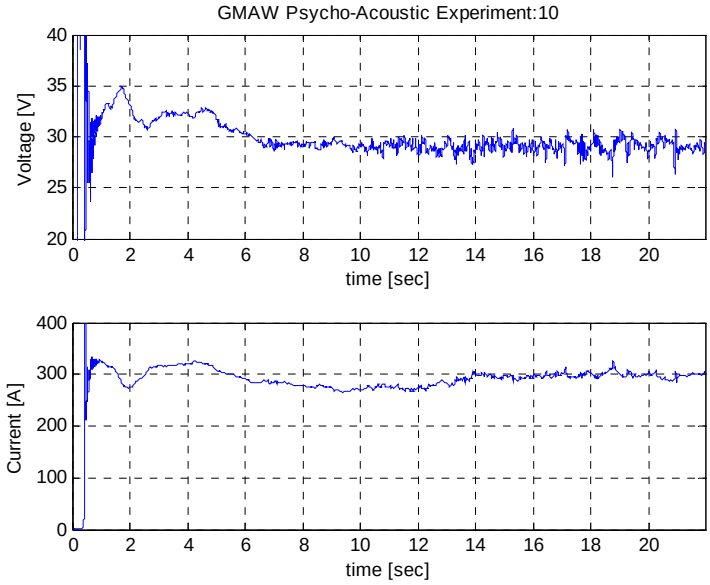

Figure 3-24: Welder 2 - Voltage and current traces of 150Hz + Harmonics attenuation experiment.

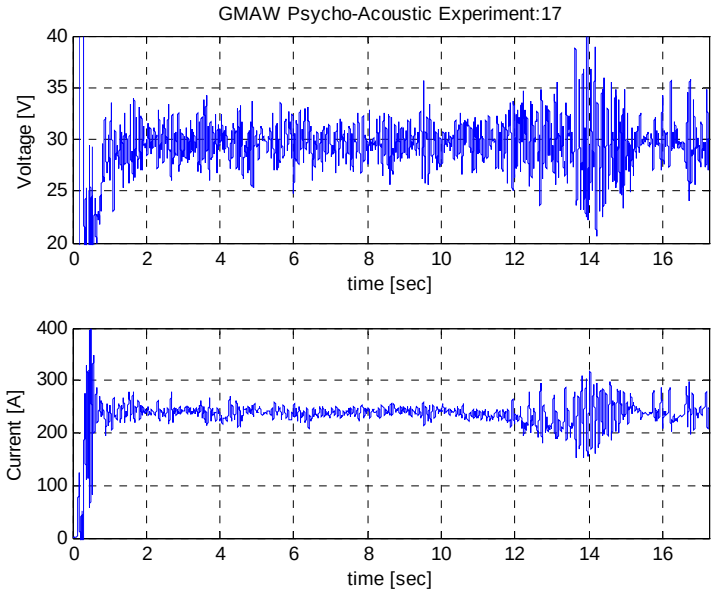

Figure 3-25: Welder 3 - Voltage and current traces of 220Hz + Harmonics attenuation experiment.

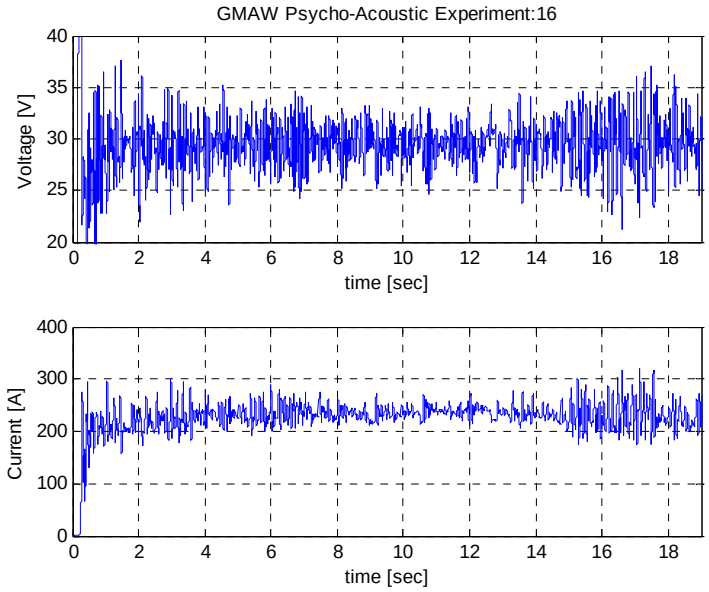

Figure 3-26: Welder 3 - Voltage and current traces of 150Hz + Harmonics attenuation experiment.

In support of these conclusions, the TLX data supplied by the welders distinctly show that they experienced more frustration when harmonic bands are attenuated. Moreover, their overall perceived task-load is generally higher when dealing with the 150Hz and 220Hz harmonic attenuations.

Incidentally, the three professional welders who participated in this study have had varying lengths of welding experience. By correlating their years of experience in GMAW and their performance, our study also found that as experience increases, the reliance on sound seems to decrease.

Chapter 4
Artificial Neural Network Inverse Model

4.1 Overview

The previous chapters identified correlations between acoustic spectral parameters and welding input parameters. Significant effects in acoustics are observed due to changes in voltage, wire-feed-speed (WFS), and contact-tip to work-piece distance (CTWD). In light of these findings, this chapter will present and demonstrate how these analytical methods are employed in conjunction with intelligent computing methods namely, an artificial neural network (ANN).

Coupled with methods developed in previous investigations [23, 24, 26] into the mapping of acoustic spectral shapes to transfer mode and weld quality, an ANN has the potential to perform an inverse mapping from acoustic characteristics to GMAW input parameters. If successful, this ability will allow us to effectively interpret acoustic signals in GMAW and translate into welding parameters, and thus implement a closed-loop controller based on acoustic feedback (Figure 4-1).

This chapter will present the fundamentals of how artificial neural networks work and how they are trained and tested. Furthermore, using data gathered from a new set of parametric experiments, we will demonstrate how the ANN learns and predicts weld parameters given specific acoustic characteristics. We will also discuss how ANN performance is assessed through a series of parameter sensitivity analyses. Finally, we verify the ANN's ability to predict weld parameters given acoustic data.

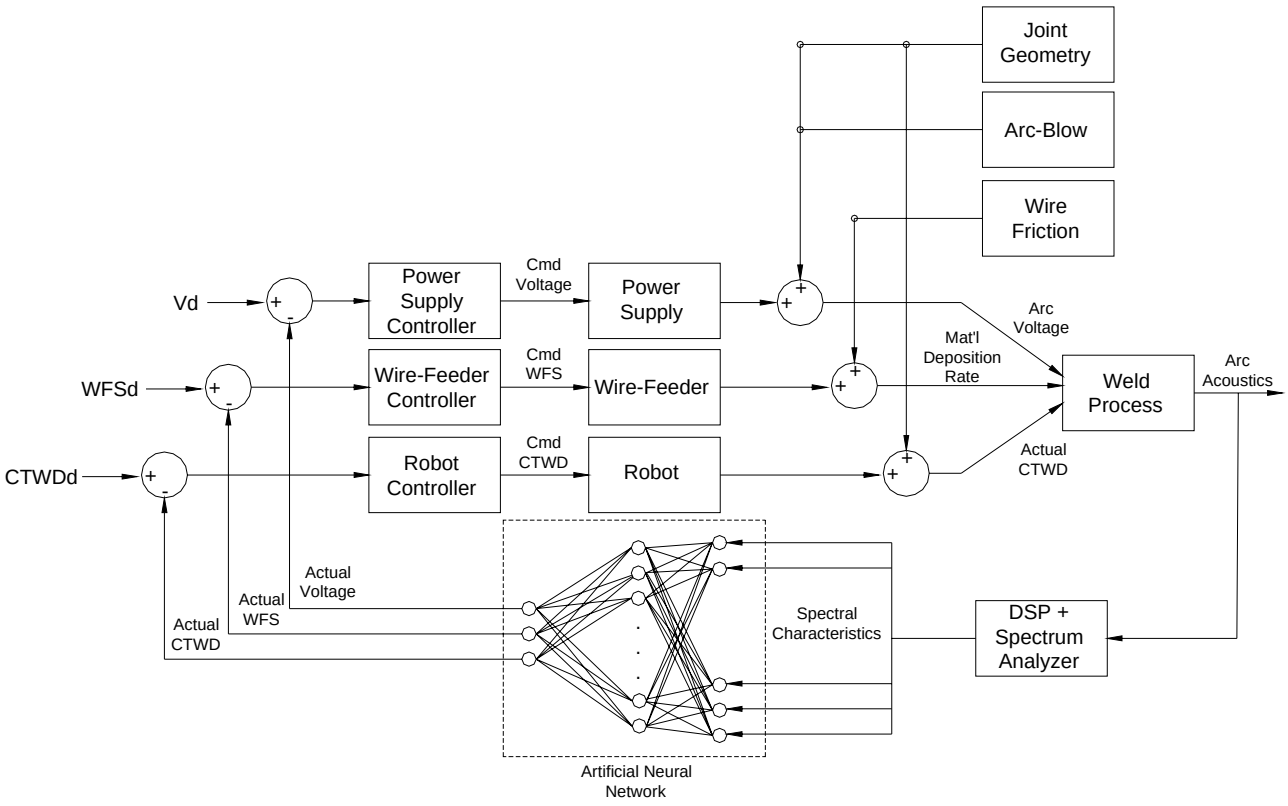

Figure 4-1: Close-loop control model of GMAW process using arc acoustics interpreted through an ANN.

4.2 Artificial Neural Network System (ANN)

Artificial neural networks were developed based on the mechanics of learning observed in human brains. Although crude in comparison to a human brain, ANNs have the demonstrated ability for pattern recognition, clustering, classification, system identification, and behavior prediction. More importantly, ANNs have the ability to learn, and given a sufficient set of training data, are capable of generalizing results based on new data. However, this ability is restricted within the parameter space initially established by the training set.

In this section, a brief discussion on the operation and architecture of multi-layer ANNs will be presented. We will then present the concept and method of back propagation training. Following this, details concerning the construction of the ANN are discussed, including; input/output training data, layer and neuron selection, activation functions, learning parameters, and verification data.

4.2.1 Neurons and Activation Functions

An artificial neural network consists of several layers of interconnected neurons. Each neuron is a basic computing element that receives several signals from its input links. These weighted input signals are summed and mapped through an activation function to produce an output signal (Figure 4-2).

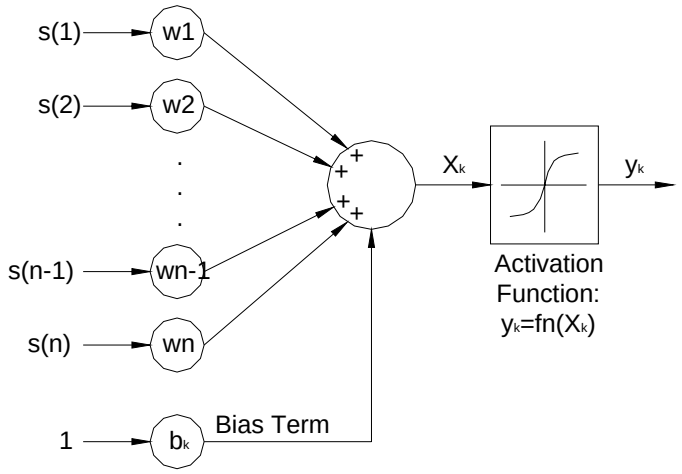

Figure 4-2: Block diagram of basic neuron computing element.

The output level of each neuron is determined by its activation function. Practical activation functions, as listed in [30], are the step, sign, sigmoid, hyperbolic-tangent and linear functions (Table 4-1). Depending on the application, some activation functions have been shown to be better suited than others. Table 4-1 provides a brief description of each.

Table 4-1: Typical activation functions utilized in artificial neural networks.

Step	Sign	Sigmoid
$Y_{step} = \begin{cases} 1, \text{ if } X \geq 0 \\ 0, \text{ if } X < 0 \end{cases}$	$Y_{sign} = \begin{cases} +1, \text{ if } X \geq 0 \\ -1, \text{ if } X < 0 \end{cases}$	$Y_{sigmoid} = \frac{1}{1+e^{-X}}$
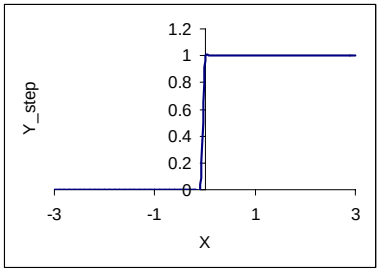	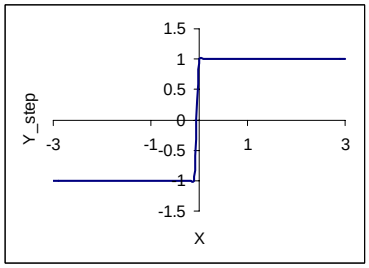	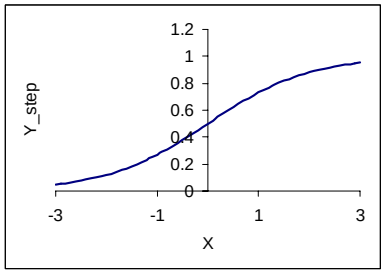

Hyperbolic-Tangent	Linear
$Y_{sign} = \frac{1-\exp(X)}{1+\exp(X)}$	$Y_{linear} = X$
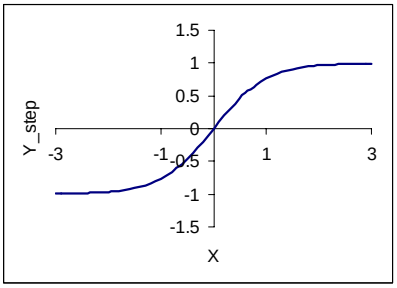	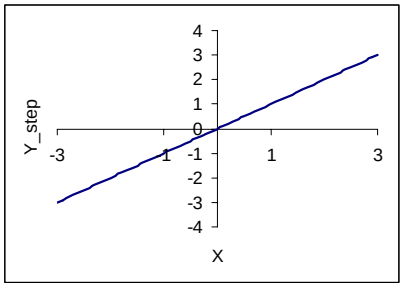

An added degree of freedom is introduced to the ANN by having a bias term in each activation function. This term shifts the center of the function away from zero, thus altering the transition sensitivity of the associated neuron. This will be elaborated on further when discussing algorithm implementation.

4.2.2 Multilayer ANN Architecture

Multilayer networks with a single hidden layer are capable of identifying and representing any continuous input/output relations. Networks with more than one hidden layer are capable of representing discontinuous functions with increasing complexity, but at an exponentially increasing computing cost. In our application, the relationships between acoustic characteristics and welding parameters will likely be non-linear but not discontinuous over our operating range, and as such, should be suited to a single hidden layer network.

A general feed-forward network is shown in Figure 4-3. In general, the input layer neurons do not perform computations and thus, do not process input patterns [30]. The connection weights to the hidden layer neurons represent the features being presented by the input neuron outputs. The output layer then determines the output pattern provided by these features.

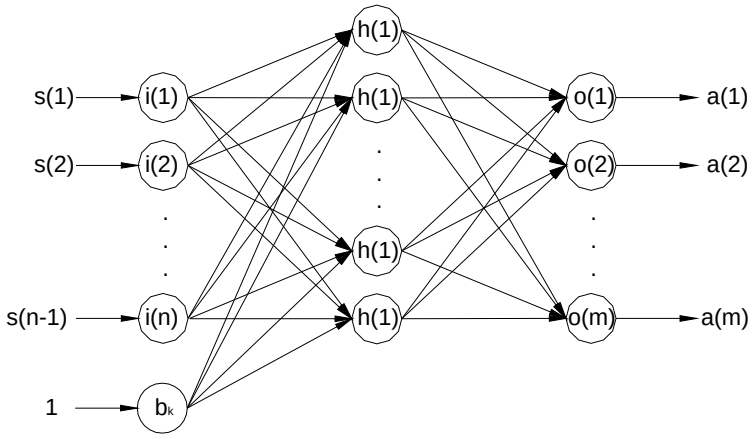

Figure 4-3: A general feed-forward ANN using a single hidden layer.

4.2.3 Back Propagation Training

Several methods of supervised and unsupervised training methods exist. We will use the most popular supervised learning method in our application, back-propagation [32]. The four steps to back propagation are; weights initialization, forward network propagation, weights correction, and iteration.

First, interconnection weights are initialized, typically using a random numbers selected from within some small range [30]. Furthermore, threshold levels or bias of activation functions are also initialized. Second, a set of training input parameters are presented to the network and propagated in the forward direction to produce output, y_k.

The network output error for neuron k at the output layer, at iteration p, is computed using the computed output $y_k(p)$, and desired (or target) output $y_d(p)$ and is defined by:

$$e_k(p) = y_{d,k}(p) - y_k(p) \tag{16}$$

The next step involves propagating the errors in the reverse direction through the network to adjust weights. Knowing the output error, the learning rule for output layer weight adjustment $\Delta w_{jk}(p)$ is implemented using the error gradient $\delta(p)$:

$$\Delta w_{kj}(p) = \alpha \times y_j(p) \times \delta_k(p) \tag{17}$$

$$\delta_k(p) = \frac{\partial y_k(p)}{\partial X_k(p)} \times e_k(p)$$

Where:

$\Delta w_{kj}(p)$: Change in weight value between hidden neuron j, and output neuron k

α: Output layer learning rate

$y_j(p)$: Output of hidden layer neuron j at iteration p

$y_k(p)$: Output of output neuron k at iteration p

$X_k(p)$: Net weighted input to neuron k at iteration p

$\delta_k(p)$: Error gradient of output neuron k at iteration p

$e_k(p)$: Output layer error

Similarly, weight correction for the neurons of each subsequent hidden layer is computed by the same weight adjustment equation (Eq.(17)), albeit using a different error gradient:

$$\delta_j(p) = y_j(p) \times [1 - y_j(p)] \times \sum_{k=1}^{l} \delta_k(p) w_{kj}(p) \qquad (18)$$

Where:

$W_{kj}(p)$: Weight value between hidden neuron j, and output neuron k

With the new weight values, the process is repeated and iteration continues until acceptable convergence of errors or some maximum number of iterations (or epochs) is reached.

Of significance to the success of ANN training is the selection of activation functions, learning parameters, and training data. The next section will summarize the parameters used in developing the ANN for correlating GMAW acoustic emissions to welding parameters.

4.2.4 ANN Parameter Selection

As mentioned before, since we expect a continuous, non-linear response between spectral characteristics and welding parameters, our ANN will be a single hidden layer system with acoustic characteristics as input and GMAW welding parameters as output. In accordance with our acoustic spectral analysis techniques, there are five spectral clusters each containing three characterizing

parameters: cluster mean; cluster scatter; and maximum frequency. ANN output parameters include voltage, WFS, and CTWD, resulting in a 15 input, 3 output network (Figure 4-4).

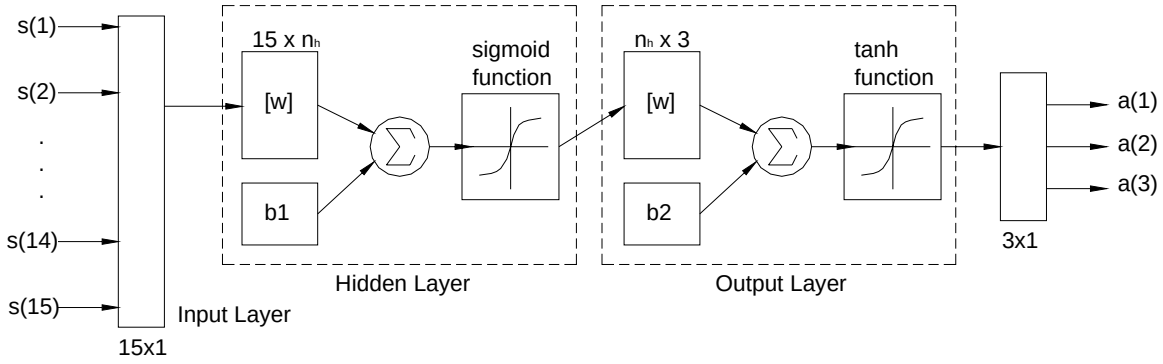

Figure 4-4: 15 input, 3 output ANN used in relating arc-acoustic characteristics to GMAW process parameters.

To complete the basic design of the ANN architecture, we have to decide on the number of neurons in the hidden layer. The appropriate number of neurons for hidden layers varies depending on the application and is best determined by experiment. Heuristically, most researchers agree [30] that the more neurons used in the hidden layer, the higher the effective 'bandwidth' represented by the network. However, if too many neurons are used, it is possible for the network to over-train and end up memorizing the training set patterns. For our network, we decided that some experimentation with the number of neurons would be acceptable assuming fast training times.

The next step is to decide on activation functions for each layer. As mentioned earlier, only the hidden and output layers contain activations functions. We decided to use a sigmoid function for the hidden layer and a hyperbolic-tangent function for the output layer. The sigmoid function guarantees

a bounded output from the hidden layer while the hyperbolic-tangent function has been shown to increase network learning rate [30].

The selection of learning rate values cannot be determined a priori. Learning rates are considered optimal if back propagation achieves convergence at a global minimum in a minimum amount of time. Since our system is relatively small, it is possible to run a sensitivity analysis to determine a suitable set of learning rates.

4.3 Algorithm Implementation

The *Matlab* algorithm implemented in our research has been adapted from existing code [31] for our data size and batch training. This section will summarize how the code is organized as well as specifics on implementing the ANN training algorithm. In general, the code is segmented into three major sections: data preparation, back-propagation training, and network simulation.

The input and training are initially normalized between -1 and 1. Normalization is necessary to accommodate varying orders of magnitude in data. Similarly, outputs being generated by the ANN are subjected to de-normalization to retrieve data in its original units. In our application, we decided to use the maximum and minimum values in our training data sets for each parameter as the basis for normalization. Each value is then normalized according to:

$$X_N(i) = \frac{x(i) - \frac{\max(x(i)) + \min(x(i))}{2}}{\frac{\max(x(i)) + \min(x(i))}{2}} \tag{19}$$

Back propagation is implemented as described previously. Hidden and output layer weights are set initially based on a random number between 0 and 1 according to:

$$W_{hidden} = \frac{randn}{N_{inputs}} \tag{20}$$

$$W_{output} = \frac{randn}{N_{outputs}} \tag{21}$$

With the selection of a sigmoid and hyperbolic-tangent activation functions for the hidden and output layers, respectively, we need to evaluate their derivatives in order to evaluate the error gradient function (Eq.(17)). For the sigmoid function:

$$\begin{aligned} y(X(p)) &= \frac{1}{1+\exp(-X(p))} \\ \frac{\partial y(p)}{\partial X(p)} &= \frac{\exp(-X(p))}{[1+\exp(-X(p))]^2} = y(p)\times(1-y(p)) \end{aligned} \tag{22}$$

Similarly for the hyperbolic-tangent function:

$$\begin{aligned} y(X(p)) &= \tanh(X(p)) \\ \frac{\partial y(p)}{\partial X(p)} &= 1-\tanh^2(X(p)) = 1-y(X(p))^2 \end{aligned} \tag{23}$$

In addition to the stated training inputs, the ANN includes an additional unity input that serves as an active bias adjustment term. As mentioned before, the bias term allows a shift in the activation function of each neuron. The mechanism by which the unity input provides an equivalent bias term to each neuron is not immediately apparent. Since each hidden layer neuron has a connection to the extra input, and because of its unity gain, the weights for each neuron connection act as an effective bias term. Similarly, the bias weights for the output layer are adjusted, albeit via a convoluted fashion as the effect is embedded with the other input weightings through the hidden layer. As the system is

back propagated, the weights associated with the extra input are adjusted to minimize error, and as such automatically realizes optimal bias terms for the ANN.

The two conditions that can terminate the back-propagation sequence are error convergence or reaching maximum epoch limit. Training data is provided in batch form to the ANN. In other words, all of the training data are presented to the ANN simultaneously, but still back-propagated in sequence. As such, forward propagation of the network results in as many output sets as there are training input sets. The output error $e_k(p)$ at iteration p is thus calculated for each resulting set. As such, overall output error for each parameter is computed using:

$$\sum_{i=1}^{n} e_k(p)^2 \qquad (24)$$

In the case where a maximum number of epochs have elapsed, our algorithm retains the weight values at which minimum overall error occurred.

Network simulation is basically a single data-set execution of the forward network propagation using the weights obtained from training. Again, input data is normalized before application to the network. Likewise, output data is de-normalized to obtain proper units.

4.4 Training and Verification Data Generation

Training data for our ANN was generated from a series of parametric experiments. Since this network was developed to determine whether or not an ANN is capable of learning an inverse relationship from acoustic characteristics to welding parameters, we decided to vary only three primary welding variables: voltage, WFS, and CTWD to generate the necessary training and

verification data. The parameter values used in these experiments are summarized in Table 4-2 and are effectively the target output parameters for training the ANN.

Table 4-2: Experiment parameters for generating training and test data for the ANN

Experiment	Voltage [V]	WFS [in/min]	CTWD [mm]
1	26	550	14
2	26	550	16.5
3	26	550	20
4	26	600	14
5	26	600	16.5
6	26	600	20
7	26	650	14
8	26	650	16.5
9	26	650	20
10	28.5	550	14
11	28.5	550	16.5
12	28.5	550	20
13	28.5	600	14
14	28.5	600	16.5
15	28.5	600	20
16	28.5	650	14
17	28.5	650	16.5
18	28.5	650	20
19	31	550	14
20	31	550	16.5
21	31	550	20
22	31	600	14
23	31	600	16.5
24	31	600	20
25	31	650	14
26	31	650	16.5
27	31	650	20

To ensure a large enough training data set, each parameter combination was performed three times. Data analysis of the recorded acoustic signal includes four averaged spectra from each weld. Each spectrum is subjected to the cluster identification algorithm as described earlier resulting in the scatter, geometric mean, and maximum frequency for each of the five clusters. From this analysis, a total of 324 sets of spectral parameters were generated. Two thirds of these data were used for batch training the ANN while the other third was reserved for verification.

Additional verification from welds performed using parameters different from, but within the parameter space of, the training data. These data will provide final verification of the effectiveness of using ANNs in this application.

4.5 ANN Training Performance Assessment

Optimization of ANN performance is accomplished by sensitivity analyses on training rates and number of hidden layer neurons. For both these training parameters, the objective function of interest was the overall error for a given number of epochs. In the interest of reasonable computation times, the number of epochs was set at 15000. The assumption is made that the trends shown for 15000 epochs reflect those for a higher number of epochs. Once good training parameters are identified, they are utilized to train the ANN until convergence is achieved.

The resulting training rates assessment is shown for each welding parameter in the contour plots of Figure 4-5 through Figure 4-7, respectively. The trend from CTWD and Voltage sensitivities (Figure 4-5 and Figure 4-6) shows that their overall errors are more sensitive to eta2, the output layer learning rate. Specifically, as eta2 increases CTWD error increases while Voltage error decreases. Based on this observation and inspection of the two figures, an optimal value of eta2 is 0.007 was

recommended. From Figure 4-6, eta1, the hidden layer learning rate would produce minimal error values if set at 0.005. The sensitivity of WFS on learning rates does not reveal any apparent trends for our system, Figure 4-7.

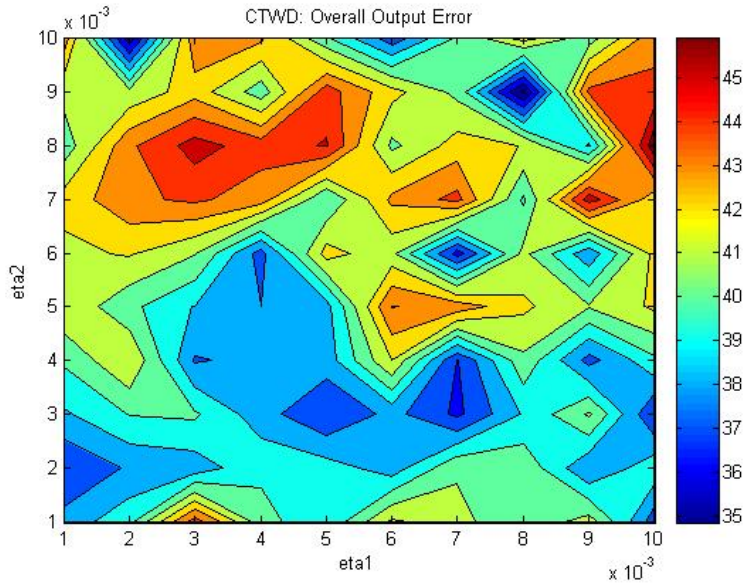

Figure 4-5: Overall CTWD output error - training rates sensitivity

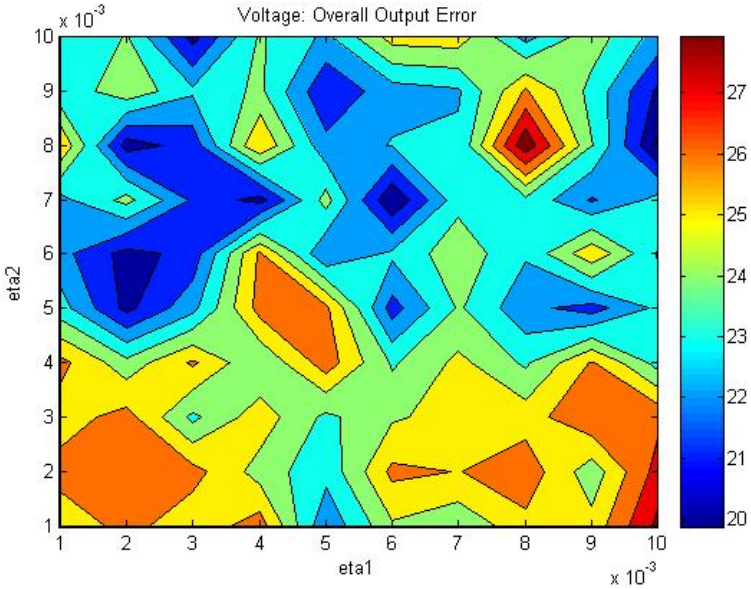

Figure 4-6: Overall Voltage output error - training rates sensitivity

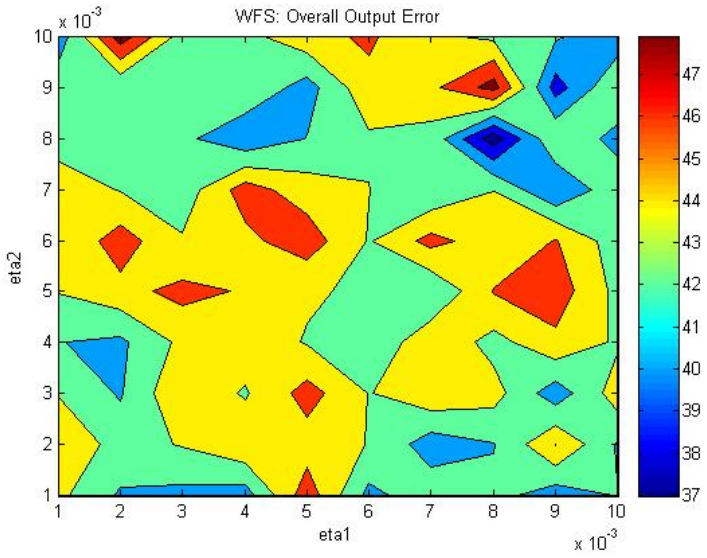

Figure 4-7: Overall WFS output error - training rates sensitivity

Figure 4-8 illustrates the sensitivity of overall ANN error to the number of hidden layer neurons. From this assessment, we can see a dramatic drop in overall output error with 22 hidden neurons. However, this level of performance becomes consistent only after using 26 hidden neurons. As such, we used 26 hidden layer neurons in our ANN application to ensure consistently small output errors.

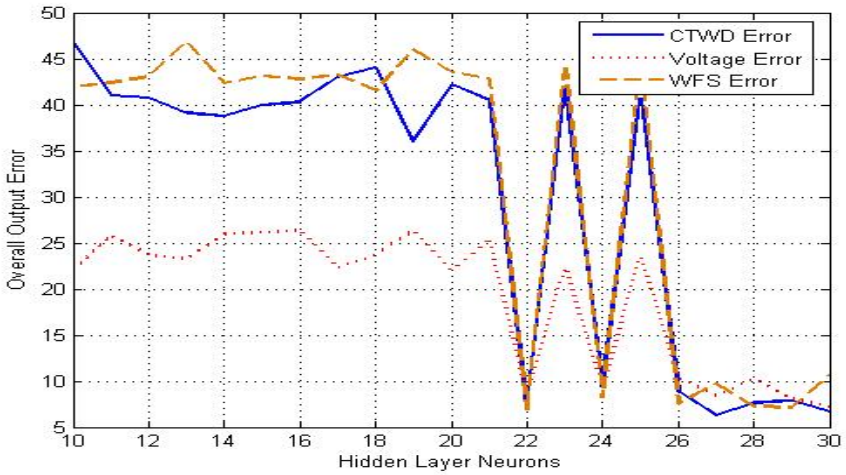

Figure 4-8: Overall output errors – Number of hidden layer neurons sensitivity

Having selected the necessary training parameters, the back propagation algorithm is executed using 150000 epochs with a convergence overall error of 0.1. Figure 4-9 shows the error convergence of our ANN using the training data specified earlier.

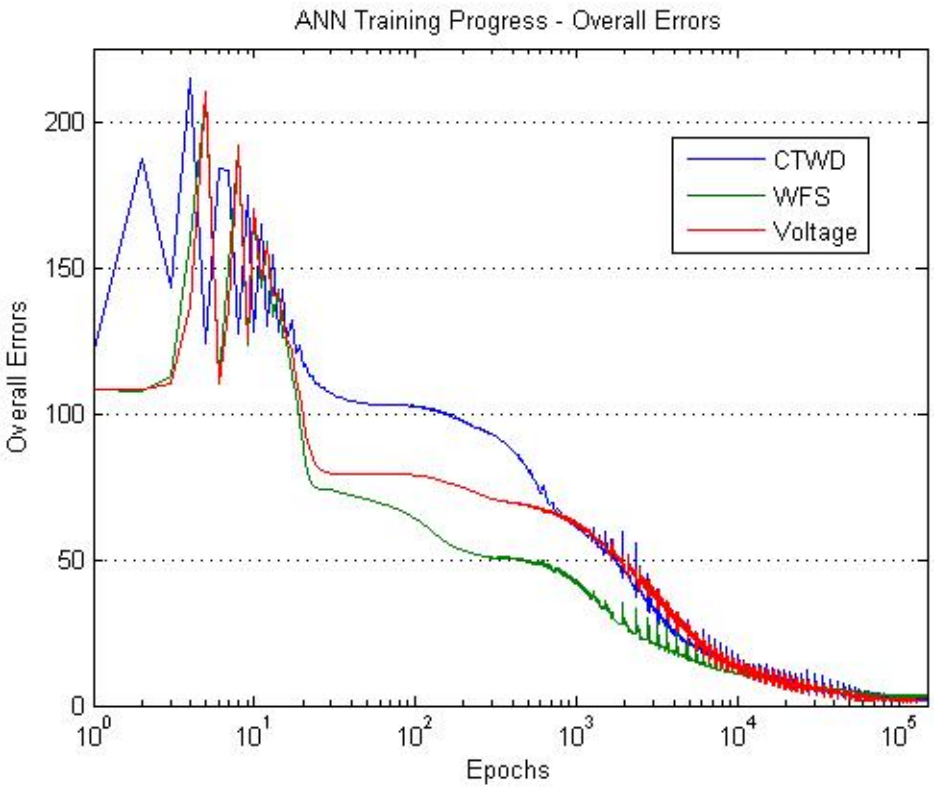

Figure 4-9: ANN training progression - Overall errors vs. number of epochs

4.6 ANN Verification

Once trained using the parameters determined above, the ANN needs to be verified. We assess the final ANN using both training data and test data. As mentioned before, training data are the spectral parameters used in training the ANN while test data are spectral parameters that the ANN has not

"seen" before. Nonetheless, since both sets of data are extracted from the experiments we ran, they are all within the training parameter envelope.

4.6.1 Verification Using Training Data

If the ANN is working properly, it should, at a minimum, be capable of predicting the welding parameters when presented with the training data. Figure 4-10 through Figure 4-12 illustrates the ANN's capability of doing this for the three welding parameters.

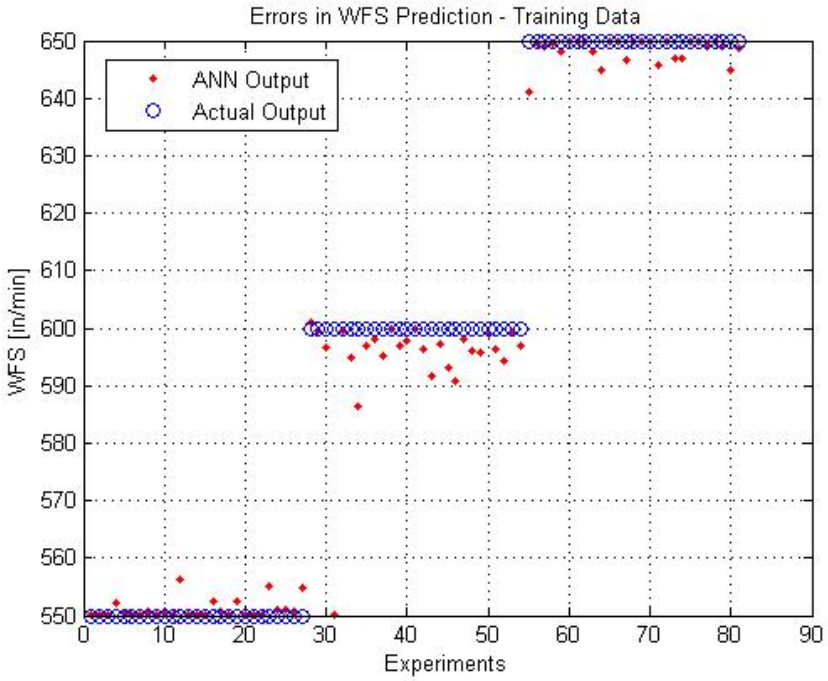

Figure 4-10: ANN predictions for WFS using training data.

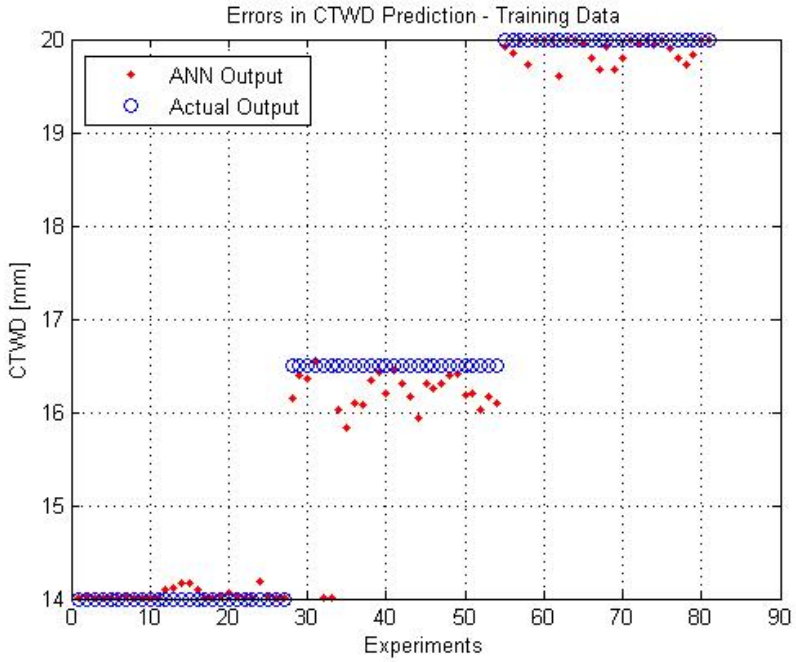

Figure 4-11: ANN predictions for CTWD using training data

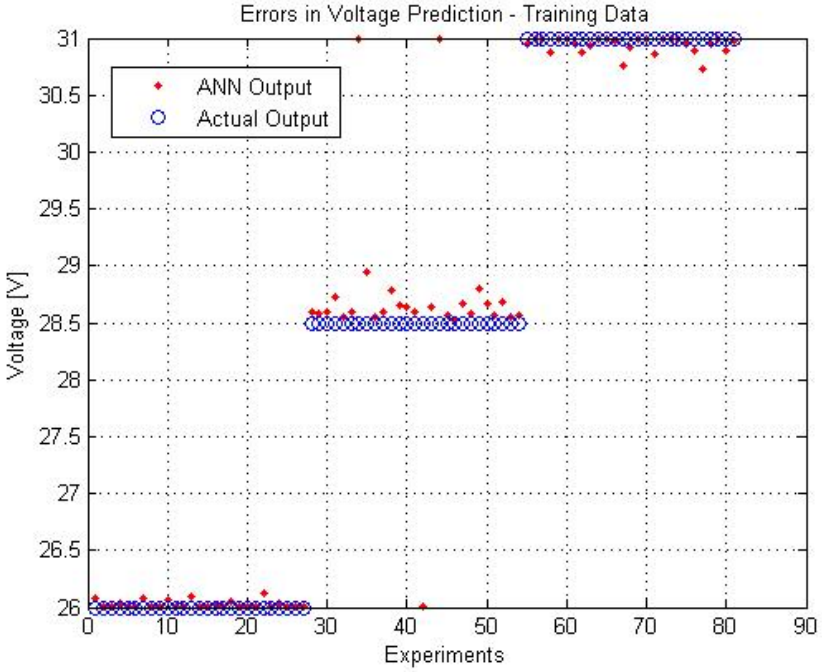

Figure 4-12: ANN predictions for Voltage using training data

4.6.2 Verification Using Test Data

Having shown that the ANN is capable of predicting weld parameters using training data, we proceed to verify the network using test data. Since we know that the test data is extracted from the same steady-state signals as the training data, we expect good agreement between ANN outputs and actual welding parameters.

Disappointingly, we found that network performance is well below anticipation. Figure 4-13 through Figure 4-15 shows the results of network verification using test data. Specifically, we observed that the network is least capable of predicting mid-level welding parameters. The wide level of scatter and inability for proper prediction is baffling and prompts an investigation into the richness and repeatability of the data, as will be presented as part of the next chapter.

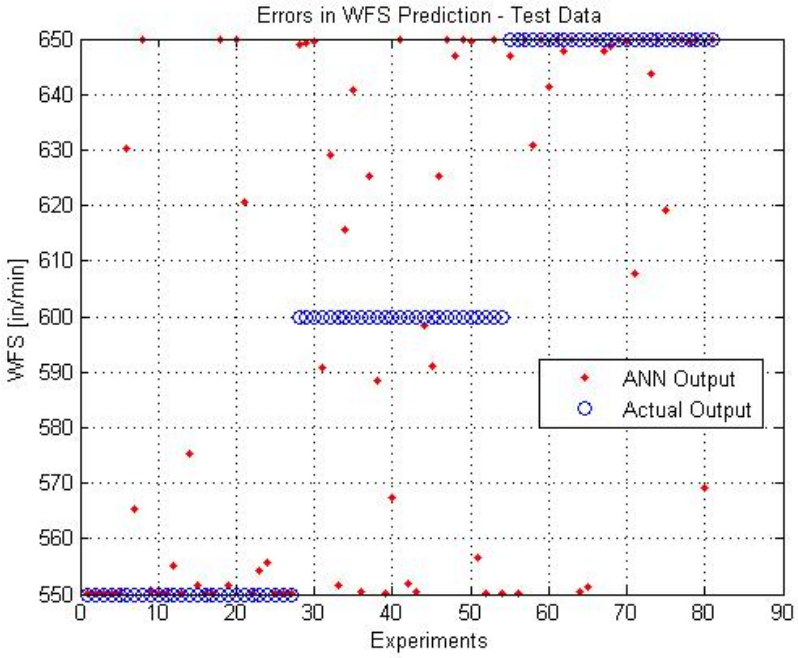

Figure 4-13: ANN predictions for WFS using test data.

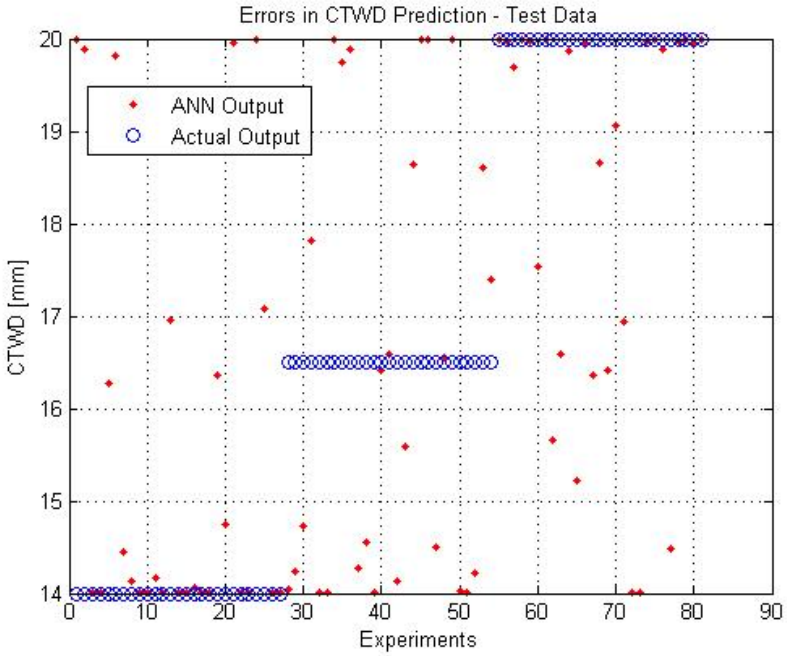

Figure 4-14: ANN predictions of CTWD using test data.

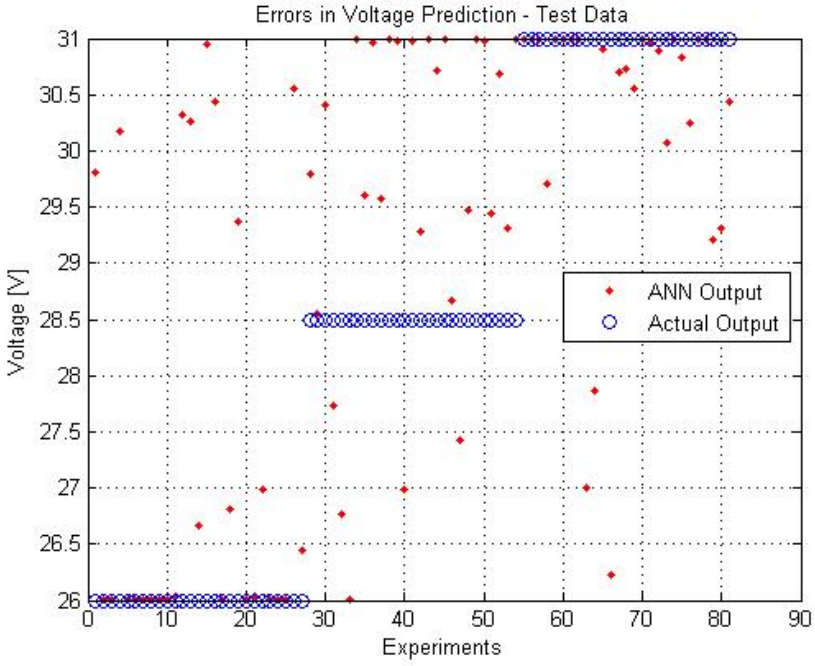

Figure 4-15: ANN predictions of voltage using test data.

Chapter 5
Conclusions and Recommendations

The objective of this thesis, to identify salient acoustic spectral characteristics in gas metal arc welding (GMAW) for control feedback, was partially achieved. In particular, experiments and robust techniques to isolate sound signal characteristics insensitive to noise intrusion were explored. The conclusions of these developments along with limitations to techniques and equipment are discussed below. Recommendations and future developments for addressing these issues are also presented below.

5.1 Conclusions

The objective was approached using three different techniques including Taguchi experiments, psycho-acoustic human experiments, and inverse mapping using an artificial neural network. The apparatus for performing these experiments was developed to allow accurate data acquisition of acoustic and power supply data. Moreover, a digital signal processing system was used in providing real-time altered acoustic feedback to assess expert welder reliance on arc-acoustics.

A cursory study using short-time Fourier transforms was conducted on acoustic signals collected while continuously changing weld parameters. The resulting spectral contour plots from this study were used as a generalized picture of what to expect in subsequent experiments. From the plots, the most prominent observation was that above 31V, there is an abrupt shift in the spectral content from the 6.0 kHz – 10.0 kHz range down to the 200 Hz – 400 Hz range.

Using the data-acquisition aspects of the apparatus, a parametric study was designed using Taguchi methods to ensure orthogonality amongst parameters. These experiments were then conducted to study the effects of changing weld parameters on acoustic characteristics. These characteristics were formally defined and identified using a cluster-identification algorithm applied to a series of fast-Fourier transforms performed on the recorded sound signals. Level-average, signal-to-noise, and frequency of occurrence analyses were performed on identified spectral characteristics resulting in a mapping of acoustic characteristic trends to welding parameters. Based on this analysis, it was shown that voltage played the largest role in affecting changes to arc-acoustics. More specifically, both level-average and frequency of occurrence trends show an increase in base frequency values (from 200Hz to 2000Hz) as voltage increased indicating an increase in droplet transfer rate. Disappointingly, this result contradicts with the cursory study performed using STFT suggesting an inadequacy in the analysis technique.

Despite conflicting results, it was decided that performing experiments with the dominant frequencies characterized in the Taguchi study using expert human welders may yield further insight as to which ones are truly salient and useful to human welder control. Efforts in designing and debugging the experimental apparatus revealed several application realities in the use of DSPs including limitations in finite-impulse-response (FIR) lengths as well as difficulties in manipulating lower frequency content.

In the process of improving response fidelity, preliminary trials with expert welders revealed that improper arc-acoustic feedback results in an inability to judge welding parameters. In other words, the necessity of acoustic feedback in GMAW was confirmed. Additional experiments conducted

using loud music to mask arc noise further confirmed these findings. The DSP was also used to introduce time-delays into the acoustic feedback. Analysis of voltage and current data indicated that at 400 milliseconds of delay, a professional welder will exhibit complete instability in process control ability. Furthermore, the corroborating evidence from a task-loading index (TLX) shows that welders experience increased frustration and decreased self-assessed weld quality as the time-delay increases. This result was consistent amongst all welders tested.

Spectral dependency tests conducted on professional welders utilized the DSP to playback band-attenuated acoustic signals. The results generally showed that 150 Hz and 220 Hz bands and their associated harmonics play a role in delivering encoded information to the welder. Unfortunately, due to a small number of subjects, and more importantly, the inability to remove duality components from visual feedback have resulted in inconclusive results concerning welder spectral dependency. Nonetheless, test results indicate that as welder experience or age increased, the dependency on acoustics reduced, as indicated by a lower frustration level in the TLX and better performance. This may be attributed to deteriorating hearing with age or better experience.

Prompted by the inconclusiveness of the previous deterministic approaches in characterizing GMAW acoustics, an artificial neural network (ANN) was implemented to apply a more “black-box” attempt to the task. More importantly, the ANN was judged to have the potential to provide a direct inverse translation from arc-acoustics to power-supply parameters and could be implemented in a closed-loop process controller. Using a full factorial set of experiments conducted within the spray-transfer mode envelope; changes in voltage, wire-feed-speed (WFS), and contact-tip to workpiece distance (CTWD) were considered. The recorded data then underwent cluster identification resulting in cluster means,

cluster scatter, and cluster maximum frequencies. In conjunction with the experiment welding parameters, these data was used for back-propagation training of the ANN. The trained network was tested using the original training data as well as test data that the network never "seen" before. Resulting ANN performance showed that the algorithm successfully learned based on the training data. However, when presented with the new data, the ANN was unable to properly predict welding parameters used.

The methods used in this study were determined to be objective, repeatable, and accurate. Despite their inconclusive results, the overall philosophy of examining spectral attributes of the acoustic signal is a significant improvement over existing correlation techniques using overall sound pressure levels (SPL) in that these techniques are relatively immune to ambient noise. Nonetheless, due to the complexity of the GMAW process and stochastic properties of acoustic signals, it is believed that richer data sets and more extensive experimentation are necessary to make these techniques successful.

5.2 Recommendations

Based on the experiences and results of this study, the following extensions and improvements are recommended for future work:

- From this study and others investigating arc-acoustics, there seems to be a strong correlation between arc-voltage and arc-noise. It would be interesting for future investigations to synthesize an acoustic feedback signal using the voltage signal. Playing this back to the welder and using the experiment techniques developed in this study while using the TLX as

an assessment of their frustration and performance can reveal how much of a correlation there really is. If welders are successful at tuning an arc using this feedback, then extracting acoustic characteristics from the voltage signal would yield a cleaner and more consistent feedback signal for use in close-loop control.

- A less time-consuming and more extensive study of expert welder judgment using arc-sound may be conducted in an "off-line" fashion. Participants can be invited to sit in an anechoic chamber and asked to judge a welding process purely based on arc sounds being played to them. These signals can be spectrally modified using a DSP to judge whether or not the welder recognizes any changes in welding parameters.

- This study suggests a correlation between metal-transfer rate and acoustic signals. Investigations into what this correlation is could yield valuable results in controlling droplet deposition dynamics using arc-sound. A possible approach would be to use high-speed laser-strobe video to measure droplet transfer rates and performing a correlation analysis with collected audio signals.

- The ANN developed in this study serves as an excellent platform upon which acoustic feedback can be utilized as a control signal. It is recommended that a richer training data set be used in training the ANN specifically within the spray-transfer operation envelope. Also, other characterizing spectral attributes should be examined in order to find those that are most relevant to achieving successful GMAW parameter prediction.

- With the existing ANN data, it may be possible to obtain improved training if 90% of the data was used to train the network, while only 5% of the data was used to verify it. Also, it is possible that some of the test data is highly irregular. If this is the case, it may be beneficial to train the network using different combinations of the existing data to see if this is so.

Appendix A

File Listing for Accompanying CD

File Name	Location	Description
ANN_Data.zip	..\Data\ANNExperiments-Data\	Data collected for training and verification of artificial neural network.
ANNExperiment-DataListing.zip	..\Data\ANNExperiments-Data\	Listing of experiment parameters corresponding to files located within ANN_Data.zip.
Power_Traces_Welder_01.doc:	..\Data\PsychoAcousticExperiments-Data\Welder_01\DAQ_Data\	Power supply traces recorded for welder 1.
Welder01_data.zip	..\Data\PsychoAcousticExperiments-Data\Welder_01\DAQ_Data\	Data collected during psycho-acoustic experiments performed on welder 1.
H_01.xls to H_19.xls	..\Data\PsychoAcousticExperiments-Data\Welder_01\TLX_Data\	TLX data collected with welder 1
TLX_Summ_Welder_01.xls	..\Data\PsychoAcousticExperiments-Data\Welder_01\TLX_Data\	Summarized TLX results of psycho-acoustic trials.
Power_Traces_Welder_02.doc:	..\Data\PsychoAcousticExperiments-Data\Welder_02\DAQ_Data\	Power supply traces recorded for welder 2.
Welder02_data.zip	..\Data\PsychoAcousticExperiments-Data\Welder_02\DAQ_Data\	Data collected during psycho-acoustic experiments performed on welder 2.
H_01.xls to H_19.xls	..\Data\PsychoAcousticExperiments-Data\Welder_02\TLX_Data\	TLX data collected with welder 2

TLX_Summ_Welder_02.xls	..\Data\PsychoAcousticExperiments-Data\Welder_02\TLX_Data\	Summarized TLX results of psycho-acoustic trials.
Power_Traces_Welder_03.doc:	..\Data\PsychoAcousticExperiments-Data\Welder_03\DAQ_Data\	Power supply traces recorded for welder 3.
Welder03_data.zip	..\Data\PsychoAcousticExperiments-Data\Welder_03\DAQ_Data\	Data collected during psycho-acoustic experiments performed on welder 3.
H_01.xls to H_19.xls	..\Data\PsychoAcousticExperiments-Data\Welder_03\TLX_Data\	TLX data collected with welder 3
TLX_Summ_Welder_03.xls	..\Data\PsychoAcousticExperiments-Data\Welder_03\TLX_Data\	Summarized TLX results of psycho-acoustic trials.
STFT_Data.zip	..\Data\STFTExperiment-Data\	Data collected for short-time Fourier transform experiments
STFT_Data_File_Listing.xls	..\Data\STFTExperiment-Data\	Listing of experiment parameters used to generate data in STFT_Data.zip
035Wire_Data_File_Listing.xls	..\Data\TaguchiExperiments-Data\035WireData	Listing of experiment parameters used to generate data in 035Wire_Taguchi_Data.zip
035Wire_Taguchi_Data.zip	..\Data\TaguchiExperiments-Data\035WireData	Data collected using 0.035” diameter wire for Taguchi experiments
0625Wire_Data_File_Listing.xls	..\Data\TaguchiExperiments-Data\0625WireData	Listing of experiment parameters used to generate data in 0625Wire_Taguchi_Data.zip
0625Wire_Taguchi_Data.zip	..\Data\TaguchiExperiments-Data\0625WireData	Data collected using 0.0625” diameter wire for Taguchi experiments
500k_epocks.jpg	…\Matlab_Code\ANN_Matlab_files\Fi	Error plot of ANN backpropagation

	gures\	after 500 thousand epochs.
L_Sensitivity.jpg	…\Matlab_Code\ANN_Matlab_files\Figures\	Error sensitivity of ANN based on number of hidden layer neurons
L15_C**k_****.jpg	…\Matlab_Code\ANN_Matlab_files\Figures\	Contour plots of error sensitivity based on learning rates.
PSD_comp_**.jpg	…\Matlab_Code\ANN_Matlab_files\Figures\	Figures to compare PSDs of training data sets.
Veri_****_testdata.jpg	…\Matlab_Code\ANN_Matlab_files\Figures\	Verification of ANN performance using test data.
Veri_****_traindata.jpg	…\Matlab_Code\ANN_Matlab_files\Figures\	Verification of ANN performance using training data.
Exp##_##_results.mat	…\Matlab_Code\ANN_Matlab_files\Vector_Load_Data	Training data vectors loaded and prepared from raw data files.
data_prep.m	…\Matlab_Code\Matlab_files	- scales voltage, current, and acoustic data from DAQ - searches voltage trace for arc-start and arc-extinguish and segments data - generates time vector based on sampling frequency
f2oct.m	…\Matlab_Code\Matlab_files	- transforms frequency vector into octave bins
FFT_Mk1.m	…\Matlab_Code\Matlab_files	- performs FFT of length N on given data segment returns power spectral distribution of

		given segment
getfile.m	…\Matlab_Code\Matlab_files	- retrieves data from experiment file sequence - calls data_prep.m to prepare data - returns time vector, core acoustic, voltage, and current data
octaves.m	…\Matlab_Code\Matlab_files	- performs geometric mean banding of frequency components based on 1/nth octave scale. - returns "banded" power-spectral distribution
recurse.m	…\Matlab_Code\Matlab_files	- determines optimal cluster boundary positions - uses recursive algorithm to sort through all cluster combinations and assesses cluster scatter using Kmeans.m
kmeans.m	…\Matlab_Code\Matlab_files	- computes scatter and mean of given data set
identify.m	…\Matlab_Code\Matlab_files	- identifies significant frequency bands from octave-banded frequency plots using known cluster sets - Note: algorithm was NOT used in final analysis of data
batch_01.m	…\Matlab_Code\Matlab_files	- data retrieval - spectral anaylsis - recursive cluster identification - identify cluster information / characteristics

		- saves data
summarize.m	…\Matlab_Code\Matlab_files	- summarizes cluster identification data graphically
data_prep.m	…\Matlab_Code\STFT_Matlab_files	- scales voltage, current, and acoustic data from DAQ - searches voltage trace for arc-start and arc-extinguish and segments data - generates time vector based on sampling frequency
getfile.m	…\Matlab_Code\STFT_Matlab_files	- retrieves data from experiment file sequence - calls data_prep.m to prepare data - returns time vector, core acoustic, voltage, and current data
STFT_2k5.m	…\Matlab_Code\STFT_Matlab_files	- retrieves and conditions data from file - high-pass filter acoustic signal - performs STFT on core segment of all three data segments: acoustic, voltage, and current - plots resulting contour map of STFTs along with voltage and current traces
BP.dpj	…\Programs\DSP_Code\BP	Bandpass project file for DSP
*******.h	…\Programs\DSP_Code\BP	Filter coefficients
Arb_Filter.m	…\Programs\DSP_Code\BR_Filters	Matlab file for generating arbitrary filters
*******.h	…\Programs\DSP_Code\BR_Filters	Filter coefficients
Ckt_Filter.m	…\Programs\DSP_Code\BR_Filters	Matlab file for generating experiment

		circuit compensation filter.
BP.dpj	…\Programs\DSP_Code\Delay_BP	Bandpass project file with time delay capacity for DSP.
*******.h	…\Programs\DSP_Code\Delay_BP	Filter coefficients
Bp_0#.csv	…\Programs\DSP_Code\Kernels	Filter coefficients for band-reject experiments developed in excel for DSP.
Gather.dsp	…\Programs\PCI9114gather\	PCI9114 data acquisition file written for data collection on welding rig.
CktFreqResponse.xls	…\Results\PsychoAcoustics-Results	Circuit response as found using frequency identification technique
Taguchi_Analysis-Results-Set1.xls	…\Results\Taguchi_Analysis-Results	Level average analysis of Taguchi methods data from experiment set 1
Taguchi_Analysis-Results-Set2.xls	…\Results\Taguchi_Analysis-Results	Level average analysis of Taguchi methods data from experiment set 2
Taguchi_Analysis-Freq_Occur_Results.xls	…\Results\Taguchi_Analysis-Results	Frequency of Occurrence analysis

Appendix B

Microphone Circuit

Description:

This circuit powers and amplifies an electret microphone while subjecting the resulting signal to a 6th order low-pass 6th order Butterworth filter for anti-aliasing.

Schematic:

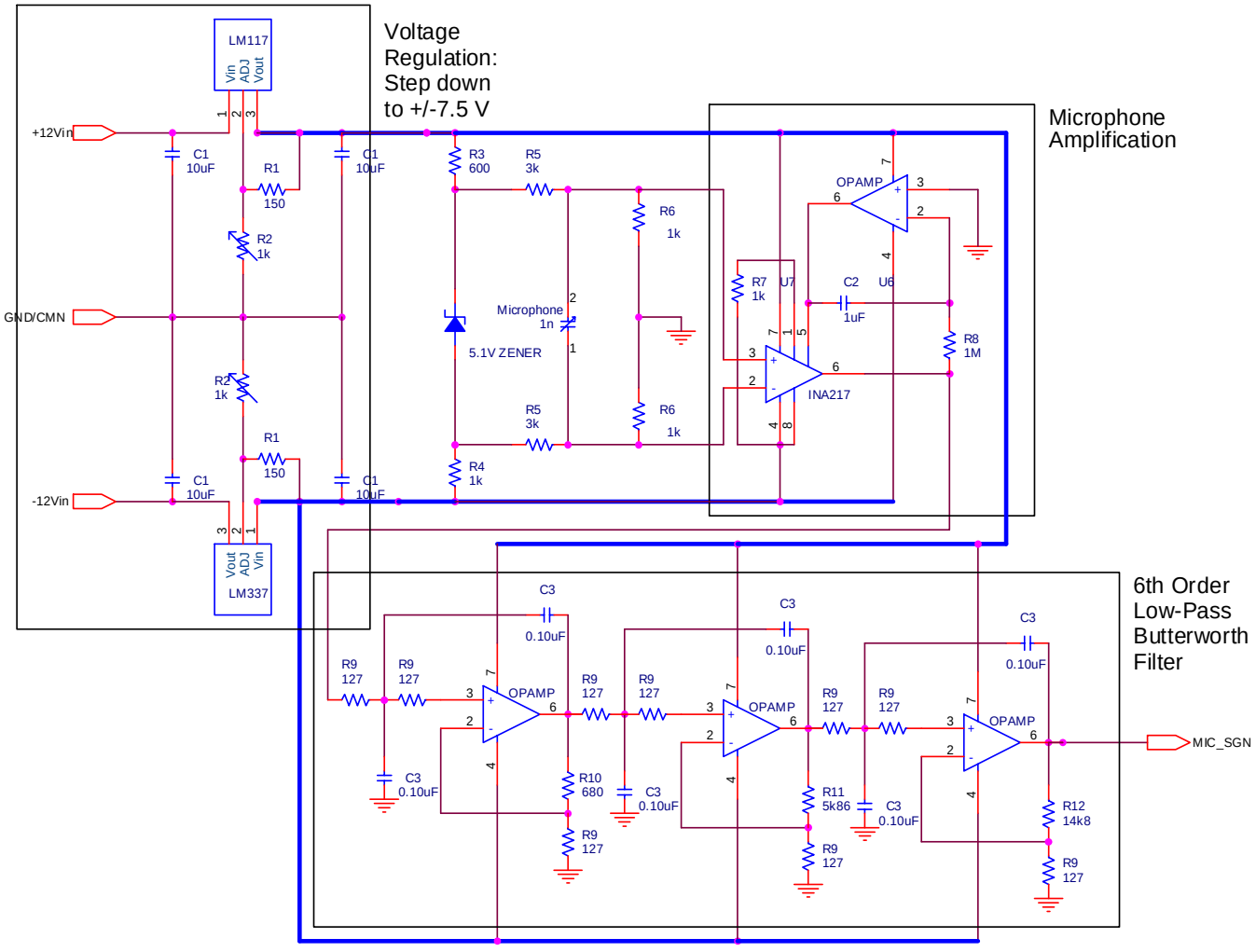

Circuit Design:

Voltage regulators LM117 and LM337 provide the necessary step-down capability to supply the circuit components with +/- 7.5V. Two 10uF capacitors filter out high-frequency noise from the regulated supply.

Chosen for near flat frequency response, the electret condenser microphone is a Panasonic WM-60A. According to manufacturer specifications, the operational parameter for this microphone requires a 2.0V charge potential and presents maximum 2.2kΩ impedance. Based on this, a 5.1V zener diode was chosen to "float" the supply voltage supplied to the microphone. Two 3kΩ resistors provide the necessary load to provide the necessary 2.0V to the microphone. Two tantalum capacitors and 1kΩ resistors provide the necessary DC content removal from the raw signal to be supplied to the amplification stage.

Signal amplification is accomplished using an INA217 instrumentation amplifier. Amplifier gain is dictated by the gain-set resister, R7, by $G = 1 + \frac{10\text{k}\Omega}{R_7}$. Using a 1kΩ resistor for R7, the circuit achieves a gain of 11. A DC control loop is implemented to eliminate DC drift of the amplifier output signal. The control loop provides a *negative* DC offset voltage to the pin 5 of the INA217 and effectively forms a feedback voltage follower.

Finally, anti-aliasing is provided by the 6^{th} order Butterworth filter. Filter design is based on a 12.5 kHz cut-off frequency with a -60dB/decade roll-off. Cascading three second-order Sallen-Key topology op-amp filters allow for easy implementation of this filter.

Appendix C

Headphone Amplification Circuit

Description:

This portable circuit was designed to amplify the arc-acoustic signal from the DSP for headphone output. It is powered by a 9V cell provides a maximum signal gain of 11.

Schematic:

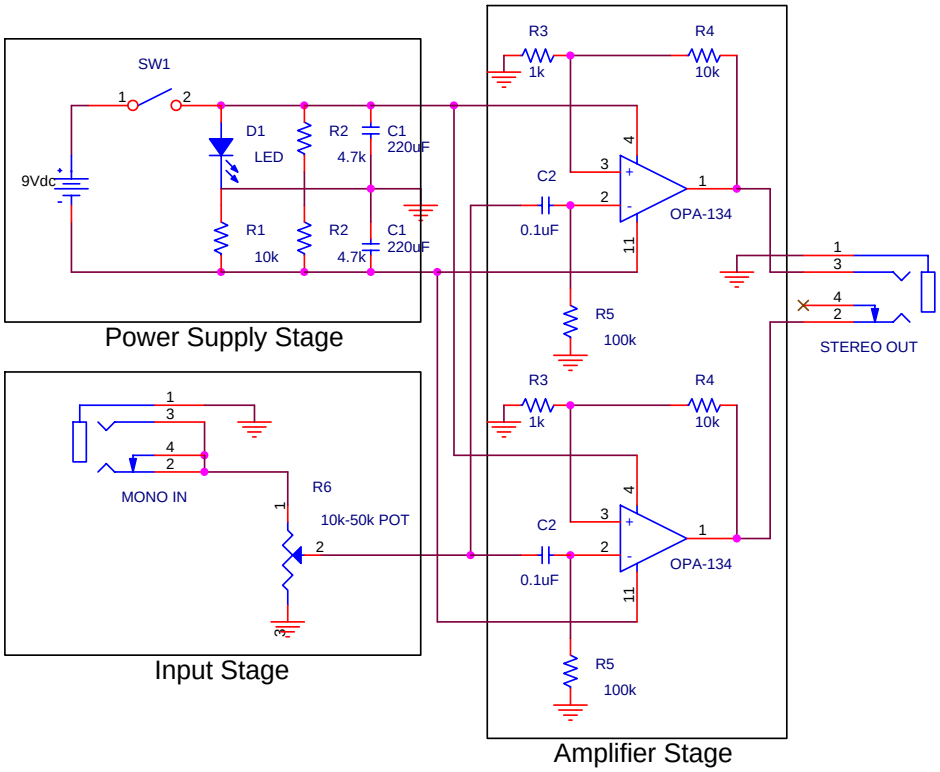

Circuit Design:

The 9V source is divided into +/- 4.5V using two 4.7k resistors (R2). This is used to power two OPA134 op-amps configured with a non-inverted gain of 11, as dictated by R3 and R4. The incoming mono-signal volume is controlled by a 10k–50k logarithmic potentiometer. C2 and R5 rejects any DC content from the incoming signal configured with a 15Hz cut-off.

References

[1] Liburdi Engineering "Automated Welding Systems: LST – Laser Seam Tracker". Nov. 2003. <http://www.liburdi.com/web_pages/aws_laserst.shtml>

[2] Matteson A., Morris R., Tate R, Real-Time GMAW Quality Classification using an Artificial Neural Network with Airborne Acoustic Signals as Inputs, *Conf. Modelling and Control of Joining Processes*

[3] Ogawa, Y et al. Analysis of Acoustic Signals on CO2 Arc Welding. *Proceedings of the Fifth (1995) International Offshore and Polar Engineering Conference*, The Hague, The Netherlands, June 11-16, 1995. ISBN 1-880653-16-8. pp. 131-136

[4] Lucas, W et al. Real-Time Low Cost Data Acquisition Systems for Weld Monitoring. *Computer Technology in Welding*. Proceedings, 8th International Conference, Liverpool, UK, 22-24 June 1998. Abington Publishing; ISBN 1-85573-415-X. pp.42-51

[5] Smith, JS; Lucas, W. Putting Intelligence into Welding – rule based systems, fuzzy logic and neural networks. *Welding and Metal Fabrication*, vol.67, no.10. Nov.-Dec.1999. pp.7-9

[6] Taylor-Burge, K et al. The Analysis of Airborne Acoustics of SAW using Neural Networks. *Computer Technology in Welding*. Proceedings, 5th International Conference, Paris, France, 15-16 June 1994. Abington Publishing for TWI; ISBN 1-85573-183-5. Paper 28.

[7] Doumanidis, C et al. Multivariable Control of Arc welding Processes. *Advances in Welding Science and Technology*. Proceedings, International Conference, Gatlinburg. ASM International; 1986. ISBN 0-87170-245-2. pp.449-460

[8] Hellinga, M Development of a Process Modelling Method for Welding Control., MASc Thesis, University of Waterloo, 1996

[9] Doumanidis, C. GMA Weld Bead Geometry: a lumped dynamic model. *International Trends in Welding Science and Technology*. Proceedings, 3rd International Conference on Trends in Welding Research, Gatlinburg, TN, 1-5 June 1992. ASM International; 1993. ISBN 0-87170-476-5. pp.63-67

[10] The Welding Handbook, 8th ed., American Welding Society (AWS), Miami – FL, 1987-1998

[11] Kralj, V Biocybernetic investigations of hand movements of human operator in hand welding. IIW/IIS Doc. 212-140-68, 1968

[12] Jolly, W.D. Acoustic emission exposes cracks during welding. *Welding Journal* 48 (1969) pp. 21-27

[13] Drouet M.G. and Nadeau F. Pressure waves due to arcing faults in a substation. (1979) *IEEE Trans*. PAS-98 1632-5

[14] Drouet M.G. and Nadeau F. Acoustic measurement of the arc voltage applicable to arc welding and arc furnaces. *Journal of Physics E: Scientific Instruments*, vol.15. 1982. pp.268-269

[15] Arata, Y. et al. Investigation of Welding Arc Sound (Report 1) - Effect of Welding Method and Welding Condition on Welding Arc Sound. *Reports Japan Welding Research Institute* (1979)

[16] Arata, Y. et al. Investigation of Welding Arc Sound (Report 2) –Evaluation of Hearing Acuity and Some Characteristics of Sound. *Reports Japan Welding Research Institute* (1980)

[17] Mansoor, A and Huissoon, JP. An investigation of the arc sound produced during GMA welding. MASc Thesis, University of Waterloo, 1997

[18] Prezelj, J and Čudina, M. Noise as a Signal for On-line Estimation and Monitoring of Welding Process. *Acta Acustica United with Acustica*, Vol. 89 (2003) pp. 280-286

[19] Chawla, KS and Norrish, J. Real time quality monitoring using analysis of the arc sound. *Computer Technology in Welding*. Proceedings, 4th International Conference, Cambridge, UK, 3-4 June, 1992. Abington Publishing for TWI; 1992. ISBN 1-85573-086-3. Paper 17

[20] Kaskinen, P. and Mueller, G. Acoustic Arc Length Control. *Advances in Welding Science and Technology*. Proceedings, International Conference, Gatlinburg. ASM International; 1986. ISBN 0-87170-245-2. pp.763-765

[21] Murugesan, M. et al. Characterization of Electric Arc-Spraying Process using Sound Signals. *Manufacturing Science and Engineering* 1994, PED 68, Vol. 1 (1994)

[22] Matteson et al. An Optimal Artificial Neural Network for GMAW Arc Acoustic Classification. *International Trends in Welding Science and Technology* (1993) pp. 1031-1035

[23] Tam, J. and Huissoon, J. Characterizing Arc Acoustic Feedback in GMA Welding. Submitted to *Science and Technology of Welding and Joining*, 2005.

[24] Tam, J. and Huissoon, J., Characterizing Arc Acoustics in GMA welding, 14th Int'l Conf. *Computer Technology in Welding and Mfg*. 2004, Sheffield Hallam University, UK

[25] G.S. Peace, Taguchi Methods – A Hands-On Approach, Addison-Wesley Publishing Company, Reading, Massachusetts (1993)

[26] Tam, J. and Huissoon, J. Psycho-Acoustic Experiments in GMA Welding. Submitted to *Science and Technology of Welding and Joining*, 2005.

[27] Smith, Steven W., The Scientist and Engineer's Guide to Digital Signal Processing, 2nd Edition., California Technical Publishing, San Diego – CA, 1997

[28] Wilson, Charles E., Noise Control – Measurement, Analysis, and Control of Sound and Vibration, Krieger Publishing Company, Malabar – Florida, 1989

[29] Hollands, J and Wickens., Engineering Psychology and Human Performance. 3rd ed. Upper Saddle River, NJ: Prentice-Hall Inc.

[30] Negnevitsky, Michael., Artificial Intelligence – A Guide to Intelligent Systems. 2nd ed. Addison-Wesley – Essex, England, 2002

[31] Melek, William. Artificial neural network code (Neural-net4.m) adapted with permission. 2003

[32] Rumelhart, D., G. Hinton, and R. Williams. 1988. Learning internal representations by error propagation. In Neurocomputing, edited by J. Anderson and E. Rosenfeld, 675-695. Cambridge, MA: MIT Press.